



POLITECNICO DI MILANO
DEPARTMENT of ARCHITECTURE BUILT ENVIRONMENT AND CONSTRUCTION
ENGINEERING
ABC DOCTORAL PROGRAM - XXXI CYCLE

Effect of the Uncertainty in Outdoor Boundary Conditions on Building Performance Simulation

A dissertation
Presented to
The Academic Faculty

By:
Maryam Meshkin Kiya

Supervisor:
Dr. Riccardo Paolini, University of New South Wales

Tutor:
Dr. Claudio Del Pero, Politecnico di Milano

PhD Program Coordinator:
Dr. Marco Scaioni, Politecnico di Milano

Politecnico di Milano
April 2019

DEDICATION

I dedicate this PhD thesis to my family.

ACKNOWLEDGEMENT

I would like to express my special appreciation to the former PhD coordinator of Department of Architecture, Built Environment and Construction Engineering, professor Enrico De Angelis, for facilitating the path of my PhD research.

A special thanks to Fondazione Fratelli Confalonieri for placing their trust in my research. I am grateful for their financial support during my PhD study through the scholarship of “Borsa per dottorandi di ricerca delle Università Milanese”, without which, I would not have been able to develop my scientific discoveries.

My sincere thanks also go to Professor Jan Hensen and Dr Roel Loonen for hosting me at the Department of Built Environment and Building performance in Eindhoven University of technology which supported me to develop parts of my investigations.

Last but not least, I would like to express my deepest gratitude to my family, friends and especially my husband. This dissertation would not have been published without their love, patience and endless support.

PREFACE

The following dissertation is submitted for the degree of Doctor of Philosophy at the Department of Architecture, Built Environment and Construction Engineering of Politecnico di Milano. The PhD research was conducted under the supervision of Dr Riccardo Paolini and tutored by Dr Claudio Del Pero in the Department of Architecture, Built Environment and Construction Engineering, and funded by Fondazione Fratelli Confalonieri as a PhD scholarship.

To the best of the author's knowledge, this work is original and has not been submitted for any degree or qualification at any other university or institution.

Table of Contents

DEDICATION.....	3
ACKNOWLEDGEMENT.....	4
PREFACE	6
Table of Contents.....	7
List of Figures.....	9
List of Tables.....	14
Summary	1
Chapter 1 - Introduction.....	3
Foreword.....	3
1-1 Building energy performance gap.....	4
1-2 Microclimate as a source of the performance gap	6
1-3 Solar irradiance research area and challenges	8
1-4 Research questions	10
1-5 Aims and objectives	11
1-6 Summary.....	12
Chapter 2 – Research background	14
2-1 Uncertainty in building energy simulation.....	14
2-2 Urban canyon features	17
2-3 solar radiation in urban canyon and effects on buildings.....	18
2-4 Solar models.....	18
Chapter 3 – Methodology.....	21
3-1- Data acquisition	21
3-1-1 Collecting data.....	21
3-1-2- Quality control tests	22
3-1-3 Infilling missing data.....	23
3-2 The theory of uncertainty	25
3-2-1 Uncertainty analysis	25
3-2-2 Sampling and propagation methods	25
3-3 Model fine tuning.....	32

3-3-1 Solar model calibration.....	32
3-3-2 Building energy model fine tuning.....	35
Chapter 4 – Case study.....	51
4-1 Data acquisition and refinement	51
4-1-2 Data Description.....	51
4-1-3 Result and Discussion.....	51
4-1-4 Conclusion	55
4-2 Model fine-tuning.....	55
4-2-1 Solar model calibration.....	55
4-2-2 Building energy model fine-tuning	68
4-2-3 Uncertainty of solar radiation and daylight analysis	81
4-2-4 Connect solar radiation analysis to building energy simulations.....	92
4-2-5 Conclusion	100
Chapter 5 - Conclusions	101
5-1 Summary.....	102
5-2 Future studies	103
References	105
Annexes:.....	116
Annex 1: Basis of DIVA solar radiation simulations.....	116
Annex 2: Uncertainty propagation - Code in MATLAB and connection to Grasshopper	117
Annex3: Building energy model assumption in WUFI Plus	120

List of Figures

Figure 1- Climate scales which effects on building energy performance [3]	3
Figure 2 - Urban canyon originally is defined by building and street between them, however, other existing elements inside a canyon can affect the energy balance.....	4
Figure 3 - Components of the solar radiation propagating within an urban canyon	9
Figure 4 - Uncertainty and building life cycle [58]	14
Figure 5 - Diagram of a vanilla neural network	24
Figure 6- Transformation of possibility distribution to belief function.....	28
Figure 7- illustration of the hybrid approach: (A) Series of random samples are generated by a probabilistic approach from PDF (P_1, \dots, P_n). (B) Sample generated based on possibilistic approach through selecting an a-cut (F_1, \dots, F_m). (C) The final set of samples are a combination of PDF and a-cuts, where each probability sample is repeated for each a-cuts of PDF and a-cuts, where each probability sample is repeated for each a-cuts (M($P_1, \dots, P_n, F_1, \dots, F_m$)). [177].....	31
Figure 8 - Framework of calibration method using Subset Simulation.....	32
Figure 9 - Equivalent lines for each class of sky and Perez coefficients (left). Interpolation of the lines (right)	34
Figure 10- Radian map component of DIVA in Grasshopper. Main inputs and possible outputs	36
Figure 11- Modules to transfer coordinates to 3D model	39
Figure 12- Module to create random height and WWR for each building	40
Figure 13- Modules to convert one floor to multi-floor buildings with the possibility of variation in height, WWR, and material	41
Figure 14- Modules to model trees with uncertainty in crown diameter and material.....	42
Figure 15- Module to create a car with the possibility of variation in material.....	43

Figure 16 – A sample of final complex canyon geometry	44
Figure 17- Geometry of simple canyon, typical consideration of urban canyon in building energy analysis	44
Figure 18 - A sample of Radiance material definition.....	45
Figure 19- The geometry of body divided to detailed segments to fed to raytracing simulation (Up), predicated projected area for standing and seated posture (Down: right=standing, left=seated) [189].....	48
Figure 20- The network of weather stations of this study. The red points refer to stations which used as the input features. The star refers to the target of the prediction of missing value in hourly temperature.....	51
Figure 21- An example of how encountering missing values in inputs can result in weak predictions @ ANN3 with MSE=1.22 and R=0.9923	53
Figure 22 - Difference between the features in ANN3 and ANN5; the presented scheme is representative of the entire input matrix. All vectors include a time offset of ± 2 hours. These samples are not used for training as they have missing values in the target and are only used for evaluating the performance of the trained model.	54
Figure 23- Estimation of missing data for Lacchiarella weather station with ANN3	54
Figure 24- Estimation of missing data for Lacchiarella weather station with ANN5	54
Figure 25- Illustration the performance of SuS. According to the proposed method, after 20 th subset, the thresholds reach to a stable minimum level	57
Figure 26- Comparison between original and calibrated Perez for Eindhoven.....	59
Figure 27- ASHRAE 90.1, Large office. The case-study building energy model.	61

Figure 28- Comparison between the produced energy by simulated PVs based on Base-EP and Modified-EP, an illustration of the probability distribution. PVs are located with (a) 15°, (b) 30° and (c) 90° of inclination..... 63

Figure 29- Comparison of incident solar irradiation on vertical surface 64

Figure 30 - Reliability assessment of the proposed cooling system 65

Figure 31- Incident solar radiation on building facades(W/m²), comparison of Base-EP and Modified-EP 66

Figure 32- Samples of sensor direction and orientation settings in DIVA. (a) The camera (assumed as a sensor) is faced due to the south, collecting data on the vertical surface, (b) The camera is facing up, collecting data on horizontal surface 68

Figure 33- A screenshot from Diva4Rhino forum. Suggested values for tree transmittance for summer and winter [196] 70

Figure 34 - Studied area (Up), Comparing the effect of trans material on two geometry for trees (Down) 71

Figure 35- Contrast incident solar radiation on south facade affected by shadows from trees as box and as sphere..... 71

Figure 36- Detailed tree model is compared with the simple model..... 72

Figure 37- Sensitivity analysis of detailed tree modeling, the decision about modifying the material transparency or precise model..... 73

Figure 38- Possibility distribution of (a) transmittance of trees, (b) cars reflectance 75

Figure 39- A sample of how each generated sample is assigned to Building geometry in Grasshopper 75

Figure 40- Uncertainty analysis of incident solar radiation on south façade on three floors: (a) ground floor, (b) middle floor, (c) top floor..... 77

Figure 41 - Simple canyon vs. uncertainty propagated canyon - Daily profile of 21 March..... 79

Figure 42- Simple canyon vs. uncertainty propagated canyon - Daily profile of 20 Jun 79

Figure 43- Simple canyon vs. uncertainty propagated canyon - Daily profile of 22 Dec 80

Figure 44- Incident solar radiation (W/m^2) on building facades during 21 Jun and 21 December in two candidate scenarios: low (Left) and high (Right). For a better presentation of the results, trees and cars are hidden however the effects are clear. 81

Figure 45 – Comparison of percentage of the year when the illuminance is occurred in UDI metrics for three scenarios. (a) ground floor, (b) middle floor and (c) top floor..... 83

Figure 46- Comparison of percentage of the year when the illuminance is exceeded of UDI metrics for three scenarios. (a) ground floor, (b) middle floor and (c) top floor..... 84

Figure 47- Comparison of percentage of the year when the illuminance is lower than UDI metrics for three scenarios. (a) ground floor, (b) middle floor and (c) top floor..... 85

Figure 48 - Daylight factor (%), comparison between simple, low and high scenarios. Depth of room refers to distance of each point from the window. Window is located at 1 86

Figure 49 – Risk of glare based on variation in WWR on the **low scenario for ground floor** ... 89

Figure 50 - Risk of glare based on variation in WWR on the **high scenario for ground floor**... 89

Figure 51 - Risk of glare based on variation in WWR on the **low scenario for the middle floor** 90

Figure 52- Risk of glare based on variation in WWR on the **high scenario for the middle floor** 90

Figure 53 – Fraction of floor subject to glare in the ground floor. A comparison between high scenario (a) transparent mesh, and low scenario (b) solid 91

Figure 54- Fraction of floor subject to glare in the middle floor. A comparison between high scenario (a) transparent mesh, and low scenario (b) solid 91

Figure 55- Fraction of floor subject to glare in the **top floor**. Similar performance of high and low scenario..... 92

Figure 56- building energy model in WUFI, the middle zone, and its external walls are simulated 93

Figure 57- Projected area factor (f_p) based on solar azimuth and altitude for seated posture [189] (a) and (b), interpolate fit on the value of projection factor (c)..... 95

Figure 58- Variation of PMV and MRT solar in high and low scenarios for ground (a), middle (b) and top (c) floor..... 96

Figure 59- Frequency of different thermal sensation based on ASHRAE division and PMV calculations. 97

Figure 60- Variation hours in PMV categories affected by uncertainty in building surroundings98

Figure 61- Variation of thermal sensation based on simple and complex urban canyon scenarios 98

Figure 62- Contrasting the effect of probabilistic and possibilistic variables on thermal comfort99

Figure 63 - WUFI weather generator..... 120

Figure 64 - Exterior wall assembly..... 121

List of Tables

Table 1 – Description of the most common variables in UA and SA	15
Table 2 – Keywords of SA and UA and related literature in building energy performance topics. UA category consists of three most popular sampling methods in building topic: LHS (Latin Hypercube Sampling), SS (Simple Sampling), QMC (Quasi Monte Carlo). SA category consists of three most popular sensitivity methods in building energy topics: MM (Meta-Model), SRC (standard Regression Coefficient) and Morris.....	16
Table 3 - Range test and relation test thresholds	23
Table 4- Sampling methods and tools.....	26
Table 5- original Perez irradiation coefficients	33
Table 6 - Candidate factors related to the uncertainty of solar radiation on urban canyon	38
Table 7- Seasonal effect of trees by measured solar radiation under the trees, in winter and summer period and with no shade and shaded conditions [185].....	46
Table 8 - predicted mean vote (PMV) thermal sensation, ASHRAE scales	50
Table 9- Description and performance of different combinations of input features for training the network. (T: Temperature, MM: Month, DD: Day, HH: Hour of each sample, AI: Anomaly Indicator).....	52
Table 10- Availability of measured data in Eindhoven site	55
Table 11 - BMS sensors details [192].....	56
Table 12- The numeric value of Perez irradiance coefficients after calibration for Eindhoven sky	58
Table 13 - Performance of the proposed calibration method based on Eindhoven data. The units of the statistical indicator are as following: RMSE(W/m ²), CV-RMSE (%), MAE (W/m ²).....	60

Table 14 - Performance of proposed calibration method based on Colorado (BMS) data. The units of the statistical indicator are as following: RMSE(W/m ²), CV-RMSE (%), MAE (W/m ²)	60
Table 15 - Comparison of energy produced between the Base EP and Modified EP	62
Table 16- Indoor temperature frequency in free-floating conditions	64
Table 17 - Effect of calibrated Perez model on the estimations of heating and cooling loads	65
Table 18- Cooling and heating energy consumption in ASHRAE large office, comparison the effect of calibrating Perez model in Base-EP and Modified-EP	67
Table 19- Comparison of different ambient bounces and simulation results for estimation solar radiation.....	69
Table 20- uncertain parameters in urban canyon and range of variation.....	73
Table 21- Solar radiation (W/m ²) among the 60 random samples in 75th and 90th percentiles..	78
Table 22 -Annual lighting energy used per grid (kWh).....	87
Table 23- Input parameters for calculating MRT solar, Units and used values in the following calculations.....	94
Table 24 – Hours outside of comfort in candidate scenarios, results of PMV solar-based	95
Table 25 - Percentage of hours outside the comfort condition, A comparison of adaptive comfort model and PMV solar based.....	100
Table 26 - Opaque and glazed area on target building façade	120
Table 27 -Window properties: Detailed of simulated building energy model in WUFI	120
Table 28- Exterior wall: Detailed of simulated building energy model in WUFI.....	121

Summary

The term “performance gap” is attributed to the mismatch between actual and estimated building performance. Building simulation tools deal with several inputs which are known as one of the most important sources of the performance gap. Among the uncertain input parameters, assumptions of climatic properties – which are typically implemented through the weather data – are of great importance. Re-scaling the climatic parameters from the mesoscale to the microscale is one of the proposed solutions to reduce the climate-related uncertainty. Among the weather parameters, the incident solar radiation on building facades is associated with uncertainty from two main perspectives, i.e., the accuracy of calculation models as well as the inputs fed into the models. The inadequacy of measurements and lack of interoperability between simulations tools are the main barriers for these kinds of studies. Therefore, there is a necessity for a holistic framework which describes proper quantification, propagation, and post-processing of uncertainty in an urban canyon. This Ph.D. study is an attempt to tackle the raised challenges while rendering the effects of opting for a suitable uncertainty treatment framework.

To simulate the building performance with the proper climatic resolution, measured or modelled climatic parameters at the microscale are necessary. While microscale data are seldom available, to develop a robust estimation the quality and integrity of a dataset is of primary importance. In fact, measured climate data series often are affected by missing values due to either instrument error or data maintenance error. Machine learning methods including neural networks are suggested as a reliable tool for predicting missing values. The presented study, as a first step, introduces a method to estimate long-term (two weeks) missing values using a neural network for parameters of temperature and relative humidity. The method is developed based on measured values from a network of weather stations locating in the north of Italy.

Re-scaling the solar radiation to a specific microclimate context by only relying on the measured climatic parameters from a network of stations within a city, is not adequate. In fact, projecting the measured global horizontal radiation on the vertical plane does not take into account the influence of shadowing or reflectance from the surroundings. The incident solar radiation on building surfaces is subject to multiple reflections within the urban canopy and is affected by shadowing and masking by different obstructions including adjacent buildings and vegetations. All these factors add uncertainties to the estimation of the incident solar radiation. The shadowing effects, reflectance and transmittance of trees on the buildings are among the main parameters which embed the uncertainty to estimations of incident solar radiation on building facades. Also, the accuracy of models to compute the diffuse fraction of solar radiation and to compute the

incident irradiance on a tilted surface is subjected to debate in the literature, which mainly refers to the uncertainties in the sky and solar position information.

The accuracy of a solar radiation calculation model (Perez sky diffuse model as one of the most popular models in building energy simulation tools) is evaluated by calibrating the model based on measurements performed in Eindhoven, Netherlands. The method uses the subset simulation approach which significantly reduces the computational time. Also, the calibrated Perez model is implemented in EnergyPlus. Applying the calibrated Perez model in EnergyPlus revealed how under/over-estimation of incident solar radiation by the default model can affect the reliability of estimations in building energy loads and photovoltaic performance.

In the context of uncertainty quantification, the choice of uncertainty representation can significantly affect the final range of variations. Introducing possibilistic and hybrid approaches for uncertainty propagation aside from the conventional probabilistic approach is discussed in this study. It is shown that based on the nature of the uncertainty and availability of data, choosing the correct approach for representing and propagating uncertainty within the model can affect the knowledge for decision support.

In this study, the complexity of modeling urban canyons as the basic module of cities is challenged and compared with the current simplifications concerning building surroundings. It is observed that details of urban canyon such as variation in height of adjacent buildings and reflectivity or transparency of surroundings can drastically affect the thermal and visual comfort, as well as lighting energy consumption. It is also shown that the effects of complexity in urban canyons are sensitive to the target height and vary on different floors. The annual electricity is highly sensitive to uncertainties in the canyon. Also, the experience of the indoor comfort for different floors may vary noticeably, due to the uncertainty in the urban canyon parameters. It is found that treatment of uncertainty according to the theory of possibility, can noticeably affect the range of variation when compared to that of the theory of probability. Detailed modeling of trees is also deeply discussed and the suitable representation of trees for uncertainty analysis is proposed. The proposed model is a balance between complexity and simplification. Also, the importance of considering the uncertainty in building surroundings during the design phase of windows are investigated. The results reveal how building surroundings can affect the potential of the glare based on the different window to wall ratios.

This PhD study is an attempt to show how re-scaling building's boundary conditions from mesoscale to microscale can provide further insight into the building performance assessment. It is shown that the initial requirements of this kind of studies are locally measured data and a meta-heuristic attitude towards the inputs of building performance estimations. The main outputs of this study can be used as supporting information for designers and decision makers including architects, building engineers, urban designer/planners and policymakers.

Chapter 1 - Introduction

Foreword

Urban areas provide a dominant contribution (i.e., 71%) to the global greenhouse emissions, 30% of which is related to the construction sector [1]. A significant fraction of total building energy consumption is associated with cooling systems. Meanwhile, (1) air temperature and (2) solar radiation are regarded as the most influential climatic parameters that affect cooling demand in buildings [2]. Buildings in urban areas experience different microclimate conditions, depending on the urban features and morphologies [3]. The Meteorology Glossary of American Meteorological Society (AMS) labels a climatic condition as the “microclimate” up to the scale in which the variation of climatic can be explained by physical properties of earth’s surfaces [4]. However, building energy performance is also affected by smaller scales as presented in Figure 1.

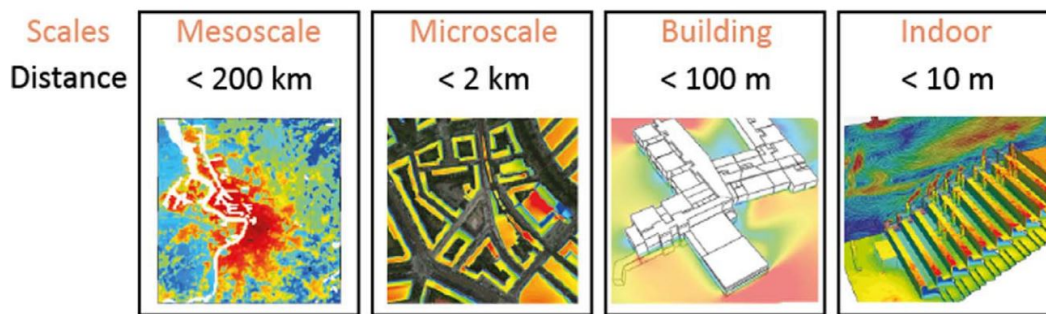


Figure 1- Climate scales which effects on building energy performance [3]

Urban shape and density, as well as the optical and thermal properties of materials, are amongst the most important characteristics which affect the urban microclimatic [5]. These properties can severely affect the climatic characteristics of the urban environment. For instance, air temperature is often increased in highly dense areas of the urban environment, when compared to rural areas, a phenomenon commonly known as the Urban Heat Island (UHI) effect [6]. Also, the incident solar radiation on building facades within the urban areas is highly correlated to the urban form and density, and therefore, could drastically affect the visual and thermal performance of buildings, as in [7].



Figure 2 - Urban canyon originally is defined by building and street between them, however, other existing elements inside a canyon can affect the energy balance.

An urban canyon is the basic module of cities [8], delimited by the walls and street between two adjacent buildings (Figure 2). Aside from walls and the street, the urban canyon is composed of urban furniture (e.g., trees, vehicles). The features of the urban canyons affect the local urban climate and also determine the interaction between the urban canopy layer and the first atmospheric level where exchanges with the urban boundary layer occur, influenced by the macro and mesoscale synoptic conditions [9]. These complex interactions are not easy to isolate with measurements or modeling. Since the surrounding environments highly influence buildings, there is a discrepancy between the estimations of buildings' energy balance and the actual response of the built environment [10]. A possibility to obtain a better perception of microfeatures in urban canyons is quantifying the inherent uncertainty embedded in the urban canyon features. The mentioned uncertainty can be related to canyons geometry (dimension, window to wall ratio, positioning), material properties (reflectivity, transparency) and time-series schedules (seasonal effects, shading operation).

Based on all remarks, for uncertainty quantification of building performance within the urban canyon, it is necessary to identify the most effective features through sensitivity analysis. Regarding the strong interaction between the buildings and their contexts, these kinds of evaluations can help decision-makers and building energy assessors to obtain a better perception about the discrepancy between estimated and actual performance of the buildings.

1-1 Building energy performance gap

The estimation of buildings' energy consumption before and after occupation, in both cases of energy retrofit and new constructions, is necessary. Many tools and methods are developed to estimate and optimize the Building Energy Performance (BEP). However, due to the mismatch between the real energy consumption and the estimations of BEP, the reliability and accuracy of building energy modeling tools, as well as the data used as inputs is still subject to debate [11].

The mentioned difference often referred to as the “Energy Performance Gap (EPG)” [12] is deeply studied in various aspects of BEP, such as building energy retrofit, high-performance buildings, and building energy optimization [13]–[15]. As mentioned, building energy simulation tools are dealing with an extensive number of inputs, and therefore, imprecision and randomness are inevitable. These factors are also known as uncertainties are major contributors to the gap between simulated and measured building energy performance. However, it is commonly believed that obtaining a correct understanding of imprecisions as well as increasing the knowledge over unknown contributors can result in better predictions.

The initial investigations on the building EPG were performed by Hass et al. in the '90s [16]. They highlighted that in building retrofit, the predicted energy saving through engineering practice (white box calculations) could differ between by 15-30% when compared to real measurements, and often fails to meet the expected CO₂ emission reduction

A framework by [17] proposed a deep investigation on the EPG, stressing that to bridge the gap one should deal with the uncertainty of the parameters. The study underlined that the lack of adequate certainty over the data strongly affects the outcomes of simulations. This uncertainty is often ignored in the design stage, despite their important role in the estimations. Building occupant behavior, weather data, and real thermal or hygrothermal performance of building components are among these parameters, which are associated with uncertainty in the design stage and greatly affect the future performance of buildings.

Post-occupancy evaluations show the effect of uncertainty in human-dominated activities, and the consequent effects on the performance of a building after becoming operational. A focus on the patterns of occupant behavior and electricity needs in the UK showed that taking post occupancy into account can reduce the performance gap by 3% in non-residential buildings [18].

The physical characteristics of the building components as built and during their service life differ from the lab-tested properties that are used as input at the design stage [19]. For instance, using actual measurements of air permeability and U-value in a typical small home construction revealed that the EPG could be reduced by 2.4% [13]. It is important to note that the results above were obtained from a simplified recreation of boundary conditions, in which the building is protected from the weather effects on the boundary conditions.

Therefore, improving the estimation of the building energy performance depends on a better representation of uncertainty, which may eventually lead to reducing the performance gap. More measurements from different aspects of building energy performance provide more accurate initialization for uncertainty investigation on performance gap.

1-2 Microclimate as a source of the performance gap

As mentioned before, there is a mismatch between the realistic and expected thermal-energy performance of building systems. Building energy simulations are normally performed based on typical meteorological years to evaluate the outdoor climatic conditions of the area where the building of interest is located [20]. The Typical Meteorological Year (TMY), International Weather Years for Energy Calculations (IWEC) and Weather Year for Energy Calculations (WYEC and WYEC2) are some of the commonly available datasets, used by building energy simulation tools. These datasets are mostly collected in rural or suburban areas, while buildings within the city context are subject to different climatic conditions. The temperature in urban areas frequently exceed by more than three °C the rural records due to the UHI effect [6], which strongly affects the estimation of a building's performance when compared to rural areas. This difference is reported up to 20% for each 1°C increasing on temperature by UHI [6]. Chan et al. [21] reflected the impact of UHI on other weather parameters, i.e. dry bulb temperature and air velocity in four locations in the city center with similarity in surrounding physical environments. By modifying the existing typical weather dataset with actual measurements, a +10% difference was observed for the estimated cooling demand while considering the UHI effect.

Royapoor et al. [22] calibrated the building energy performance to reduce the performance gap by considering the uncertainty in HVAC system parameters, the physical characteristics of the building, as well as actual measurements of weather parameters around the studied building. The study developed based on ASHRAE calibration criteria reported that the calibrated model could improve the estimations of inside air temperature by 90% while considering the deviation error of ± 1.5 °C [22].

The impact of uncertainty in TMY weather data on building energy performance has been investigated through the effects on design choices for cool roofs [23]. Comparing TMY with Actual Meteorological Year (AMY) displayed overestimation of building's cooling energy estimation for both reflective and dark roofs.

Based on these remarks, the correlation between using actual weather data with more accurate estimations of building energy has been proved. Modifying typical datasets with local measurements has a growing trend in recent studies. However, the limitations of AMYs has caused most studies to rely on typical datasets. Limited locations, short-term availability of data, the inadequacy of measured weather parameters and missing values within the datasets are among the major issue in using AMY datasets. Typical weather datasets are created by weather generators based on statistical methods and derived from long-term data collections [24]. These datasets are not updated frequently, and therefore, cannot reflect the recent climate change effects.

Cities influence the climate through construction-related parameters (urban morphology) as well as air quality related parameters. Urban geometry, materials, vegetated area and air pollution are the most acknowledged parameters that are affected by the urban fabric [25]. The microclimate within the urban areas is also known as one of the primary sources of uncertainty in building energy estimations. The importance of considering micro-scale weather conditions within the urban area has been the subject of recent studies [26]–[31]. Although collecting actual weather data in microclimates scales was initiated, maintenance and equipment cost are the leading causes of limited data.

Liu et al. [29] tried to present microscale weather data with respect to actual measurements of weather parameters and urban physical variables. Building-related parameters such as the aspect ratio and area of surrounding walls, pavement, greenery, and sky factor were among the urban texture parameters considered in the study. Three different areas with a radius of 50 m were studied. Results showed that considering the proposed microscale climatic conditions (rather than the traditional weather datasets) can reduce the EPG by 10%.

The importance of considering microclimate conditions for developing new districts is discussed by [32]. The study focused on modeling solar radiation, wind velocity and outside temperature in different design choices. The study highlights the importance of incorporating microclimate characteristics as support for design decision-making. It is important to note that the study was developed by modeling the weather parameters. However, the study stresses the necessity of real measurements for calibration of results as future work.

Sun et al. [33] suggested a framework to deal with the uncertainty at the microscale while considering major weather parameters. They presented statistical models to quantify the uncertainty in local wind speed, temperature, wind pressure, and solar radiation. The study recommends embedding the statistic models of microclimate parameters in building energy simulation tools, rather than opting for traditional weather data, Microclimate in an urban area [33].

Solar irradiation is among the microclimate parameters that is investigated through different approaches. Some studies focused on solar availability in the urban area and the variation of urban morphologies. These studies vary from urban scale to district scale and urban canyons, mostly focusing on building energy performance [34]–[37]. The solar availability on building facades is the major subject of these studies, with the main concern over active solar technologies such as PV panels and solar [38], [39]. On the other hand, research from an urban perspective tried to assess the solar-based comfort aspects in urban canyons [40], [41].

The highlighted studies stress on the strong role of solar radiation on the interaction between building and surrounding elements. Regarding the inadequacy of data, uncertainty in solar radiation is inevitable; however, this uncertainty and effective features are not deeply investigated.

1-3 Solar irradiance research area and challenges

Regarding the important effect of solar radiation on the thermal-energy performance of non-isolated buildings, this section presents an introduction of solar radiation, components, related features and challenges of estimations of solar radiation inside of urban canyon. The global solar irradiance has three components: direct, diffuse and ground reflected solar irradiance (Figure 2). These components can be measured or calculated on horizontal and tilted surfaces. The measurements of global solar irradiance are mainly performed on horizontal surfaces, while measured data on tilted surfaces are very scarce and available only at experimental sites (e.g., ref). Measuring the direct and diffuse components of solar irradiance is mostly performed on the horizontal surface and in limited locations [42], while seldom measurements of ground reflected radiation data are also available [43].

Moreover, the building envelope is composed of different elements having various tilts and orientations. Therefore both horizontal and tilted solar irradiance affects the building's energy performance. TMY datasets include the global horizontal, direct and diffuse solar irradiance, while the ground reflected component is mostly calculated inside the building energy simulation tools based on the ground albedo.

Building simulation tools compute the incident solar irradiance on building surfaces with various tilts and orientations. Mostly these models use a set of observed global solar irradiance data to extract the diffuse solar irradiance [44]. Solar models are developed based on data collected at different locations and different climatic conditions. However, it is argued by many studies that solar models cannot be considered as generally valid models and the uncertainty in calculations based on these models is inevitable [45] [46].

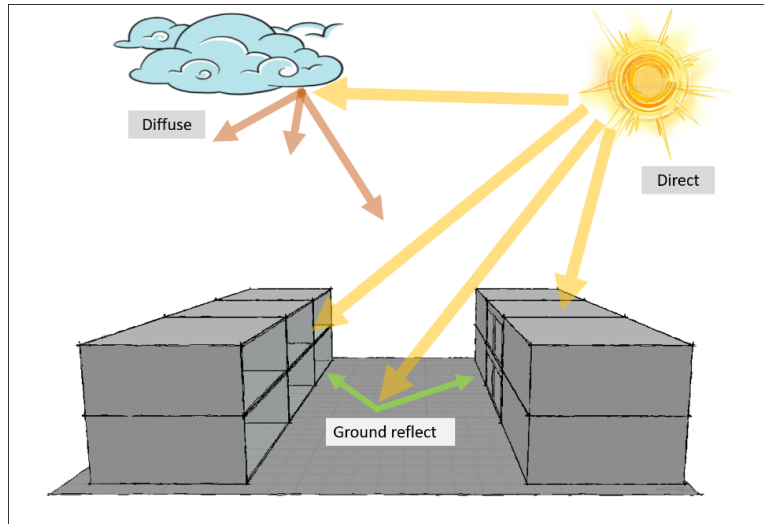


Figure 3 - Components of the solar radiation propagating within an urban canyon

Figure 3 shows a simplified schematic of an urban canyon and solar availability as adopted in many studies, however, in reality (Figure 1), this representation is much more complex. As mentioned earlier, the urban morphology incorporates a considerable amount of uncertainty into the microclimate and therefore, the input parameters for calculations. Urban obstructed solar irradiance, inconsistent reflection from the surroundings, urban vegetation and future modifications on the surroundings are among the main factors that can impact the total solar irradiance in urban canyons. Considering the fourth component of solar irradiance inside the canyons, i.e. the reflected solar irradiance from the adjacent buildings is a topic suggested in the literature [47].

The canyon geometry is composed of the street width, building aspect ratio, orientation, the shape of the roofs and building façades. These quantities determine the amount of direct and reflected solar irradiance inside a canyon. Most of the previous studies investigate the effects of these parameters on the total amount of direct solar irradiance received inside the canyon [48]–[52]. Studies have shown how the canyon geometry affects the amount of direct solar irradiation during a day whether in summer and winter conditions. These attempts clarify that assessing the performance of passive strategies, which work based on the position of the sun, should be considered in the case studies while their interaction with the surrounding environment ought to be accurately quantified.

The reflected solar irradiance is directly related to the albedo from the environment. Studies showed that the overall albedo of a canyon might differ from the albedo of the street. Qin [53] presented a numerical method to evaluate the streets albedo based on the variation of reflectivity in a canyon's components. The results of calculations stress the impact of the canyon's proportions, namely the canyon's aspect ratio. As suggested in the study, the effect of reflectivity of different components may vary in summer and winter. Aside from the seasonal effects, the

reflectivity of the roof or urban facades can change over time [54]. This phenomenon also known as weathering and soiling effects can influence the performance of the components that are exposed to the canyon's environment. Paolini et al. [19] measured these effects on roofing membranes for different durations of exposure. Their study revealed that the reduction of reflectance of roofing membranes could reduce the energy saving of this technology up to 34%.

The type and density of vegetation during the seasonal change are also investigated from a shading point of view [55], as well as their impact on thermal comfort inside the canyons [56], [57]. However, these investigations lack the assessment of the albedo of the canyon considering the vegetation impressions. It is evident that such considerations will alter the design choices since the sensitivity analysis will reveal different correlations between the design choices and the canyon properties.

1-4 Research questions

Reaching the targets of the Paris agreement, which ask for an urgent attempt to decrease the climate change effects, is achievable with a coherent movement of all related groups. Built environment as one of the major contributors has a vital role in meeting this goal. As previously discussed, the role of buildings on the overall CO₂ emission is synonymous with their strong potential to mitigate climate change. The central attempts to reducing this portion are related to estimations of building energy performances before retrofit or construction. Although there is significant progress in building energy simulation tools, the mismatch between estimations and real energy consumption remains an issue. The solar irradiance in the microclimate around the buildings has been introduced as one of the primary sources of this mismatch and is the topic of recent studies.

This research study tries to find an answer to this question, i.e. how increasing the precision of modeling, as well as the input parameters in the urban canyons can reduce the gap between measurements and estimations of building energy consumption. The solution to this major challenge comes with some minor questions.

- What are the input parameters in building energy estimations, which affect the variation of solar irradiance in microclimates?
- When modeling solar radiation in an urban canyon, which inputs parameters are associated with uncertainty?
- How can the uncertainty in solar radiation affect building energy estimations?
- How to propagate uncertainty while minimizing the loss of valuable information?
- How can more accurate modeling of the urban canyon support decision-making in building envelop design?

1-5 Aims and objectives

This Ph.D. research tries to present a new approach for the suitable treatment of uncertainty while quantifying solar irradiance on the building envelope. Therefore, it tries to determine the effectiveness of more realistic models of building surroundings, through an in-depth investigation of the uncertainties and the model's sensitivity to each parameter. The final objective of this Ph.D. is to quantify the uncertainty in the incident solar radiation that is received on the building envelope within the urban canyon, and the consequent impacts of this variation, on the performance of visual and thermal comforts as well as energy performance. For reaching the main objective, some secondary objectives will be addressed. The original contributions of this Ph.D. study include:

1. Determining the most important parameters that affect the variation of incident solar radiation on the building surfaces.
2. Exploring the possible ranges and variation of each parameter and the possible correlation between them.
3. Defining the correct approach for representing an uncertain parameter, i.e. probabilistic (random) or possibilistic (fuzzy).
4. Exploring different strategies for optimizing simulation time based on the diversity of parameters and the range of their variation.
5. Developing a methodology to support the assessment of envelope design amidst uncertainty.

The current study is specifically tailored to enhance design and decision supports for a range of audience. Therefore, the developed framework will provide decision-supporting information for architects, building engineers, urban planners/designers, as well as policymakers.

- Architects define the façade of the building and often choose the properties of opaque and transparent surfaces. The framework introduced in this study, not only helps architects to assign proper characteristics to the transparent surfaces (glazing) of their building placed within a canyon but also, to evaluate the effect of the buildings glazed and opaque reflections (specularity) of other buildings within the canyon.
- Building engineers who work alongside architects can evaluate the performance of their shading devices and consequently the availability of daylight, occupant comfort, and energy performance with more realistic realizations of the surrounding environment.
- Urban designers and planners who define the aspect ratio of the urban canyons, as well as the urban furniture (vegetation, parking spaces, etc.), ought to have a deep understanding of the interaction between the buildings as well as urban furniture within an urban canyon. Therefore, resorting to the framework in this study will not only provide them with

adequate knowledge to assess the suitability of characteristics of urban canyons but also deliver well-informed foundation for new design and planning.

- Policymakers working in the municipal, district, and national levels can opt for the introduce framework to set regulations and policies regarding the overall characteristic of a canyon, be it minimum and maximum range of specularity and reflectance, suitable margins for tree spacing and species, as well as regulations on the canyon skyline.

1-6 Summary

Based on these remarks, quantifying solar irradiance is a significant challenge of recent studies in different aspects. One challenge is related to calculations (models) of solar irradiance on titled surfaces. This issue calls for developing calibration models where the measured data in titled surfaces are available. The other issue is related to the model inputs and the inherent uncertainty associated with these parameters. The former issue can be addressed through calibration of model hyperparameters while the latter calls for uncertainty quantification of the variability associated with the input parameters.

This research study structured in 4 main chapters. In Chapter 2, a review on previous studies in the area of uncertainty in building energy estimations, the energy balance of urban canyon, solar radiation as parameters in urban canyon and model of calculation of solar radiation presented. These investigations resulted in extracting the effective features in urban canyon related to uncertainty in solar radiation, state of the art related to the method of uncertainty analysis, and current challenges about solar radiation model of calculations.

Chapter 3 introduce the methods and frameworks which are developed based on the needs of this study. This chapter starts with a challenge related to the quality of collecting and control tests on data. An application of neural networks for infilling the missing values in measured weather data is presented in this chapter. A deep discussion about uncertainty analysis, methods, propagation approaches presented in Chapter3. Finally, the methods for building energy model fine-tuning argued. Model fine-tuning evaluated from two aspects: (1) Calibration an existing solar model (Perez sky diffuse model) for calculating the incident solar radiation on the tilted surface, (2) Uncertainty quantification of solar-related parameters within the urban canyon.

The presented methods are implemented in real case studies in Chapter 4 to highlight the effect of building energy performance. The section about data acquisition relies on actual measured data from a network of a weather station in Milano, Italy. Method to calibrating the Perez model is developed based on measurements of solar radiation on a tilted surface in Eindhoven, Netherlands

and tested with another measured data from Colorado, USA. The uncertainty quantification of the urban canyon also performed for an actual canyon located in Milan, Italy. Regarding that, the geometry data collected from in site survey. Also, the range of variation related to other quantities collected from the literature.

Finally, in Chapter 5 an overview of all results, suggestions and possible future developments of this study is stressed.

Moreover, more details and some supplementary materials including developed scripts explained in Annexes.

Chapter 2 – Research background

This chapter presents an overview of previous studies in the area of uncertainty in building energy performance, urban canyon features, and microclimates within the canyons.

2-1 Uncertainty in building energy simulation

The propagation of the uncertainty in the building's lifecycle grows exponentially. The quantity of probabilistic uncertainty is subtle in the initial phases of the building design procedure. At this stage, the unknown information consists of possibilistic uncertainties which will be transformed into probabilistic quantities throughout the life cycle of the building (Figure 4) [58].

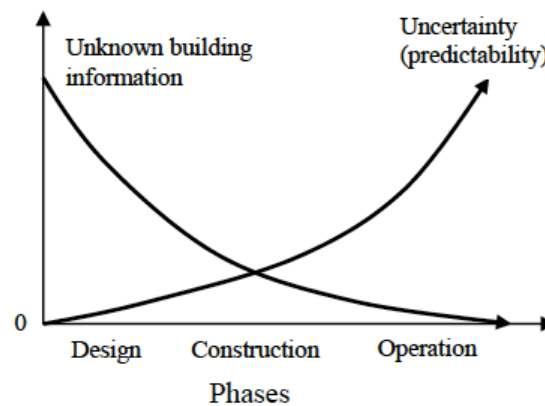


Figure 4 - Uncertainty and building life cycle [58]

Before the investigation on UA and SA, identifying the source of uncertainty in input data in the context of building energy performance is necessary. The source of uncertainty can be addressed through different sources. In studies based on the approach of research, several categories are defined. Kim and Augenbore [59] are considered on the type of data as the source of uncertainty. Therefore, they focused on two phases of uncertainty: Scenario and statistical. First one is related to the uncertainty external and future environment of the building. The second one is based on statistical data. Hopfe and Hensen [60] declared three sources: uncertainty in physical, design and scenario parameters. They consider on physical properties of wall, roof and floor area as the physical uncertainty. The uncertainty in design parameters is referred to different design strategies, which are adopted in the planning process. Finally, the scenario uncertainty comes from the future life of the building. The occupancy and future weather condition are the main causes of this kind of uncertainty. The most complete description is offered by Macdonald [61]. He believed that the source of uncertainty in building energy should be investigated in five questions about the model, input data, stochastic process, software simulation, and design variation.

Identifying the aim of sensitivity analysis is the initial task. Uncertainty and sensitivity analysis are covering two major aims in building performance topics. A group of research is evaluating the embedded uncertainty in early design parameters [62], while the others take the UA and SA as support to validate measurements [63], [64].

After defining the aim of UA and SA, the first step will start with selecting model parameters and determining the range of variation with a mathematical interpretation. Based on previous studies, building performance parameters can be divided into three main categories, i.e. physical, Operation and weather. Different subgroups are defined from the mains, which consist of a wide number of parameters. Table 1 is the essence extracted from the literature. The variable column contains a limited number of variables, which are popular in studies. The mathematical interpretation of uncertainty can be demonstrated through distributions or scenarios. Using a distribution function is recommended for variables with continues uncertainty, while for discrete variables application of scenario uncertainty is suggested.

Table 1 – Description of the most common variables in UA and SA

Parameters	Type	Variable
Physical	Geometrical	Area, Size, Number of zones, Wall and Roof thickness, Shape, Orientation, Window to wall ratio
	Thermo-physical	Material thickness, U-Values
	Hygro-thermal	Heat capacity, Moisture
Operation	Qualitative assessment	High, Mean, Low
	Quantitative parameters	Indoor temperature, Infiltration rate, Internal heat gain, HVAC utilization
Weather	Year type	Hot year, Medium year, Cold year
	Weather parameter	Dry bulb temperature, Wind, Solar radiation, Relative humidity

An overview of recent literature concerning UA and SA in building energy performance is gathered in Table 2.

Table 2 – Keywords of SA and UA and related literature in building energy performance topics. UA category consists of three most popular sampling methods in building topic: LHS (Latin Hypercube Sampling), SS (Simple Sampling), QMC (Quasi Monte Carlo). SA category consists of three most popular sensitivity methods in building energy topics: MM (Meta-Model), SRC (standard Regression Coefficient) and Morris.

Ref.	Building type			Input variable			Target					UA			SA					
	Office	Recreational	Residential	Environment	Operation	Physic	Carbon emission	Energy consumption	Energy demand	Energy need	HVAC Performance	Moisture content	Peak load	LHS	SS	QMC	MM	Morris	Sobol	SRC
[65]	X				X	X							X							X
[66]			X		X			X							X			X		
[62]			X		X	X		X							X					X
[67]			X		X			X					X	X	X				X	
[68]			X	X	X	X		X					X							X
[69]	X					X			X				X							X
[70]			X	X	X	X				X			X					X		
[71]					X			X	X						X					
[72]	X				X	X		X	X				X					X		
[73]	X				X	X		X					X					X		
[74]			X	X	X	X		X					X					X		
[75]				X		X					X			X						
[60]	X				X	X		X		X				X						X
[76]	X				X	X		X						X						X
[77]			X		X	X				X	X					X				X
[59]				X	X	X			X											
[78]	X							X					X					X		
[79]	X				X	X		X				X		X						X
[80]	X			X		X			X					X				X		
[81]		X		X	X	X		X						X						
[58]	X				X						X		X					X		
[82]			X		X	X		X	X				X							X
[83]	X				X	X		X						X					X	
[84]	X				X	X		X					X				X			X
[85]	X			X	X	X		X					X							X
[86]	X				X	X		X					X							
[87]	X			X	X	X	X			X			X				X			X
[88]	X				X	X				X			X					X		

2-2 Urban canyon features

An urban canyon is the basic module of the urban energy balance which typically defines by the ratio between the height of the adjacent building and width of the street as the main identification [8], [89]. The ratio between the height of buildings and street width address as “aspect ratio” and in parallel with the orientation was targeted in many studies in urban canyon energy balance analysis [48], [90]–[92]. Aspect ratio and orientation of the buildings are the first parameters in urban canyons can affect the building energy performance inside a canyon.

The effect of aspect ratio and orientation of urban canyon on climatic parameters is investigated by Toudert et al. [48]. Results in different combinations of aspect ratio and urban canyon orientations showed the thermal comfort has a strong relationship with the aspect ratio. Emmanuel et al. reported the higher rate of comfort with a wider aspect ratio regarding the variation of shading patterns [93]. The effect of aspect ratio on thermal comfort is also investigated in the difference in the nighttime and daytime effects. Recorded higher temperature during the night hours in the canyon with the higher aspect ratio is reported [94].

The canyon orientation is important for exposing the canyon to direct solar radiation and wind speed inside the canyon [95]. The effect of orientation on canyon thermal analysis vary based on the latitude and weather characteristics of each location [48]. The orientation of the canyon has different behavior in summer and winter time. A canyon which extended along the E-W comparing to an N-S canyon receives more amount of solar radiation in the summer period while the situation in the winter period is notably different [90].

The impact if urban canyon geometry on the flow rates and reducing the heat gains by building surfaces is also investigated in many studies in the area of urban microclimate. This effect varies in the canyon with the uniform building heights to more dense geometries in city centers. The air exchange in the urban canyon also depends on asymmetry and aspect ratio of the canyon which [3], [96], [97].

The sky view factor (SVF) is also another important parameter related to urban canyons energy assessments. The SVF define based on the ratio between visible sky to total sky hemisphere from a certain point in the canyon. This parameter can tackle solar availability and heat escape from the canyon [98]. The adjacent building heights and shading devices, trees and other vertical elements inside the urban canyon are the parameters that determine the amount of SVF.

The vegetated area is discussed from two points of view: the shadowing effect and transpiration [95], while shadowing effect of trees is discussed in the next section. The vegetation in urban canyon include the vertical and horizontal, i.e., trees, green facades, and green roofs as well. Incident solar radiation on urban facades trapped in the urban canyons and change to heat radiation.

The transpiration effects of trees change the radiant heat effect of solar radiation to latent heat flux. Konarska et al. measured this conversion of solar radiation to latent heat flux not only reaching to 30% during the daytime, in the nighttime the process continuing and can convert up to 20% of heat radiation to latent heat fluxes [56].

2-3 solar radiation in urban canyon and effects on buildings

Solar radiation has a significant influence on a building's energy balance, as it affects both the potential for on-site energy generation (e.g., photovoltaic (PV) or solar thermal) [51] as well as solar heat gains [99] and daylighting [100], and optimal shading strategies [101]. Therefore, accurate estimations of the incident solar irradiance on horizontal and tilted surfaces within the built environment deem necessary.

Solar availability in urban surfaces has a strong relation with urban geometry and urban texture. The urban texture is a term that refers to reflectance and absorptance properties of building surroundings. As discussed, in the polluted conditions the reflectivity of canyon elements is reduced which cause to increasing the absorptance and resulted in higher temperature within the urban canyons [102]. Also, the aging process can change the optical properties of building surfaces and change the urban texture. Paolini et al. measured the reduction of solar spectral reflectance of material by exposing to exterior weather conditions in different durations [19]. A comprehensive research study on the uncertainty in albedo and emissivity of urban material performed by [103], both longwave thermal emittance and short-wave spectral reflectance of the material are measured and the results presented as an online library in [104].

In general, the albedo of the canyon is the key element of determining the actual solar radiation on building surfaces. The studies in the area of UHI mitigation proposed increasing the urban albedo by applying brighter colors on the urban surface and ground pavement [105]. However, it is shown that besides the heat reduction benefits, the higher ground albedo can sense by BIPVs and total PV yield increase by the 13% [106].

Tregenza [107] assessed the uncertainty in daylight illuminance in different urban canyons conditions when the SVF affected by the adjacent building. It is mentioned that “the cumulative effect of even minor changes can cause significant uncertainty in the prediction of interior illuminance”.

2-4 Solar models

While solar irradiation on horizontal surfaces is measured in numerous locations around the world, the incident solar irradiation on tilted surfaces is mostly calculated through white-box models. Specifically, the diffuse component of global solar radiation on tilted surfaces is calculated by

models that transpose the diffuse horizontal solar radiation to diffuse solar irradiation on tilted surfaces, generally referred to as diffuse solar irradiation models [108]–[114].

Most solar irradiation models are developed with input data from a few measurement sites, which are then extrapolated to cover the entire globe [115]. The increasing availability of incident solar irradiation measurements on tilted surfaces, especially at PV farms, creates the opportunity to assess the accuracy and performance of solar models in different locations [116]–[121]. Comparing solar models in different studies reveals that for obtaining more accurate estimations of solar irradiation on inclined surfaces, each location may perform better with a specific (or even a hybrid) solar model [117]. Therefore, finding the best model for a site is not easy since the mismatch between measurements and calculations can come from either the model or the measurements [122].

Uncertainty in estimated values of solar radiation on tilted surfaces is discussed by Gueymard [123] and can be attributed to observation time-step, sky conditions, ground reflectance, and model of separating direct and diffuse components from horizontal radiation. The highlighted factors mainly affect the diffuse and ground reflected components of global solar radiation on tilted surfaces. The potential improvement in estimations of solar radiation on tilted surfaces is discussed in [124]. The direct component of global radiation on tilted surfaces can be calculated based on pure geometrical equations, and therefore, the observed uncertainty in this component is often relatively low [125].

Yang [126] ranks the performance of 26 models for calculating solar radiation on tilted surfaces by two ranking approaches, i.e. linear ranking and pairwise hypothesis testing. The study suggests that the uncertainty assessment of solar model parameters (such as foreground albedo) can have a significant effect on solar radiation estimations.

Among solar models, the Perez model is frequently used in building energy and daylight simulation [127]–[129]. The model calculates diffuse irradiation on tilted surfaces based on horizontal values and estimations of the brightness and clearness of the sky [130]. The Perez model is developed based on solar radiation measurements from different climatic conditions, i.e. Temperate Maritime, Humid Continental, Mediterranean, Arid, Continental, Subtropical (See Table 2 in [130]). However, the model developer acknowledges the need for further validation of the model with future data collected from more locations or surface tilt angles.

The performance of the Perez model has been investigated for different orientations, tilt angles, and measurement time-steps. For instance, [120], [118] developed their study based on 10-minute intervals of measured data, while [131], [132], [133] focused on hourly measurements. It is shown that the accuracy of the Perez model can be affected by the surface orientation [134],[118].

The over- or underestimation of diffuse radiation through the Perez model has been recorded in different locations. While most of the studies reported an overestimation, in Egypt (Cairo) [135] the model was reported to underestimate the solar radiation on tilted surfaces.

Demain et al compared 14 common solar models, including the Perez model to find the best fit for Belgium [117]. Results show that for the mentioned location, the best performance during cloudy sky conditions is obtained by using the Perez sky diffuse model. The Perez model has also been validated for the southern hemisphere with measurements of solar radiation on two angles of 20° and 40° facing north [136]. The variation of incident solar radiation on the exterior building façade and under different sky conditions is evaluated in [119]. Loutzenhiser [137] performed an uncertainty analysis between the choice of solar model in building energy simulation tools. A 7% variation is reported for using the Perez model when compared to actual measurements.

Perez model has categorized sky conditions into eight different classes, and for each class, a set of sky brightness and clearness coefficients are specified, commonly known as Perez model coefficients

for irradiance. These coefficients are extracted empirically from a limited group of locations. Robledo [138] highlighted the sensitivity of the Perez model to location as a result of the sky coefficients. Based on the remarks concerning the variation of Perez's performance in different locations, assessing the uncertainties in the Perez model merits to be considered. Different approaches have been proposed to calibrate the Perez model to a specific location. Sun et al. proposed an uncertainty quantification of Perez parameters through a regression fit over a selection of parameters [139], resulting in an improved version of the Perez model for the intended location. As an alternative approach, Yang et al. used a "Least Square Method" to optimize the Perez irradiance coefficients for tropical sky conditions, stressing that the intended location was not among the original experimental data that was used to develop the Perez model [140].

In this study, we propose a new method to tune the Perez model for a specific location. This process involves Subset Simulation, which is based on the Markov Chain process. The effect of using a calibrated Perez mode evaluated on the incident solar irradiance on inclined and vertical surfaces, and the electricity production by PV panels with different slopes, as well as the cooling and heating loads of a case study building. The method proposed in this study can successfully adapt Perez coefficients to local measurements and is easy to implement in building energy simulation models.

Chapter 3 – Methodology

The main aim of this research study is quantifying the uncertainties related to solar radiation within the urban canyons. After recognizing the major features related to this uncertainty, the next steps are exploring between different methods which can model the uncertainty of solar radiations with the features as much as possible. The method should be logical from a computational and comprehensively point of view if there is not a case-specific approach.

3-1- Data acquisition

3-1-1 Collecting data

To robustly investigate the interaction between building and surrounding climate conditions, the analysis with considering several years is suggested which increases the chance of covering different climate events. This approach is even more important when the performance of the buildings is studied for several consecutive years.

The multiple weather data can be provided from the in-site measurements which are managed by universities, weather forecast institutes or other research institutes. In some cases, the organization offers the data through the websites for any applications while others just share data to research communities.

The aim of collecting data by the institutes are also another important point to consider before using the data in a specific research study. The weather forecast institutes record weather data for both air quality and weather forecasting targets, therefore depend on the target, weather stations are installed on the ground level or roof-top level, respectively.

Also, some institutions have organized automated weather station networks among the urban and rural areas which provide a good opportunity for UHI studies. For instance, in Italy, the ARPA Institute (Agenzia Regionale per la Protezione dell'Ambiente) organized a network of weather stations which covers the whole Lombardia region (north of Italy) and presents a variety of measured weather parameters in both urban and rural contexts and for multiple years. The ARPA data is available through www.arpalombardia.it.

Collecting such a long-term dataset needs some consideration such as the overlap between starting time-step of the following year with the last time-step of the previous year or the existing leap years among the selected period.

As a part of this thesis, a network of weather stations in Milano province are evaluated. The aim was preparing a long-term (8 years) weather data to apply in building energy simulations. The intended datasets are collected from ARPA website for five main weather parameters, i.e., temperature, relative humidity, wind speed, wind direction, and precipitation.

This dataset is the material of the next two sections (3-1-2 and 3-1-3).

3-1-2- Quality control tests

New approaches in the field of building energy simulation encourage the application of actual weather measurements [141]. Using the raw weather measurements directly from weather stations resulted in new challenges since these data commonly suffer from missing values. Moreover, due to maintenance or instrument errors, the data needs constant quality control tests to ensure more accurate weather datasets [142].

Frequent sensor checking of weather stations, sensor calibration, and statistical tests are some of the quality controls that proposed to improve and ensure the quality of weather data to apply in later analysis. In more cases, the statistical tests are easier to apply to collected data since the first two need to access the actual measurement instruments.

Statistical tests which also called as validation procedure validate the collected datasets through indexing erroneous data. Table 3 provides a comprehensive guideline of statistical tests. The proper method/s could be selected among the proposed tests which depend on the availability of data and the target of the study.

To prepare long-term weather, two validation procedures applied to collected data of Temperature and Relative humidity, i.e., Range test and Relation test. The Range test ensure that the distribution of measured data for each weather parameters varies on the define thresholds which are defined based on historical observation of data in each location. The Relation test makes sure if the variation of the observed data in two following time-steps do not exceed the defined threshold.

In the studied dataset, thresholds are extracted from two sources. The Range test thresholds are stated according to identified values by Estevez et al. (see [142], Table 3). The thresholds of the relation test are defined based on statistical analysis on historical weather data e.g. standard deviation, average or 99.9th percentile [143], [144]. Accordingly, the required threshold for Relation test is modified based on Milan climate conditions through other measurements, where more reliable data is available (Table 3). The supplementary datasets belong to a weather station (Vaisala WXT 520) located in Politecnico di Milano. To state the thresholds of Relation test, a cumulative distribution is applied to the difference of two subsequent timesteps for each weather parameter. The thresholds are defined based on the 99.9th percentile of the timestep.

Table 3 - Range test and relation test thresholds

Test	Quantity	Threshold
Range test	Relative Humidity (RH)	$10\% \leq RH \leq 100\%$
	Temperature (T)	$-20^{\circ}\text{C} \leq T \leq 50^{\circ}\text{C}$
Relation test	Relative Humidity (RH)	$ RH_h - RH_{h-1} \leq 18.18\%$
	Temperature (T)	$ T_h - T_{h-1} \leq 3.85^{\circ}\text{C}$
	Wind Speed (WS)	$ WS_h - TWS_{h-1} \leq 2.3 \text{ ms}^{-1}$

3-1-3 Infilling missing data

The actual measured data in many cases suffer from missing values along the datasets. These missed areas (which mainly result of maintenance issues) observe in short-term or long-term series. Missing values in weather datasets are normally indicated with a value of “-999”. To infill the missing values along datasets a network of measured data from different instruments and duration of observations have the key roles to the accuracy of estimations.

Different methods are proposed for infilling missing weather data. Empirical methods, statistical and function fitting methods have been discussed for a variety of aspects regarding filling missing values [145]. The choice between the existing infilling method strongly is related to percent and length of sequential missing data.

3-1-3-1 short term missing data

According to [146] prediction of short-term weather values refer to missing data up to 12 consecutive hours, while the absence of weather values over 5 days are considered as long-term missing data. The simpler methods can be applied on short term missing values since it helps to reduce the computational time and in case of accessing to a proper network of data the accuracy of the method will be enough. The simple arithmetic averaging can categorize in Empirical methods. In this method, the missing values assume as arithmetic average and calculate based on making the average between corresponding values in other nodes of the network (Eq.1).

$$Val_{missed} = \frac{\sum_{i=1}^n Val_{nodei}}{n} \quad (\text{Eq.1})$$

Where:

Val_{missed} refers to a missing observation, Val_{nodei} refers to existing correspond value in other from other weather stations in the network

n refers to the total number of weather stations along the network

3-1-3-2 long term missing data

Neural Networks (NN) – which can be categorized in the function fitting groups – have been more popular in recent studies concerning climatic parameters prediction. Most of the studies in this area use a network of weather stations to predict missing values. Solar radiation is one of the climatic parameters subject to infilling by neural nets [147]. The necessity for accurate predictions regarding the incident solar radiation on photovoltaic panels resulted in the application of NN in predicting global solar radiation [148]. Studies tried to find the best set of input features from a group of weather stations to reach the minimum prediction error. Estimations of wind speed – as one of the sources of renewable energy – has also been a focus of climatic studies resorting to NN. The fluctuation and nonlinear behavior of these parameters call for a robust framework, among which NN is a strong candidate. The network weather stations method is also suggested for estimating the mean monthly wind speed [149].

The estimation of missing values among the datasets through machine learning methods demands for a series of correct samples. Each sample consists of some input features and a target (Figure 5). The performance of machine learning methods depends on selecting correct input features, the suitable training function, as well as the adequate number of samples for training and testing the network [150].

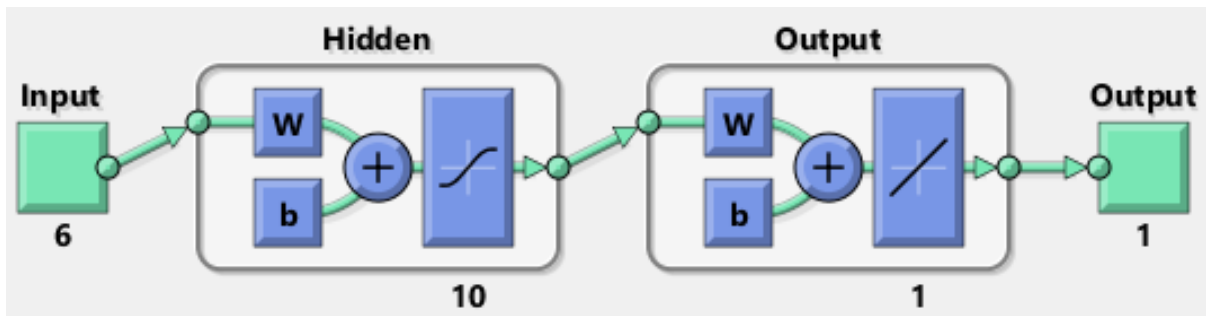


Figure 5 - Diagram of a vanilla neural network

A multilayer perceptron (MLP), which in this case is a Back-Propagated Neural Network (BPNN) trained by using the Levenberg-Marquardt algorithm. The inputs are hourly data of 9 consecutive years and are divided into three subsets of training, cross-validating and testing datasets.

To prevent confusion during the training process, the missing values (-999) eliminated from the target vector. To keep the input and target matrices consistent, the rows which had (-999) in the target also removed from the input dataset.

3-2 The theory of uncertainty

Uncertainty can be categorized into two classes, i.e., aleatory and epistemic. Aleatory uncertainty deals with randomness due to inherent variability in the system behavior (e.g., outdoor temperature fluctuation), while epistemic uncertainty is derived from lack of information on the system (e.g., the state of an HVAC system) [151]. For example, lack of accessible information on the value of a quantity, which enters as a parameter of the system or process model, can result in epistemic uncertainty (e.g., due to the difficulty of collecting accurate measurements or the lack of time for data collection).

The probabilistic theory is the most favorable approach that was developed based on betting logics [152]. In this theory, imprecise quantities are selected to form a distribution due to their inherent random behavior (aleatory). The possibilistic theory is based on the fuzzy logic theory introduced by Zadeh in 1978 [153]. The fuzzy possibility theory deals with lack of knowledge and scarce information (epistemic) on the system [Dubois]. The Uncertainty Theory was introduced by Liu in 2006 [154]. The theory deals with variables which are neither random nor fuzzy as they are simultaneously affected by both probabilistic and possibilistic behaviors.

3-2-1 Uncertainty analysis

Uncertainty Analysis (UA) deals with quantitative modeling, which cannot be associated with certainty [155]. The approach has various applications in risk assessment [156], reliability assessment [157] and decision-making (decision support) [78]. The most important aspect of UA concerns reliable mapping of uncertain inputs on to the output. Correct implementation of UA will also provide insights into the post-processing tasks (sensitivity analysis), which will be discussed afterward.

3-2-2 Sampling and propagation methods

It is important to recognize the nature of the faced problem, to tackle UA oriented problems with the right tool. Therefore, a short description of the three major uncertainty types and the related sampling and propagation approach is provided in the following sections.

3-2-2-1 Sampling with a probabilistic approach

The probabilistic approach assumes some inherent randomness in the uncertain parameters. Therefore, the sampling procedure is conducted by using random generation approaches i.e. Monte Carlo Sampling, Latin Hypercube Sampling, and Low-discrepancy sequence (quasi-random sampling, sub-random sampling) (Table 4).

Table 4- Sampling methods and tools

Method	Tool(s)
Monte Carlo	<i>Simple Random Sampling (SRS)</i>
	<i>Latin Hypercube Sampling (LHS)</i>
	<i>Quasi-Monte Carlo sampling</i>

Among the introduced sampling methods, the Monte Carlo method (MC) is the most common approach for sampling building uncertainties. Macdonald and Strachan [158] and Bucking and colleagues [62] performed Simple Random Sampling Monte Carlo (SRS) to quantify the design parameters. As another subcategory of the Monte Carlo method, Latin Hypercube Sampling (LHS) was adopted to many studies [58], [65], [69], [159]. Meanwhile, the third subcategory of MC, Quasi-Monte Carlo sampling was observed in a study by Eisenhower et al. [71]. The logic behind using numerical sampling techniques is derived from the fact that the process of building performance simulation is a complex process, which cannot be simply performed through an analytical approach.

It should be noted that Monte Carlo method (Monte Carlo sampling) is different from Monte Carlo simulation as defined in [160], where the Monte Carlo method is a technique for solving a problem, while Monte Carlo simulation uses random samples to define phenomena.

3-2-2-2 Sampling with the possibilistic approach

To better describe the applicability of possibility theory, a comparative description between the two main approaches of treating uncertainty is inevitable, i.e., the Bayesian framework and the Dempster-Shafer framework. The Bayesian theory uses data to improve the initial belief, arguing that probabilities are apt for treating all classes of uncertainty (aleatory/epistemic), regardless of the level of information that is available on the uncertain parameter. In this theory, uncertainty is represented by probabilities, where for each variable X a probability (based on available information \mathcal{E}) is assigned to each real value x in the domain θ so that [161]:

$$\sum_{x \in \theta} P(x|\mathcal{E}) = 1 \quad (\text{Eq.2}).$$

Unlike the Bayesian framework, the Dempster-Shafer (D-S) framework assigns beliefs to sets of elements (instead of single elements), where a set of all believed propositions is called a belief set [162]. The D-S framework differentiates between “true” and “certainly true” propositions, and how they represent incomplete knowledge. Although propositional calculus is defined by a binary logic of $\{0,1\}$, uncertainty can adopt a ternary form, where a proposition can be true to a certain degree. In other words, a proposition can be either 1) “certainly true”, 2) “true” to some extent, or 3) “false” based on the belief-base of the expert’s knowledge.

Although Bayesian proponents argue that the probability theory is sufficient for handling both aleatory and epistemic uncertainty [162], [163], studies have strongly challenged the probabilistic framework, highlighting its limitations in representing incomplete knowledge [164], [165]. It is argued that the application of a uniform probability distribution on the range of plausible values of an uncertain parameter (in cases of scarce information), can distort the actual knowledge and impact the calculations obtained from the model [166], [167]. For instance, adopting a uniform probability distribution for occupant density cannot correctly characterize the situation, as we are not in complete ignorance of the number of occupants, but rather, we have most plausible values within a range. Moreover, forcing a probability density function based on scarce information can produce biased results [168], [169]. For example, assigning a triangular (or Gaussian) distribution to occupant density – based on linguistic propositions of the number of occupants – will misrepresent the scarce information, as we do not know the frequency of occurrence, but rather, a range within which occupant density may vary. In this study, we seek a reliable alternative for probabilistic treatment of epistemic uncertainty, namely, a framework that can faithfully represent the imperfect knowledge without distorting the information.

An alternative to the probabilistic representation of epistemic uncertainty is based on the use of a possibility distribution $\pi(x)$ [169]. This extension of incomplete knowledge is specifically practical when the agent's knowledge is a fuzzy set, stating to what degree an event is normal, unsurprising or even expected. A possibility distribution value $\pi(x) \in [0,1]$ is allocated to each real value x in the range X . Expressing $\pi(x) = 0$, indicates that the value x is considered impossible, whereas $\pi(x) = 1$ implies that at least one interpretation of the value x is completely possible. Take for example the number of occupants in a bank at 10:00 a.m. of weekdays, where 10 employees work full-time, and 7 to 10 visitors are expected. In this example, observing less than 10 or more than 20 occupants is unexpected and surprising $\pi(x) = 0$, while encountering 17 occupants is considered normal and the routine state of affairs $\pi(x) = 1$. Any number of occupants between 10 and 17, as well as 17 to 20, would be characterized with a degree of certainty $0 < \pi(x) < 1$.

According to the theory of possibility, the likelihood of an event A is described by two limiting measures, the possibility Π and the necessity N , defined as [170]:

$$\Pi(A) = \sup_{x \in A} \pi(x) \quad (\text{Eq.3})$$

$$N(A) = 1 - \Pi(\bar{A}) = \inf_{x \notin A} (1 - \pi(x)) \quad (\text{Eq.4})$$

Let $\mathcal{P}(\pi)$ be a family of probability distributions such that for any event A , the probability measure of that event $P(A)$ is within the assigned necessity and possibility limits, i.e. $N(A) \leq P(A) \leq \Pi(A)$; then,

$$N(A) = \inf P(A) \quad \Pi(A) = \sup P(A) \quad (\text{Eq.5})$$

where the **infimum** and **supremum** probabilities represent the largest lower bound and the least upper bound of all probability measures in \mathcal{P} . This representation of uncertainty is particularly helpful when the available data is scarce or only the upper and lower bounds can be defined (e.g. uniform, triangular probability distributions). It is possible to transform a possibility distribution into a family of probability distributions (Figure 6). For this, a possibility distribution can be seen as a nested set of confidence intervals [171], which are the α -cuts of the distribution i.e. $[\underline{x}_\alpha, \bar{x}_\alpha] = \{x, \pi(x) \geq \alpha\}$. In this case, the necessity measure $N([\underline{x}_\alpha, \bar{x}_\alpha])$ gives the degree of certainty contained in the α -cuts $[\underline{x}_\alpha, \bar{x}_\alpha]$. Then, each interval is represented with a range of probability measures, such that $P(X \in [\underline{x}_\alpha, \bar{x}_\alpha]) \geq 1 - \alpha$ and $P(X \notin [\underline{x}_\alpha, \bar{x}_\alpha]) \approx \alpha$.

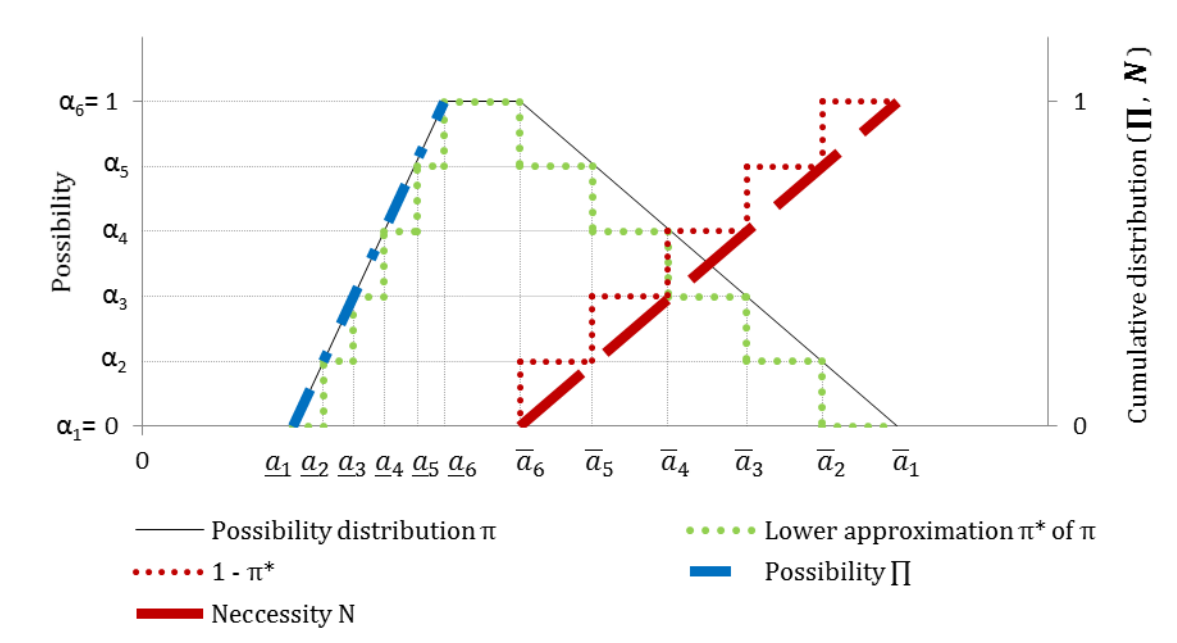


Figure 6- Transformation of possibility distribution to belief function.

The theory behind the possibilistic representation of uncertainty is a special case of evidence theory [172], which unlike probability theory (that assigns a density value to each potential value of a variable) allocates probability masses $v(E_i)$ to subsets $E_i = 1, 2, \dots, K$ of the uncertain variable domain, with $\sum_{i=1}^K v_i = 1$. Then, a quantitative description of uncertainty is given by means of the belief (Bel) and plausibility (Pl) measures, defined as follows:

$$Bel(A) = \sum_{E, E \subseteq A} v(E_i) \quad (\text{Eq.6})$$

$$Pl(A) = \sum_{E, E \cap A \neq \emptyset} v(E_i) = 1 - Bel(A) \quad (\text{Eq.7})$$

where $Bel(A)$ and $Pl(A)$ provide the minimum and maximum probabilities that can be assigned to set A , respectively. As in possibility theory, all probability values lie within the belief and plausibility interval; hence, for a probability family \mathcal{P} we obtain:

$$\forall P \in \mathcal{P}, Bel \leq P \leq Pl \quad (\text{Eq.8})$$

Since the mass distribution v of evidence theory is a generalization of both probability and possibility distributions, evidence theory provides a common framework for the hybrid modeling of uncertainty using both probability and possibility distributions.

3-2-2-3 Sampling with the hybrid approach

Uncertainty propagation is the process of numerically propagating the uncertainty associated to input quantities of the model to the outputs of that model. In this section, we describe how randomness (represented probabilistically) and imprecision (represented possibilistically) can be jointly propagated [173]. Let us consider a model $Z = f(X_1, X_2, \dots, X_k, X_{k+1}, \dots, X_n)$, in which the output is a function of n uncertain variables $X_i, i = 1, 2, \dots, n$. For ease of illustration, we consider that the first k variables are aleatory, and the remaining $n-k$ variables are epistemic. In order to propagate the hybrid uncertain information in the model, random quantities are represented by probability distributions $p_{X_i}(x), i = 1, 2, \dots, k$, and imprecise quantities are characterized with possibility distributions $\pi^{X_i}(x), i = k + 1, k + 2, \dots, n$. The procedure of propagating both types of uncertainty consists of two nested loops [174]: Monte Carlo sampling from the probabilistic distributions (outer loop) and approximation of the possibilistic distributions through α -cuts (inner loop). For this, the following steps are performed:

1. A k dimensional vector of random realizations (x_1, \dots, x_k) is generated by Monte Carlo sampling from the uncertain (probabilistic) quantities (X_1, \dots, X_k) .
2. α is set to zero and the related α -cuts of all possibility distributions $(\pi^{X_{k+1}}, \dots, \pi^{X_n})$ are found. The possibility distributions are intervals of possible values of the possibilistic quantities (X_{k+1}, \dots, X_n) .
3. The supremum and infimum values $[\bar{f}_\alpha, \underline{f}_\alpha]$ of $f(x_1, \dots, x_k, X_{k+1}, \dots, X_n)$ are calculated, where (x_1, \dots, x_k) is the vector of Monte Carlo-sampled probabilistic quantities from step 1, and (X_{k+1}, \dots, X_n) are the values of the possibilistic quantities obtained from step 2.
4. A small increment $(\Delta\alpha)$ is added to the value of α (e.g. $\Delta, \alpha = 0.05$) and the new α -cuts are found.
5. Steps 3 and four are repeated while $\alpha \leq 1$.

6. Steps one to five are repeated until the desired number of Monte Carlo samples (m) are generated.

The outcomes of this procedure are m random realizations of n ($n = \left(\frac{1}{\Delta\alpha}\right)$) possibility measures i.e. $(\pi_1^f, \dots, \pi_m^f)$. It is worth noting that the number of realizations ($m \cdot n$) should come from a tradeoff between computational cost and desired accuracy in the uncertainty description. Choosing a large value for $\Delta\alpha$ will fail to adequately describe the possibilistic representations, while selecting a small value can result in a considerable increase in computation time. Similarly, a small value of m could fail to appropriately define the probabilistic representations, while a large value could lead to a large computational time. Figure 7 presents an illustration of Hybrid approach.

3-2-2-4 Post-processing analysis of uncertain model outputs

The outcomes of the hybrid procedure can be combined by using different methods, such as separate affectation of probability and possibility descriptions [175], fuzzy prediction interval method [173] and homogenous post-processing [176]. The homogeneous post-processing method provides a tradeoff between the other two techniques. The method is based on average upper and lowers cumulative distributions of the outcomes. In this method, the possibility and necessity measures are calculated for each set A (see Eq.3 and Eq.4). This way, m pairs of measures that correspond to the upper and lower bounds of the possibility distributions are obtained. The limiting bounds allow us to obtain the belief and plausibility of any set A . Since the first k uncertain parameters are random quantities, then:

$$Pl(A) = \frac{1}{m} \sum_{i=1}^m \Pi_i^f(A) \quad (\text{Eq.9})$$

$$Bel(A) = \frac{1}{m} \sum_{i=1}^m N_i^f(A) \quad (\text{Eq.10})$$

Where, $N_i^f(A)$ is the necessity measure and $\Pi_i^f(A)$ is the possibility measure of A , obtained from the i^{th} Monte Carlo realization.

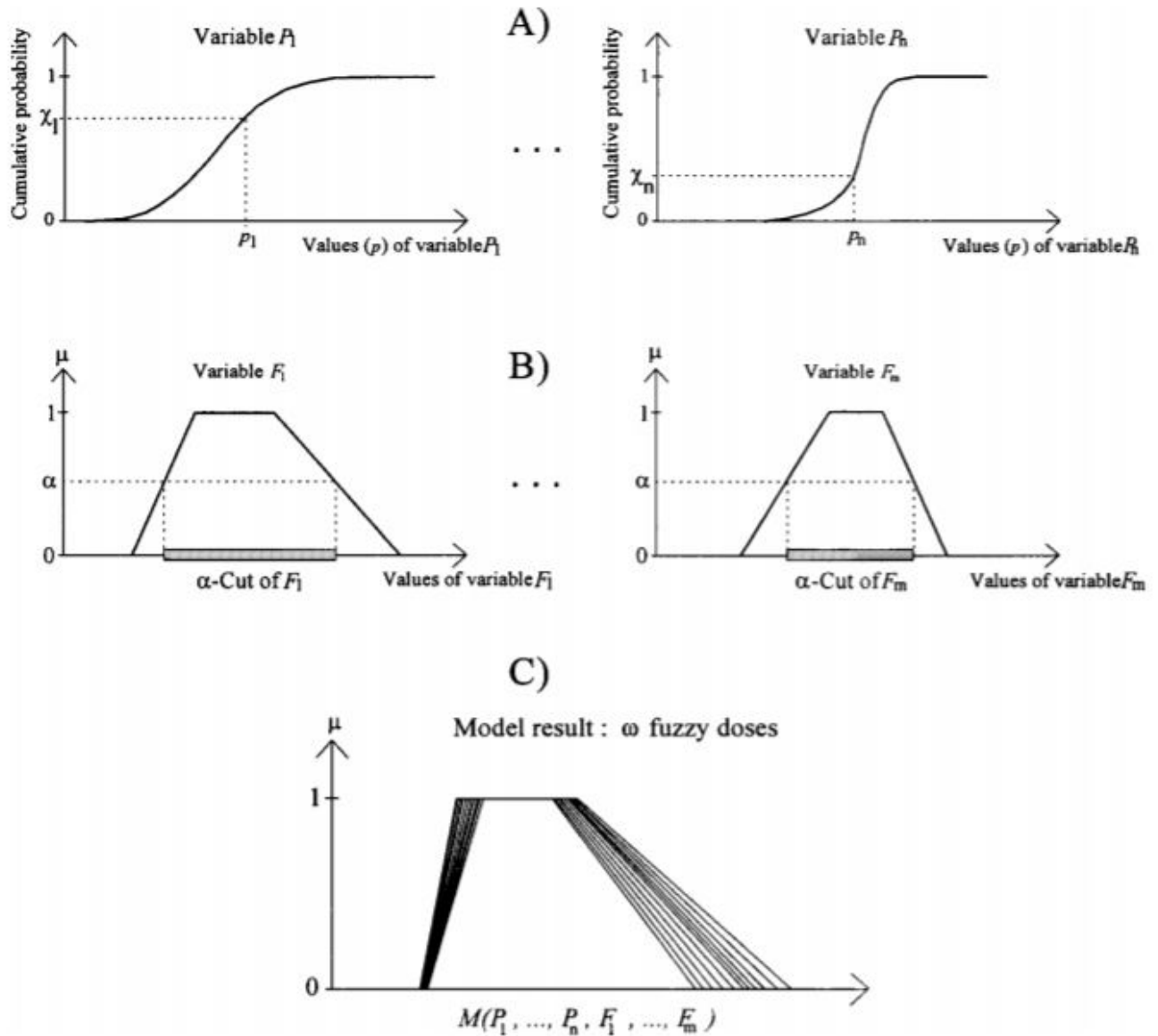


Figure 7- illustration of the hybrid approach: (A) Series of random samples are generated by a probabilistic approach from PDF (P_1, \dots, P_n). (B) Sample generated based on possibilistic approach through selecting an α -cut (F_1, \dots, F_m). (C) The final set of samples are a combination of PDF and α -cuts, where each probability sample is repeated for each α -cuts ($M(P_1, \dots, P_n, F_1, \dots, F_m)$). [177]

3-3 Model fine tuning

3-3-1 Solar model calibration

In this study, a new method is proposed to tune the Perez model for a specific location. This process involves Subset Simulation, which is based on Markov Chain Monte Carlo and Importance Sampling. The effect of using a calibrated Perez model has evaluated on the incident solar irradiance on vertical surfaces, as well as cooling and heating loads of a building. The method here proposed can successfully adapt Perez coefficients to local measurements and is easy to implement in building energy simulation models.

3-3-1-1 Subset simulation method

In this study, a Subset Simulation (SuS) is selected to calibrate Perez solar model coefficients. The application of SuS for calibration of different models has previously been adopted by Gong et al. [178]. This technique is specifically useful for complex models with high dimensions of uncertain variables and can reduce the computational time of the process. The method shifts rare probabilities to more frequent events, by resorting to Markov Chain Monte Carlo sequences, i.e. rejecting unwanted samples that have higher errors [179]. The SuS framework adopted in this study is presented in Figure 8.

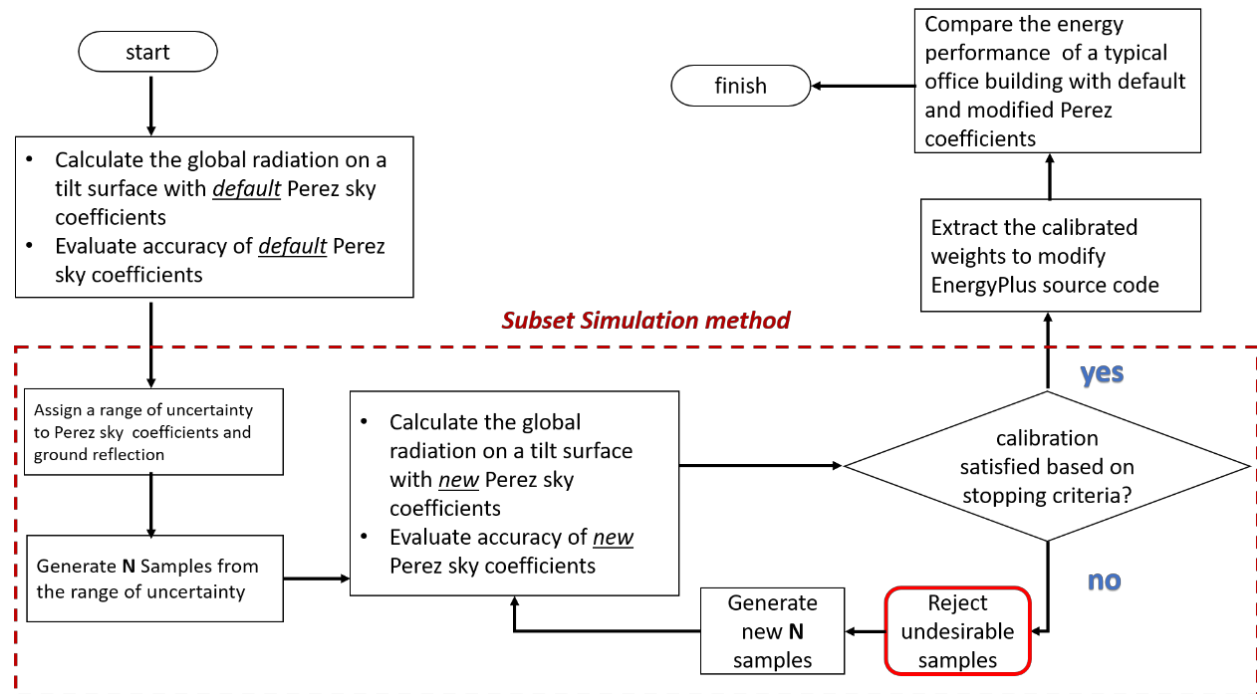


Figure 8 - Framework of calibration method using Subset Simulation

3-3-1-2 Uncertain parameters

Global irradiation on tilted surfaces is calculated from direct, sky diffuse and ground reflected irradiation. Among the three components, sky diffuse irradiation has been reportedly associated with immeasurable uncertainty [139]. In the Perez model, sky diffuse radiation is calculated through a series of predefined sky conditions. Therefore, this study tends to localize the sky conditions to obtain more accurate calculations of diffuse radiation. Perez irradiance coefficients are developed based on measured data in various sky conditions. The coefficients are necessary for calculating the circumsolar and sky brightness within the Perez model (Table 5).

Irradiance coefficients in the Perez model are presented for eight sky categories (e-Bins), which vary from overcast to clear sky conditions. Each of the sky conditions consists of six values (three circumsolar brightening coefficients and three horizon brightening coefficients), which are used as weights in Perez model equations to calculate sky diffuse radiation. Treatment of eight sky categories, each consisting of six brightening coefficients results in 48 uncertain irradiance coefficients that require calibration (Table 5).

Table 5- original Perez irradiation coefficients

	Sky clearness	F11	F12	F13	F21	F22	F23
Over cast	1 – 1.065	-0.008	0.588	-0.062	-0.06	0.072	-0.022
	1.065 – 1.230	0.13	0.683	-0.151	-0.019	0.066	-0.029
	1.230 – 1.500	0.33	0.487	-0.221	0.055	-0.064	-0.026
:	1.500 – 1.950	0.568	0.187	-0.295	0.109	-0.152	-0.014
	1.950 – 2.800	0.873	-0.392	-0.362	0.226	-0.462	0.001
	2.800 – 4.500	1.132	-1.237	-0.412	0.288	-0.823	0.056
	4.500 – 6.200	1.06	-1.6	-0.359	0.264	-1.127	0.131
Clear sky	6.200 – ...	0.678	-0.327	-0.25	0.156	-1.377	0.251

To decrease this number of uncertain parameters (48) and avoid multi-modality, a second-order curve is fitted onto each sky brightening coefficient (Figure 9). Each second-order polynomial curve consists of three constants (Eq.11 - Eq.16) and accepts a sky clearness value (e) to return a brightening coefficient.

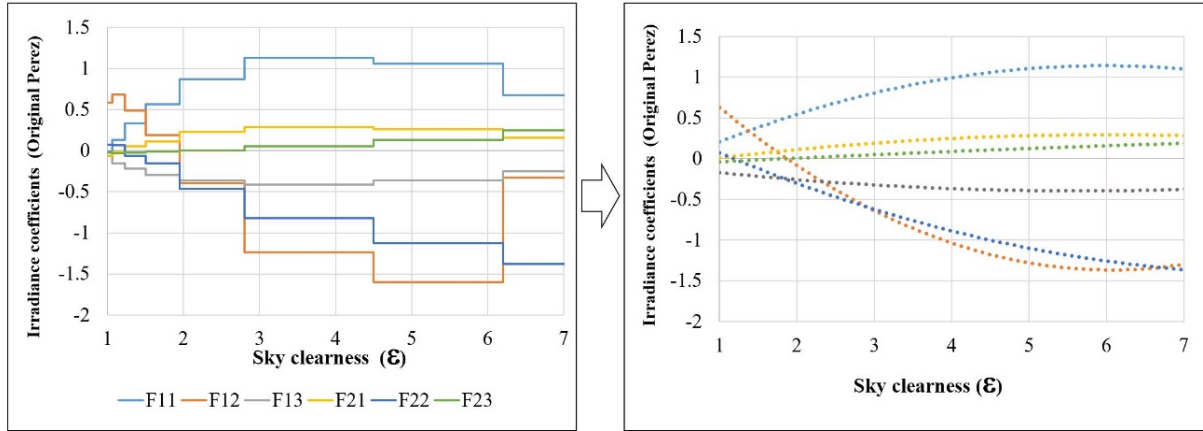


Figure 9 - Equivalent lines for each class of sky and Perez coefficients (left). Interpolation of the lines (right)

New interpolated equations:

$$F11 = -0.0378 (e)^2 + 0.4515 (e) - 0.2079 \quad (\text{Eq.11})$$

$$F12 = 0.0781 (e)^2 - 0.9457 (e) + 1.4969 \quad (\text{Eq.12})$$

$$F13 = 0.0104 (e)^2 - 0.1173 (e) - 0.0642 \quad (\text{Eq.13})$$

$$F21 = -0.0115 (e)^2 + 0.1373 (e) - 0.1173 \quad (\text{Eq.14})$$

$$F22 = 0.0269 (e)^2 - 0.4539 (e) + 0.4986 \quad (\text{Eq.15})$$

$$F23 = -0.0015 (e)^2 + 0.0502 (e) - 0.088 \quad (\text{Eq.16})$$

In fact, these constants in equations (Eq.11 - Eq.16) are considered as uncertain parameters, which require tweaking for calibration. As a result, a weight is associated with each constant that facilitates the propagation of uncertainty for calibration (Eq.17 - Eq.22). Since the Perez model consists of six brightening coefficients, and each coefficient is represented with a curve of three uncertain weights, calibrating all brightening coefficients requires (six multiplied by three) 18 uncertain parameters (A11 - C23). Therefore, converting the bins to curve equations reduces the number of uncertain parameters from 48 to 18.

$$F11 = \mathbf{A11} \times (-0.0378) (e)^2 + \mathbf{B11} \times 0.4515 (e) + \mathbf{C11} \times (-0.2079) \quad (\text{Eq.17})$$

$$F12 = \mathbf{A12} \times 0.0781 (e)^2 + \mathbf{B12} \times (-0.9457) (e) + \mathbf{C12} \times 1.4969 \quad (\text{Eq.18})$$

$$F13 = \mathbf{A13} \times 0.0104 (e)^2 + \mathbf{B13} \times (-0.1173) (e) + \mathbf{C13} \times (-0.0642) \quad (\text{Eq.19})$$

$$F21 = \mathbf{A21} \times (-0.0115) (e)^2 + \mathbf{B21} \times 0.1373 (e) + \mathbf{C21} \times (-0.1173) \quad (\text{Eq.20})$$

$$F22 = \mathbf{A22} \times 0.0269 (e)^2 + \mathbf{B22} \times (- 0.4539) (e) + \mathbf{C22} \times (- 0.4539) \quad (\text{Eq.21})$$

$$F23 = \mathbf{A23} \times (-0.0015) (e)^2 + \mathbf{B23} \times 0.0502 (e) + \mathbf{C23} \times (- 0.088) \quad (\text{Eq.22})$$

The total radiation incident on a tilted surface is also affected by the reflected solar radiation from the ground. Since the ground reflected radiation is composed of both direct and diffuse radiation and considering that the diffuse component is the subject of the study, the albedo of the ground is also associated with uncertainty and subject to calibration.

3-3-1-3 Gaussian Mixture Model

Ground reflection and Perez irradiance coefficients are the parameters that are associated with uncertainty for calibration. Therefore, the study deals with a multivariate distribution of uncertain variables, composed of 19 different parameters in total. To represent the covariation of all uncertain parameters within a single matrix, we opted for a Gaussian Mixture Model (GMM). The GMM creates a k (multi) variant distribution, where k is the number of random (or uncertain) parameters [180].

GMM works based on an Expectation-Maximization (EM) algorithm. The EM algorithm processes the multivariate distribution in two steps: E-step, M-step. In E-step, the posterior probability of each sample data is estimated. After that, in M-step these probabilities are considered as the weight for applying the maximum likelihood for each involved distribution on GMM. The EM algorithm continues iteratively to converge on a local optimum [181]. In this study, MATLAB scripting is used to create a pipeline of functions for implementing the SuS.

3-3-2 Building energy model fine tuning

3-3-2-1 Introduction of DIVA

The energy performance of a building inside a canyon can be affected by surrounding elements. This is investigated in different aspects such as the solar potential for installing PV panels, shading and thermal effect of vegetation or building obstructions and air flows within the urban canyons. However, uncertainty in optical properties of surrounding elements such as reflectance of adjacent buildings or transparency of trees resulted from seasonal changes still needs for more investigations.

DIVA (Design Iterate Validate Adapt) is a plug-in for Rhino which recognized as one of the daylight professional tools. DIVA is presented for both Rhinoceros and Grasshopper and uses RADIANCE [182] and DAYSIM [129] calculations methods equivalently [183]. DIVA-for-

Grasshopper includes different components that can cover the variety of daylight quantities from incident solar radiation to visual comforts and performance of shading devices. The flexibility of Grasshopper in parametric modeling is the strength of DIVA-for-Grasshopper for optimization or uncertainty analysis problems [184].

DIVA can calculate the incident solar radiation on building surfaces at selective nodes, and the tool can manage the calculations for different scales from urban to single building scale. Solar radiation is estimated based on the climate-based calculation method and time series (hourly) values are possible to retrieve from the simulations. DIVA can generate different images of radiation map on building surfaces for the annual values or a specific moment of the year. Figure 10 shows the Radiation Map component of DIVA in Grasshopper as well as required inputs and achievable outputs.

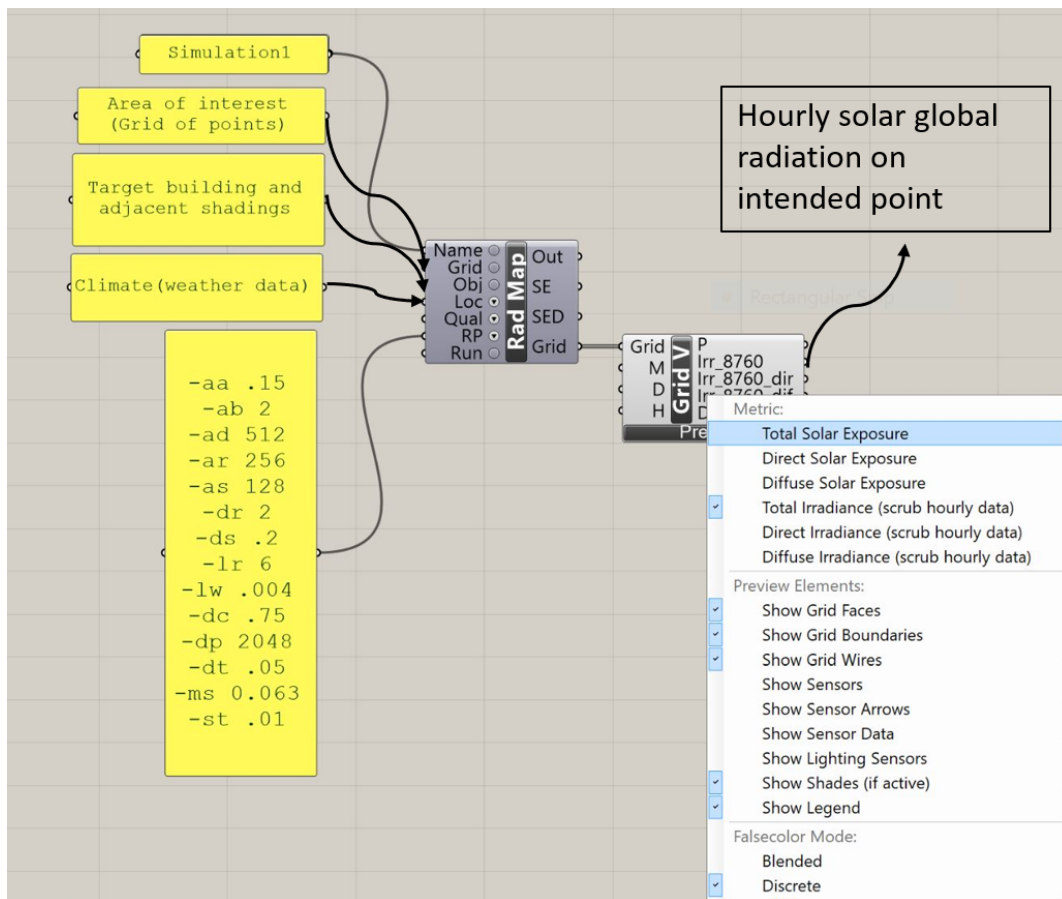


Figure 10- Radian map component of DIVA in Grasshopper. Main inputs and possible outputs

3-3-2-2 Modelling an uncertain urban canyon in DIVA

Based on the need of this study for parametric modeling, DIVA for grasshopper is chosen to develop the uncertainty quantification of solar radiation within the urban canyon.

A new framework is suggested here which can create a complex urban canyon geometry based on the uncertainty of selective parameter through Grasshopper and involve in DIVA daylight analysis. The method has the capability of generating different random samples of the whole complex canyon with variation in all selective parameters.

The proposed method works based on the following steps:

1. Define the uncertain parameters around the building and inside the canyon which can affect the estimations of solar radiation on façade.
2. Define the range of variation and the possible method to propagate uncertainty in each parameter. This information can achieve from:
 - i. Actual measurements
 - ii. On-site survey or observation
3. Connect the sampling procedure to DIVA solar radiation analysis
 - i. Sampling procedure can be done by MATLAB
4. Make the model of the urban canyon and perform DIVA-Radiation Map calculation based on recognized uncertainties.
5. Involved the quantified incident solar radiation in building performance analysis

The first step is defining the uncertain parameters, the range of variation and the appropriate propagation method. Availability of solar radiation on building façade is highly related to the skyline. This parameter can be interrupted by different obstacles such as the height of adjacent buildings and trees. Moreover, as mentioned in Chapter 2, the albedo of surrounding elements such as high reflected facades or variation in ground reflectance can manipulate the estimations of solar radiation.

Based on a literature review (Chapter 2), seven parameters are introduced as possible sources of uncertainty in the estimation of incident solar radiation on building facades (Table 6). The uncertainty in skylines are sourced from the variation in the height of surrounding buildings and

considered through assigning a ratio of variation to height of different buildings. This parameter is called “Ratio of building height” in Table 6. Within an urban canyon, different Window to Wall Ratios (WWR) for each building is among the important features which can create the uncertainty in estimations of solar radiation within an urban canyon. External shadings are other features in urban canyon which can affect the solar radiation by changing the ratio of glazed and opaque area during operation. When an external shading is closed it can change the effect of reflected radiation received from the surrounding buildings. Variation in façade material, type and size of vegetations are also among the important sources associated with uncertainty in estimations of incident solar radiation within an urban canyon. Moreover, the optical properties of cars including reflectance and specularity can affect the overall albedo of urban canyon. More details about the type and range of uncertain parameters and their variation are presented in Chapter 4.

Table 6 - Candidate factors related to the uncertainty of solar radiation in an urban canyon

	Uncertain parameters	Unit
1	Ratio of building height	%
2	WWR	%
3	External shading	On/off
4	Exterior wall reflectance	-
5	Trees crown diameter	m
6	Tree transmittance	-
7	Cars reflectance	-

After defining the variation of each uncertain parameter, the sampling procedure is performed in MATLAB. Due to the diversity in the nature of the uncertain parameters in Table 6, sampling with a hybrid approach is preferred in this framework. Parameters 1 to 5 in Table 6 have the probability distributions since a more detailed range of variation for these parameters are achievable from the in-site observation or measurements. While the possibilistic sampling approach should be adopted for transmittance of trees and car shells reflectance (6 and 7), these two are not easy to estimate and clearly there is a lack of information. Transparency of trees is measured by estimating the reduction of solar radiation under the tree canopy. The season change is the most important parameter that should be considered in trees transparency analysis. Transparency of different tree species during the summer and winter period are measured by [185] The values are reported in Table 7. Estimating the randomness of the reflectance distribution of parked and moving cars in a street can prove difficult; however, the lowest and highest reflectance values of car shells are achievable in the literature [186]. The distribution of cars reflectance can vary between [0.05, 0.58]. Therefore, creating the possibility of propagation for this parameter is also conceivable.

In this study for creating the 3D model of the complex canyon, a structure in Grasshopper is presented which converts the numeric information of a sample canyon into a 3D model. This information is:

- (1) Canyon elements numbers and coordinates (building, tree, car)
- (2) Height of canyon elements (building, tree)
- (3) Number of building floors
- (4) Window to wall ratio

The structure of the 3D model is modular, and it is possible to adopt the structure of further case studies. Moreover, the required numeric information can be retrieved from GIS databases, where available.

The following Figures (11-16) show how the 3D maker structure can create a random geometry model from the numeric information. Figure 11 shows how the developed model creates a simple geometry (box) from imported coordinates.

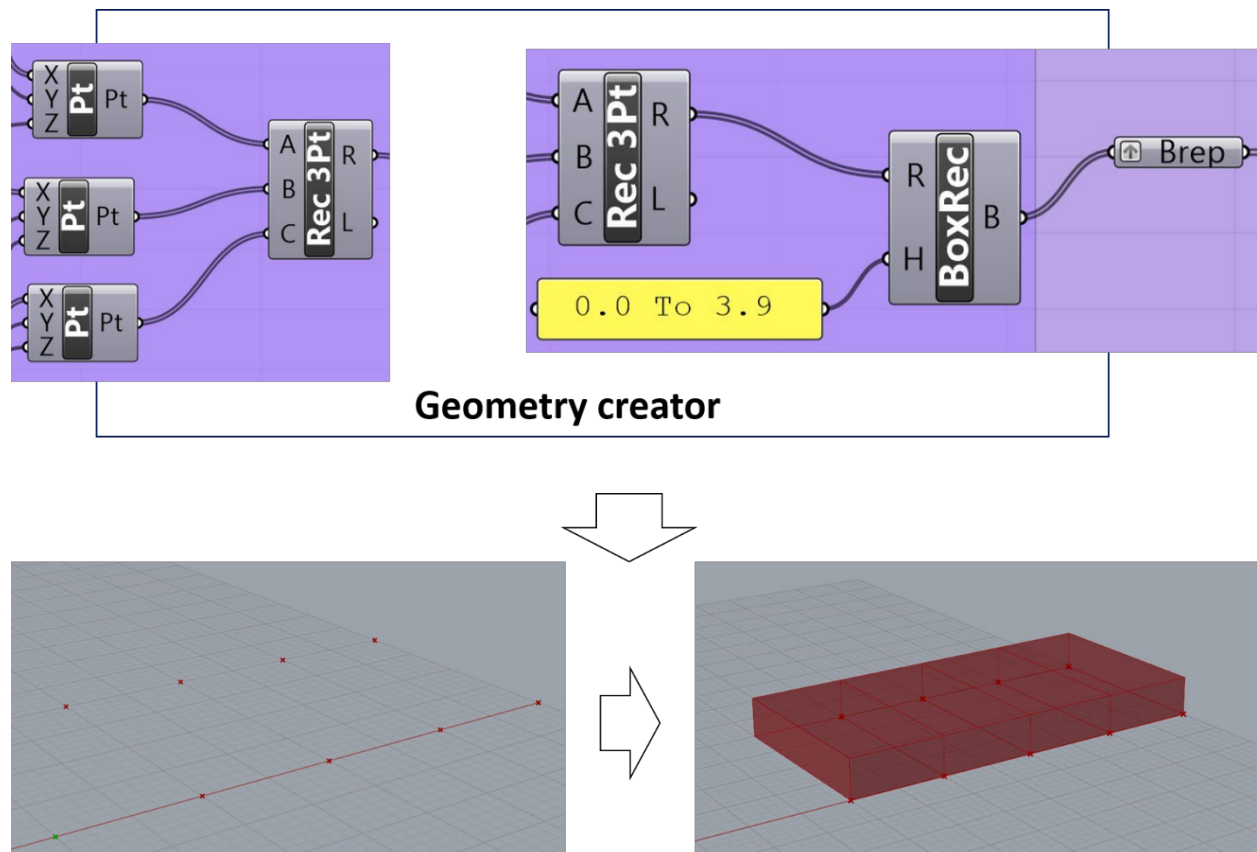


Figure 11- Modules to transfer coordinates to 3D model

Figure 12 shows the modules which combine uncertain parameters including: (1) ratio of building height, (2) WWR and (3) external shading to create the random geometry of each random sample of an urban canyon.

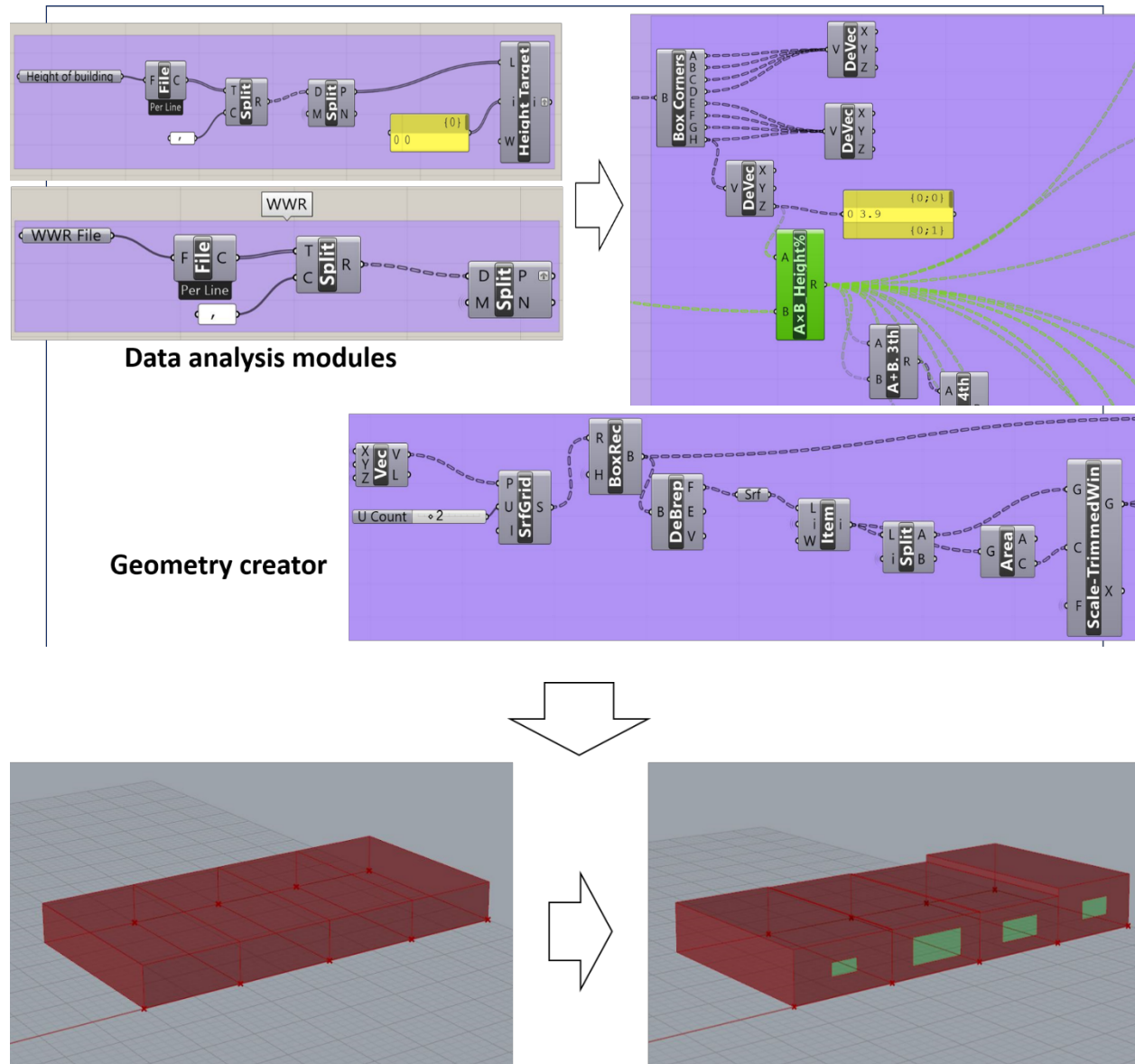


Figure 12- Module to create random height and WWR for each building

The final model of surrounding buildings with the option of assigning uncertainty in both geometry and optical properties is presented in Figure 13. The file path containing a possible range of variations of parameters subject to uncertainty (already defined in MATLAB), is addressed in data analysis modules. Associating data analysis modules with geometry creator modules shapes the final random geometry of surrounding buildings.

The same pattern is followed to model random tree and cars in Figures 14 and 15. In both cases, the model provides the opportunity to create the final random object by accepting the coordinates file and a range of variation concerning size (only for trees) and optical properties.

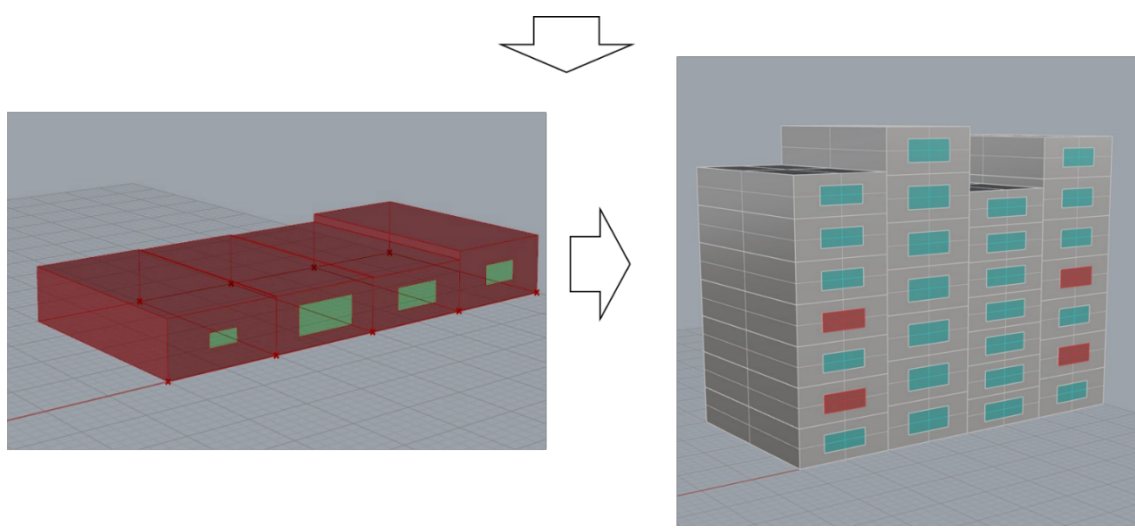
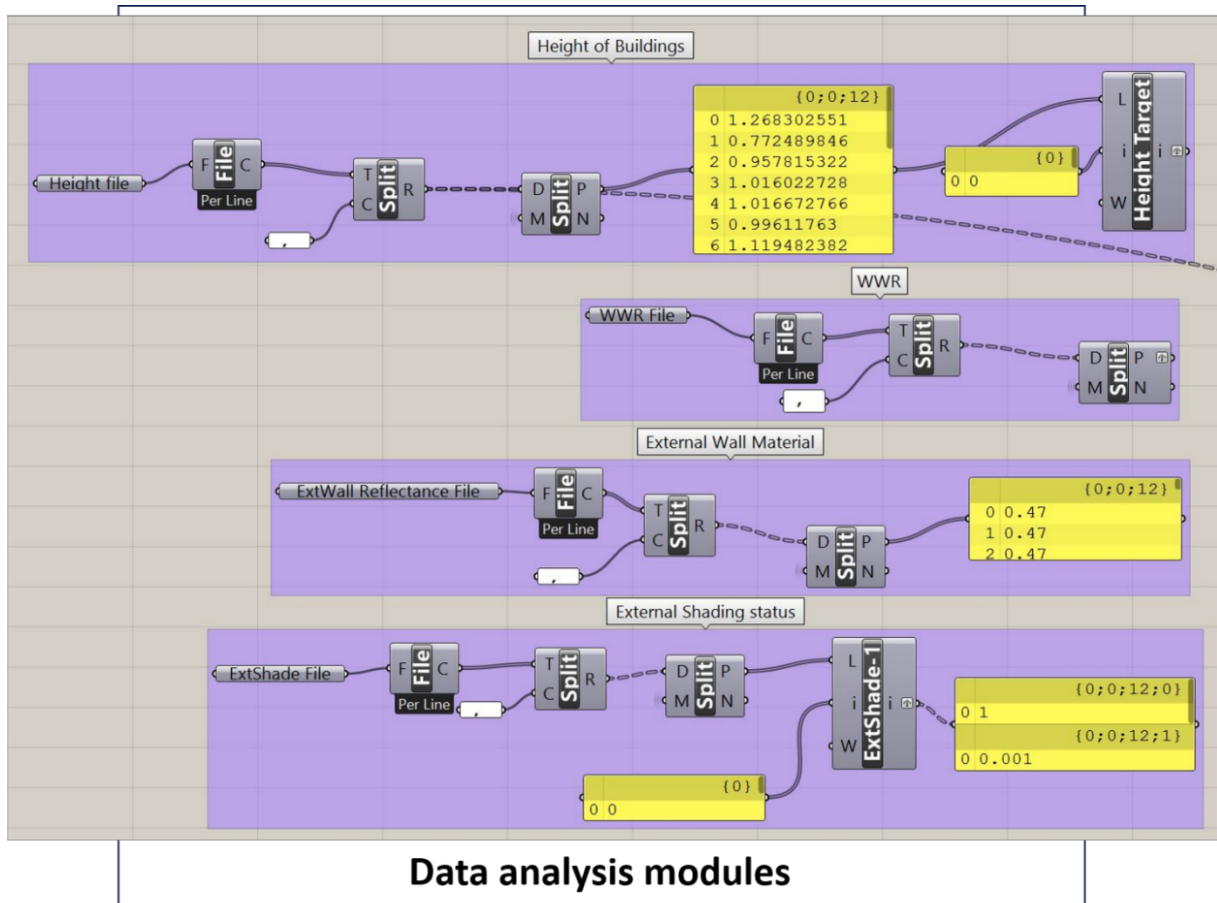


Figure 13- Modules to convert one floor to multi-floor buildings with the possibility of variation in height, WWR, and material

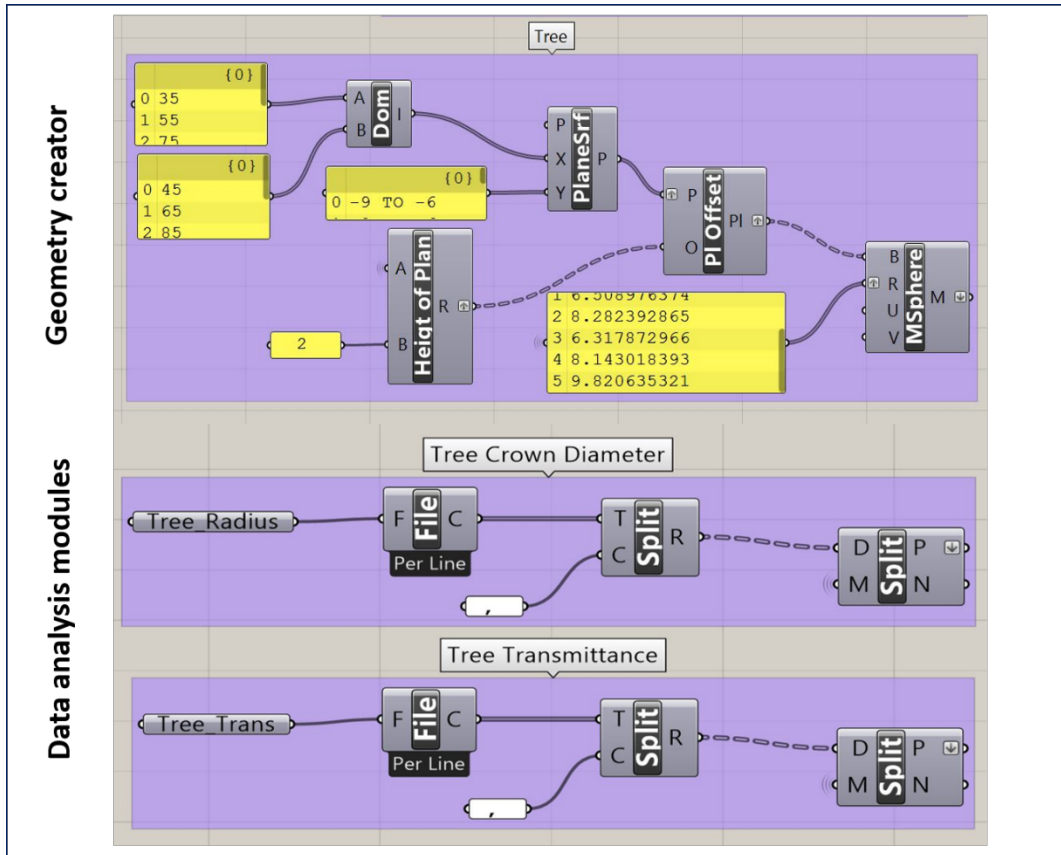


Figure 14- Modules to model trees with uncertainty in crown diameter and material

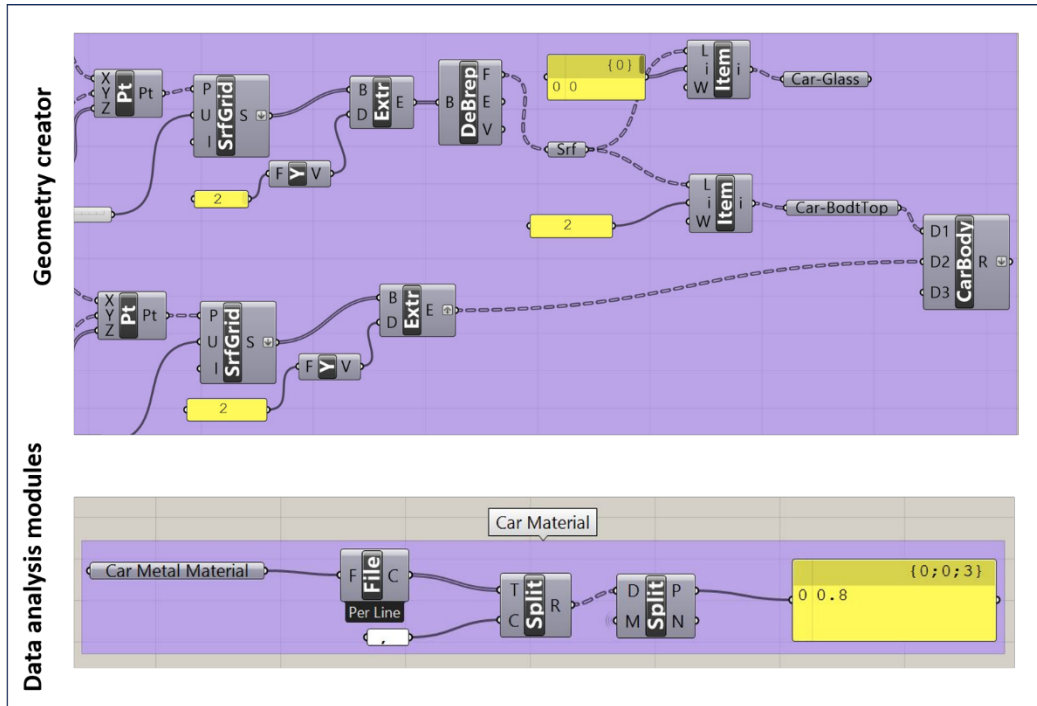


Figure 15- Module to create a car with the possibility of variation in material

A final view of the generated random canyon (through the proposed framework) is presented in Figure 16. For the following analysis, 60 different random samples are produced to perform the uncertainty analysis of incident solar radiation within an urban canyon.

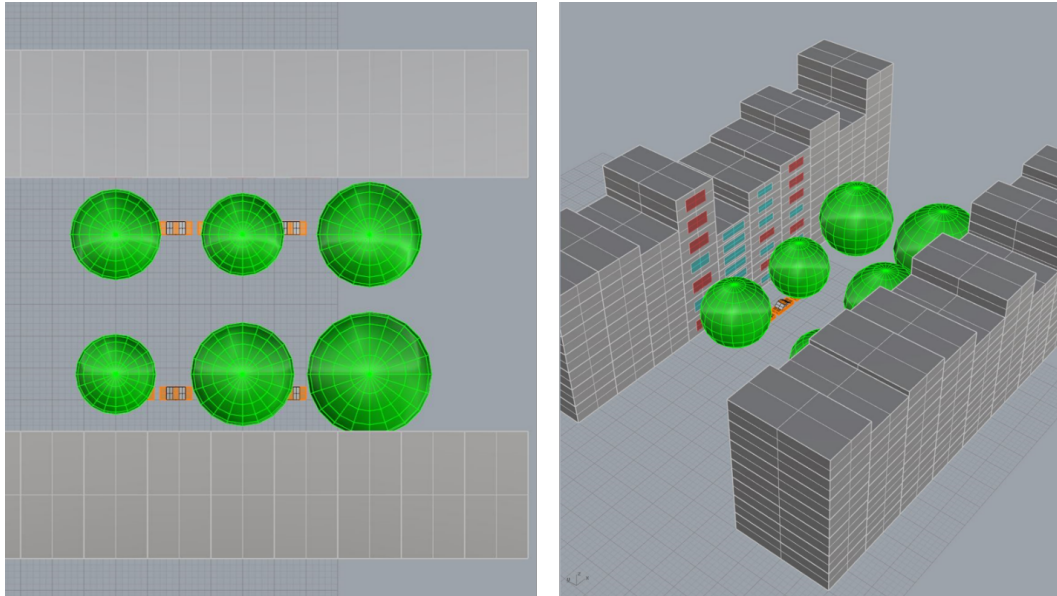


Figure 16 – A sample of final complex canyon geometry

In the following sections, the results of uncertainty in the complex canyon are compared with a Simple canyon (Figure 17) which defines as:

1. Same height for all buildings
2. Same WWR
3. No tree, No Car
4. No variation in material

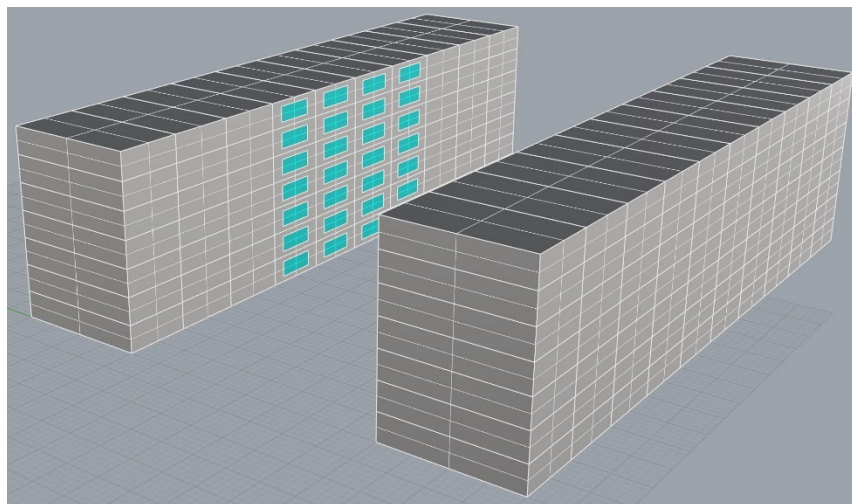


Figure 17- Geometry of simple canyon, typical consideration of urban canyon in building energy analysis

3-3-2-3 Seasonal effect of vegetation

Trees are more transparent in cold seasons because of the fact of losing the leaf while in spring and summer seasons, trees more act as shading elements, so the transmittance of the trees reduces.

Table 7 shows some actual measurements of the seasonal effect of trees on incident solar radiation through comparing the solar radiation attenuation in summer and winter [185] (for more details see Figure 2 in [185]). The solar radiation attenuation (AT) can be related to the transmittance of the trees (Eq.23) [187]. If AT is the percentage of solar reduction after passing through a transparent or semi-transparent obstacle, the transmittance (T) can be computed as:

$$AT = \frac{S_{sun} - S_{shadow}}{S_{sun}} \times 100 \quad (\text{Eq.23})$$

$$T = 1 - AT \quad (\text{Eq.24})$$

Where, S_{sun} refers to total the amount of solar radiation hitting on a surface without any obstacle, S_{shadow} returns the amount of solar radiation on the surface which affected by shading elements.

As mentioned, the optical properties of a given material are represented by RADIANCE material definition. To simulate the transparency of the trees and seasonal change in DIVA, using of a translucent object is an accepted solution [188]. A translucent object is defined by the Trans type of material in RADIANCE material database [182]. This type of material can have all reflectance, specularity, and transmittance and define as Figure 18.

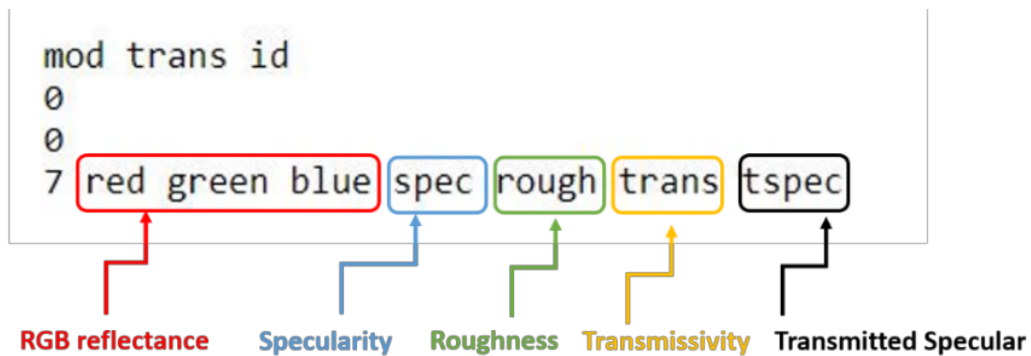


Figure 18 - A sample of Radiance material definition

Table 7- Seasonal effect of trees by measured solar radiation under the trees, in winter and summer period and with no shade and shaded conditions [185]

Trees species	Season Pinus	Solar radiation attenuated (%)
Pinus palustres	Summer	79.7
	Winter	69.8
Pinus coulteri	Summer	83.8
	Winter	78.3
Handroanthus chrysotrichus	Summer	82.8
	Winter (leafless)	46.4
	Winter (with flowers)	51.4
Jacaranda mimosaeifolia	Winter	63.8
Syzygium cumini	Summer	87.2
	Winter	89.1
Mangifera indica	Summer	89.2
	Winter	88.6
Caesalpinia pluviosa	Summer	83.8
	Winter	69.5
Lafoensia glyptocarpa	Winter	63.9
	Winter	76.0
Spathodea campanulata	Winter	55.0
	Winter	82.4
Tipuana tipu	Summer	76.2
	Summer	80.2
Delonix indica	Summer	73.5
	Winter	72.3
Senna siame	Summer	89.2

3-3-2-4 Solar-based MRT

The direct effect of shortwave radiation resulted from outside solar radiation on comfort conditions is ignored in main standards which are typically applied to building energy models. Arens et al. [99] proposed a novel model to involve the shortwave flux on mean radiant temperature (MRT). The model works based on energy flux and the occupant's body surfaces, quantifying the effect of incident direct radiation on human body surfaces.

The Mean Radiant Temperature (MRT) could be extracted based on the effective radiant field (ERF) from Eq.25. According to Arens et al. [99], the direct effect of solar radiation on MRT can be considered through Eq.26 based on shortwave solar radiant flux on the body surfaces (E_{solar}).

$$ERF = f_{eff} h_r (MRT - T_a) \quad (\text{Eq.25})$$

$$\Delta ERF_{solar} = \left(\frac{\alpha_{sw}}{\alpha_{Lw}} \right) E_{solar} \quad (\text{Eq.26})$$

Where:

In Eq.25 f_{eff} refers to the fraction of occupant body which is directly affected by solar radiation inside the building, h_r is the radiant heat transfer coefficient of surrounding surfaces in W/m²K and T_a is the indoor air temperature in °C.

The quantities of α_{sw} and α_{Lw} in Eq.26 are short-wave absorptivity and long-wave emissivity/absorptivity, respectively. α_{sw} is defined based on color skin and clothing while α_{Lw} is usually considered as a constant value of 0.95.

E_{solar} is divided into three components of direct beam radiation passing through the windows, diffuse sky radiation and reflected component from indoor floors. (See Eq 3,4,5. in [99])

And finally, the ΔERF_{solar} estimate based on:

$$ERF_{solar} = (0.5 f_{eff} f_{svv} (I_{diff} + I_{global} R_{floor}) + A_p f_{bes} I_{dir} / A_D) T_{sol} (\alpha_{sw} / \alpha_{Lw}) \quad (\text{Eq.27})$$

The f_{eff} is a fraction of the body surface which is visible to radiation from the environment and set as a constant value of 0.696 for seated and 0.725 for standing person. T_{sol} is solar transmittance of glazed area and could be exported from optical material properties. A_D refers to body surface area which is usually considered as 1.8 m². f_{svv} and A_p are determined based on the following equation:

$$f_{svv} = \frac{\left(\tan^{-1}\left(\frac{h}{2d}\right)\tan^{-1}\left(\frac{w}{2d}\right)\right)}{90.180} \quad (\text{Eq.28})$$

The f_{svv} is the fraction of the sky that affects the occupant activities. According to Eq.28., this parameter is determined based on windows dimensions (width and height) and occupant's distance from the target window.

$$A_p = f_{eff} f_p A_D \quad (\text{Eq.29})$$

A_p is the projected area of a standard person exposed to direct beam radiation which is defined based on the projected area factor (f_p).

Determining the f_p is relied on values by Kubaha et al [189]. Kubaha et al. simulate the detailed geometry of two standing and seated posture of human body with a raytracing simulation engine to estimate the f_p when the effect of direct and diffuse solar radiations is taking into account. Based on this method, the estimations of f_p based on sun azimuth and altitude during the daylight hours is possible. Figure 19 (Up) shows the body geometry studied by Kubaha et al and proposed values based of f_p (Down).

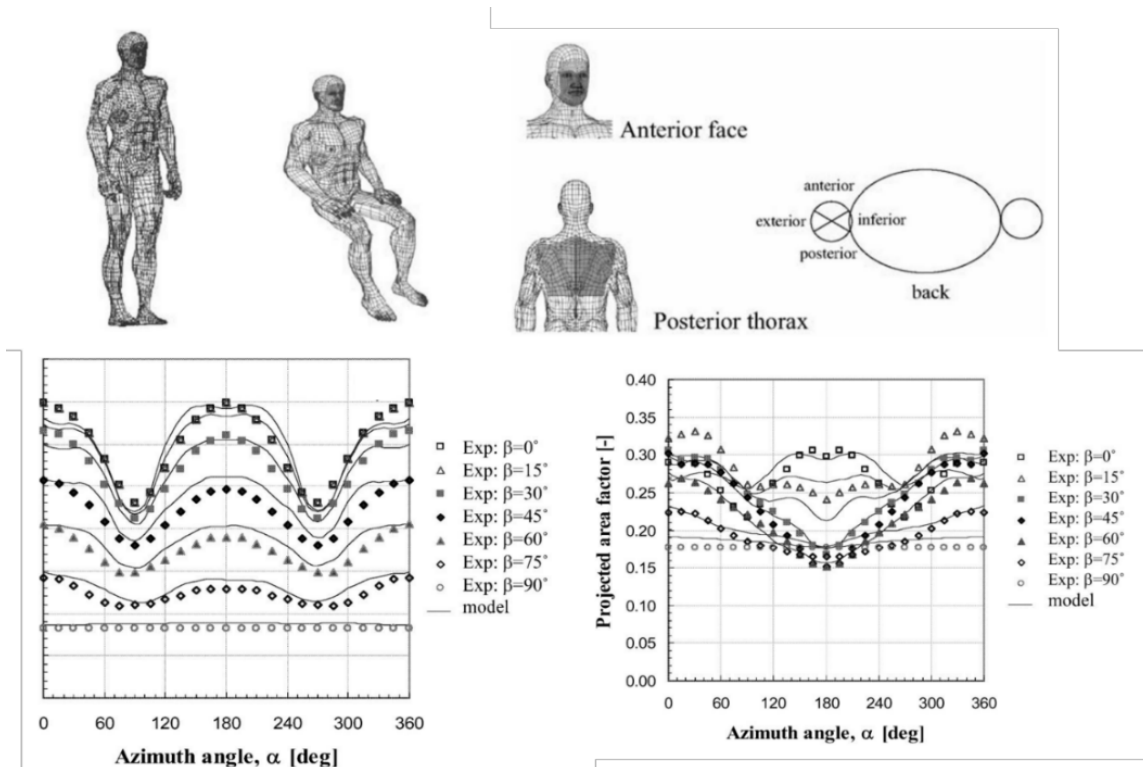


Figure 19- The geometry of the body divided to detailed segments to feed to raytracing simulation (Up), predicted projected area for standing and seated posture (Down: right=standing, left=seated) [189]

3-3-2-5 Indoor comfort metrics

Standards propose limitations to ensure the quality of indoor conditions in the initial design steps. Among these, it can be referred to as the adaptive comfort model [190] and predicted mean vote (PMV) [191]. The first one estimates the accepted indoor conditions based on indoor operative temperature and monthly mean outdoor temperature. While the latter determines the occupant feeling of comfort based on indoor air temperature, relative humidity, MRT, air movement, metabolism rate of indoor activities and finally the clothing rate of occupants.

In the previous section the direct effect of shortwave radiation resulted from outside solar radiation on MRT is discussed. Since MRT is used in PMV calculations, this section tries to associate the solar-based MRT in PMV comfort index, and study the effect of uncertainties in building boundary condition on indoor comfort sensation.

The PMV indicator is obtained from a research study from a wide range of people with the same clothing and indoor activities to understand the level of comfort sensing by different peoples [191]. After that the following equation is extracted:

$$\begin{aligned}
 \text{PMV} = & (0.303e^{-0.036M} + 0.028) \{ (M - V) & \text{(Eq.30)} \\
 & -0.00305 [5733 - 6.99(M_W) - \rho_s] \\
 & -0.42 [M - W - 58.15] \\
 & -(1.7 \times 10^{-5}) M (5867 - \rho_s) \\
 & - 0.0014 M (34 - \theta_{ai}) \\
 & -(3.96 \times 10^{-8}) f_{cl} [(\theta_{cl} + 273)^4 - (\theta_c + 273)^4] \\
 & - [f_{cl} h_c (\theta_{cl} - \theta_{ai})] \}
 \end{aligned}$$

Where:

	Parameters	Unit
M	Metabolic rate	W/m ²
W	External work	-
f _{cl}	Ratio of cloths to un-cloths body area	-
θ _{ai}	MRT	°C
θ _c	Operative temperature	°C

ρ_s	Water vapor pressure around the body	Pa
h_c	Convective heat transfer coefficient at the body surface	W/m ² K
θ_{cl}	Surface temperature of clothing	°C

Thermal comfort sensation based on ASHRAE scales, as shown in Table 8, defines three classes as the uncomfortable thermal sensation for feeling the cold and three classes for the overheating feelings.

Table 8 - predicted mean vote (PMV) thermal sensation, ASHRAE scales

PMV	Thermal sensation
-3	Cold
-2	cool
-1	Slightly cool
-0.5	Natural
0	
0.5	
1	Slightly warm
2	warm
3	Hot

Chapter 4 – Case study

In this chapter, the presented method in chapter 3 is validated through real case studies.

4-1 Data acquisition and refinement

4-1-2 Data Description

The value of hourly measured temperature, for nine years (from 2000 till 2008) is collected from seven different weather stations within the Milan city. These measured data are extracted from the network of ARPA Lombardia. Figure 20 shows the position of the weather stations under study.

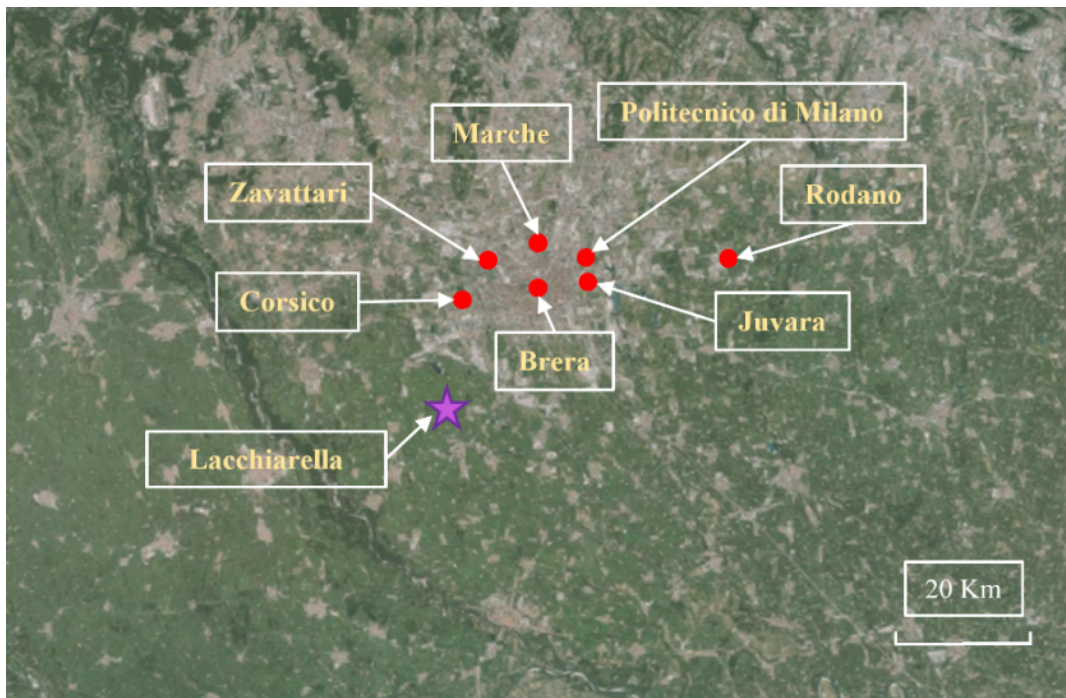


Figure 20- The network of weather stations of this study. The red points refer to stations which used as the input features. The star refers to the target of the prediction of missing value in hourly temperature.

4-1-3 Result and Discussion

The target of activities in this part is estimating the missing temperature related to “Lacchiarella” weather station. A total of 5 NN models are compared in this study. Different combinations of the hourly temperature from neighbor stations in ARPA network are stated as input features, while the hourly temperature in “Lacchiarella” station is considered as the target of prediction. Each model is trained five times, and the best performance is considered. The performance of the NN is indicative of the accuracy of the trained NN. The predicted values by NN are defined as output

(look at Figure 5). Mean Squared Error (MSE) and Regression (R) are considered as the performance indicators. Both “MSE” and “R” are defined based on measured hourly temperature values (of “Lacchiarella”) as target, and the predicted hourly temperature as the output of NN. The best trained neural network is the one with lowest MSE and highest R among the trained networks. Table 9 provides some details on each model. The first model (ANN1) was trained based on temperature values of all stations as the inputs of the network, except for Lacchiarella which is considered as the target vector. Time features including hour, day and month (HH, DD, MM) are added to ANN2. It is observed that incorporating the time features into the network (ANN2), does not improve the performance of the model. The climatic parameters have a transient property, for instance, the sensed temperature in the present hour is correlated to that of the previous hours and will affect the next ones in the subsequent time-steps. Therefore, the temperatures observed in $T_{\pm 1}$ and $T_{\pm 2}$ (at time step T) are added in the third NN model (ANN3). As it observes in Table 1 the MSE of ANN3 is reduced to 1.2241 while the R-value is increased to 0.9923.

Table 9- Description and performance of different combinations of input features for training the network. (T: Temperature, MM: Month, DD: Day, HH: Hour of each sample, AI: Anomaly Indicator)

Model	Vector size	Input features					MSE	R
ANN1	6	T _{Juv}	T _{Ber}	T _{Cor}	T _{Rod}	T _{Marc}	1.3590	0.9915
ANN2	9	T _{Juv}	T _{Ber}	T _{Cor}	T _{Rod}	T _{Marc}	1.4528	0.9909
		HH	DD	MM				
ANN3	33	T _{Juv-2}	T _{Juv-1}	T _{Juv}	T _{Juv+1}	T _{Juv+2}	1.2241	0.9923
		T _{Ber-2}	T _{Ber-1}	T _{Ber}	T _{Ber+1}	T _{Ber+2}		
		T _{Cor-2}	T _{Cor-1}	T _{Cor}	T _{Cor+1}	T _{Cor+2}		
		T _{Rod-2}	T _{Rod-1}	T _{Rod}	T _{Rod+1}	T _{Rod+2}		
		T _{Marc-2}	T _{Marc-1}	T _{Marc}	T _{Marc+1}	T _{Marc+2}		
		T _{Zav-2}	T _{Zav-1}	T _{Zav}	T _{Zav+1}	T _{Zav+2}		
		HH	DD	MM				
ANN4	33	Same features of ANN3 All anomalies are deleted					0.66575	0.9958
ANN5	63	Same features of ANN3 +					0.8451	0.9947
		AI _{Juv-2}	AI _{Juv-1}	AI _{Juv}	AI _{Juv+1}	AI _{Juv+2}		
		AI _{Ber-2}	AI _{Ber-1}	AI _{Ber}	AI _{Ber+1}	AI _{Ber+2}		
		AI _{Cor-2}	AI _{Cor-1}	AI _{Cor}	AI _{Cor+1}	AI _{Cor+2}		
		AI _{Rod-2}	AI _{Rod-1}	AI _{Rod}	AI _{Rod+1}	AI _{Rod+2}		
		AI _{Marc-2}	AI _{Marc-1}	AI _{Marc}	AI _{Marc+1}	AI _{Marc+2}		
		AI _{Zav-2}	AI _{Zav-1}	AI _{Zav}	AI _{Zav+1}	AI _{Zav+2}		

Based on Table 9 the overall performance of ANN3 is improved. However, deep investigations along the datasets reveal some poor performances of this model in some specific situations (Figure 21). The reason for this issue comes from the anomaly values (missing values indicated with -999 collected at other input stations) which are inserted as inputs into the model. As a result, experiencing missing values (-999) in the input data can also affect the performance of the network; not necessarily decreasing the performance, but rather the inability of the model to ignore anomalous (-999) values as inputs.

Measured Lachiarella	ANN3	Juvara	Zavatari	Marche	Berera	Rodano	Corsico
11.1	10.37417553	10.9	11.5	12	11.2	9.8	11.4
10.5	8.218272669	10.7	11.1	11.7	10.9	9.7	10.9
9.6	8.180377139	10.4	10.7	11.2	10.8	9.6	10.2
-999	-33.96005161	10.1	9.8	10.9	10.7	-999	-999
-999	-41.59355998	9.8	8.9	10.4	10.5	-999	-999
-999	-33.41657545	-999	-999	-999	-999	-999	-999

Figure 21- An example of how encountering missing values in inputs can result in weak predictions @ ANN3 with MSE=1.22 and R=0.9923

To detect the issue, model ANN4 is created based on the same features of ANN3 with input and target matrices cleaned from missing values. The procedure of cleaning the inputs follow the same procedure mentioned before: when a missing value is encountered in the target, the corresponding input and target vectors are removed, while this process is repeated for missing values in the input dataset. The results showed a significant improvement in the performance of this model, as the MSE of the ANN4 is reduced to 0.66575. This test model reveals that the selected features in ANN3 can provide a good estimation for the missing values, conditioned that anomaly (-999) values in the input matrices are ignored. Considering that in ANN4 around half of the whole dataset is deleted due to anomalies (-999) in input and target datasets, the model cannot represent a suitable estimator for this study.

The model ANN5 is proposed with an extra set of Boolean features. Regarding that for each temperature feature in the input dataset, we add this Boolean vector, where the value of “0” is inserted for anomalous value (-999) and the value “1” is inserted for the non-anomalous measurements (Figure 22). ANN3 was modeled with 33 features, of which 30 were measured temperatures. Therefore 30 additional vectors are added to ANN5 to ensure that the weighting procedure will detect anomalies while training the neural net. Figures 23 and 24 show the performance of ANN3 before adding the anomaly indicator and the improvement on ANN5 as the optimum model of this study after adding the Boolean features. In this example, missing values are also observed in other stations (and consequently the input data) during hours 21 to 31. Model ANN3 is affected with the anomalies in inputs (-999) and returns unreasonable temperatures (-20, -5), while the anomaly indicator (AI) features in ANN5 were able to ignore the -999 values and presented more reasonable predictions.

4-1-4 Conclusion

This study was an attempt to show the application of machine learning methods for infilling gaps within the raw weather data. Accordingly, with access to a network of weather stations, as well as an acceptable number of samples (in this case long-term weather data) and selecting the most appropriate input features is it possible to estimate the missing values. The most important challenge of this study was deal with the missing values alongside data sets. In this regard, a Boolean vector was proposed as a solution to improve the performance of the NN. Moreover, the performance of this method for the lengthy missing values is acceptable.

The presented method in this study could provide a similar accuracy with access to a network of weather stations and at least three years of recorded weather data. As mentioned before, various methods are presented for estimating gaps in climatic datasets (Empirical methods, statistical and function fitting methods). Providing comparisons among the performance of different infilling methods, and the framework introduced in this study can be a potential for future research.

4-2 Model fine-tuning

4-2-1 Solar model calibration

This study is developed based on sub-hourly measurements of solar irradiation, which are provided by SEAC/SolarBEAT. The measurement site is located at the Eindhoven University of Technology, the Netherlands, with 51.4° N, 5.5° E latitude and longitude, respectively. All measurements are performed with secondary class pyranometers from EKO Instruments B.V., which are installed perfectly due south. Table 10 provides an overview of the datasets utilized in this study.

Table 10- Availability of measured data in Eindhoven

Quantity	Tilt	Time steps	Period of data
Global, diffuse and direct irradiation	0°	15 minutes	2015-2017 / 24 months
	0°	1 minute	2017-2018 / 10 months
	90°	15 minutes	2016-2017 / 15 months
Global irradiation	30°	15 minutes	2015-2016 / 12 months
	15°	1 minute	2017-2018 / 10 months

Also, the method is validated for another dataset from Colorado, US which is provided by NREL Solar Radiation Research Laboratory, Baseline Measurement System (BMS) [192]. The measurement site is located on latitude 39.74° N, longitude 105.18° W. From BMS datasets, one year of measured solar radiation at an hourly timestep is collected which include: global, direct normal, sky diffuse radiation on horizontal and global radiation on two inclinations of 40° and 90° . Measured global solar radiation on 90° inclination is available for north, east, south and west orientations while measurements for 40° inclination is only provided for south orientation. Details regarding the sensor’s characteristics are reported in Table 11.

Table 11 - BMS sensors details [192]

Quantity	Sensor	Provider
Global horizontal radiation	CMP 22	Kipp & Zonen
Direct Normal	CHP1	Kipp & Zonen
Sky diffuse	CM22	Kipp & Zonen
Global radiation on 90°	PSP	Eppley Laboratory, Inc
Global radiation on 40°	CMP11	Kipp & Zonen

It should be noted that for performing building energy simulations in this study, climatic data are collected from the local weather station, i.e. global, diffuse and direct solar radiation incident on the horizontal plane. Therefore, the global, direct and diffuse horizontal solar irradiation in the TMY file is replaced with that of measured data in building energy simulations.

4-2-1-1 Model implementation

Prior to performing the calibration, measured solar irradiation datasets are divided into two portions; a training set and a test set. The training data consists of 70% of the measurements which are randomly selected from the entire dataset. The remaining 30% is used solely for testing the performance of the model after calibration. To increase the probability of sampling from the “area of interest” with smaller errors, it is necessary to define a threshold, based on which unwanted samples are rejected. In this study, the performance of the MCMC is evaluated based on the Euclidean distance between absolute zero and a custom measure dubbed the “Threshold”, i.e. equation (Eq.31). The Threshold is calculated from the CV_RMSE (%) and MAE of all datasets with various tilts.

$$Threshold = \left[\begin{array}{l} (CV_{RMSE_{Tilt\ 90}})^2 + (MAE_{Tilt\ 90})^2 + (CV_{RMSE_{Tilt\ 30}})^2 + \\ (MAE_{Tilt\ 30})^2 + (CV_{RMSE_{Tilt\ 15}})^2 + (MAE_{Tilt\ 15})^2 \end{array} \right]^{\frac{1}{2}} \quad (Eq.31)$$

Where:

$$RMSE = \left[\frac{1}{n} \sum_1^n (GI_{Measured} - GI_{Simulated})^2 \right]^{\frac{1}{2}} \quad (Eq.32)$$

$$CV_{RMSE} = RMSE \left(\frac{1}{n} \sum_1^n GI_{Measured} \right)^{-1} \quad (Eq.33)$$

$$MAE = \frac{1}{n} \sum_1^n |GI_{Measured} - GI_{Simulated}| \quad (Eq.34)$$

The performance of the SuS calibration method is illustrated in Figure 25. The default state which is not affected by any uncertainty is indicated by a black cross. As the first step, a Latin hypercube sampling (LHS) is applied to the uncertain parameters. The number of samples for the first LHS is defined based on the work by Loeppky et al. [193]. Regarding that, a suitable choice for the number of random samples can be considered as $n=10*d$, where ‘n’ is the number of generated random samples and ‘d’ refers to the number of uncertain variables. From Figure 25 it is visible how the SuS reduces the error between calculation and measurements of solar radiation on a tilted surface. After the 20th Subset, the minimum is obtained based on the selected thresholds, which indicate the calibrated version of default parameters.

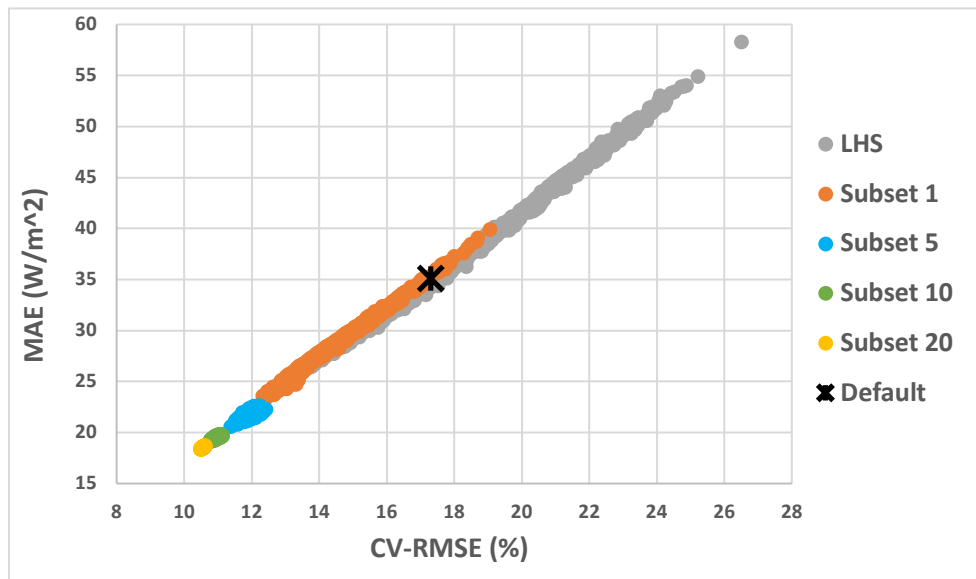


Figure 25- Illustration of the performance of SuS. According to the proposed method, after the 20th subset, the thresholds reach to a stable minimum level

As a first run, the calibration method is developed based on Eindhoven dataset. The SuS yields the calibrated parameters i.e. ground albedo and Perez sky coefficients. The calibrated ground reflectance returns a value of 0.1, which is notably smaller than the default value (0.2), yet can be explained by the fact that a black rubber mat is placed below the pyranometers in the experiment. The Perez sky coefficients fitted to Eindhoven sky conditions are presented in Table 12.

Table 12- The numeric value of Perez irradiance coefficients after calibration for Eindhoven sky

	Sky clearness	F11	F12	F13	F21	F22	F23
Overcast	1 – 1.065	0.243	0.707	-0.188	0.096	0.448	-0.001
	1.065 – 1.230	0.289	0.633	-0.200	0.113	0.425	0.004
...	1.230 – 1.500	0.373	0.499	-0.222	0.145	0.382	0.016
	1.500 – 1.950	0.503	0.296	-0.256	0.194	0.316	0.034
	1.950 – 2.800	0.709	-0.011	-0.312	0.273	0.215	0.066
	2.800 – 4.500	1.005	-0.388	-0.398	0.393	0.081	0.124
	4.500 – 6.200	1.230	-0.536	-0.475	0.495	0.006	0.192
Clear Sky	6.200 – ...	0.999	0.467	-0.469	0.463	0.244	0.274

A comparison between the lines fitted to original Perez coefficients and calibrated ones are also presented in Figure 26. Among the brightening coefficients, F12 from circumsolar brightening and F22 from horizon brightening coefficients showed the most sensitivity to associating the uncertainty on sky conditions. From Figure 26 it is inferred that the calibrated version of coefficients for overcast and semi-overcast sky conditions are close to the original Perez model, however, passing from overcast to clear sky conditions shows an underestimation of these parameters for Eindhoven sky conditions.

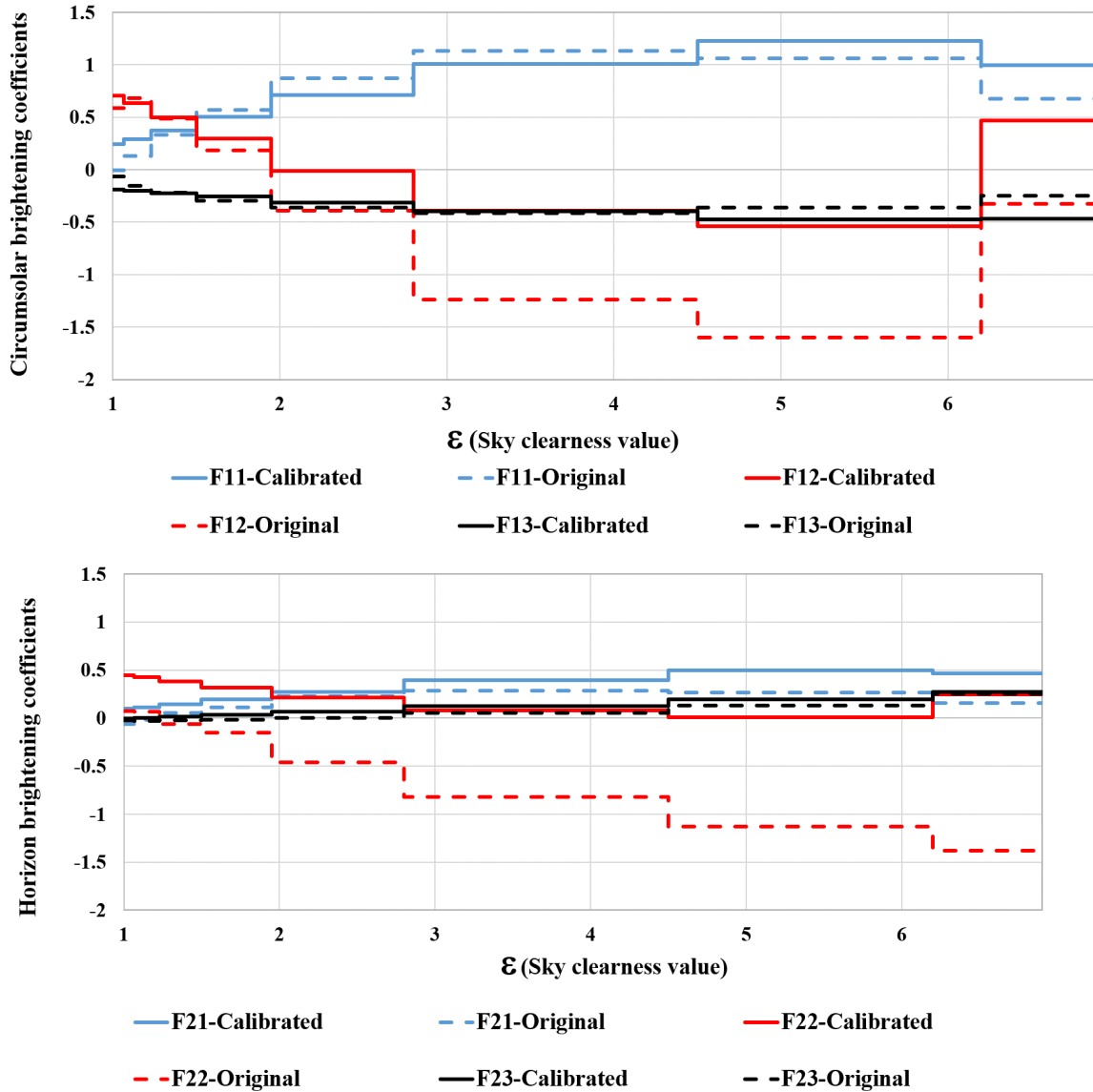


Figure 26- Comparison between original and calibrated Perez for Eindhoven

The performance of the calibration process is reported in Table 13. The improvement of estimation using a calibrated model is evaluated on the test dataset. As mentioned before, the whole dataset is divided into two portions of training and test sets. The calibration procedure is performed on the training portion of the dataset and after that the calibrated version of Perez is verified by another dataset which has not been involved in calibration procedure. Table 13 confirms that the Perez model which is calibrated based on the proposed method is not overfit on the training data. This statement is evident as the performance of the test set is close to that of the training set. The highest improvement was observed for 30° of tilt, reducing the RMSE from 57.6 W/m² to 36.6 W/m². This improvement was slightly smaller for the 90° estimations with the calibrated model.

Table 13 - Performance of the proposed calibration method based on Eindhoven data. The units of the statistical indicator are as following: RMSE(W/m^2), CV-RMSE (%), MAE (W/m^2)

		South 90°	South 30°	South 15°
Original Perez	RMSE	37.56	57.67	55.46
	CV-RMSE	13.95	13.91	21
	MAE	27.17	40.07	40.37
Training set Calibrated Perez	RMSE	32.15	36.62	40.17
	CV-RMSE	11.93	8.83	15.21
	MAE	22.33	25.67	28.07
Test set Calibrated Perez	RMSE	32.93	36.17	40.49
	CV-RMSE	12.38	8.87	15.67
	MAE	22.3	25.42	27.74

In the next step, the defined methodology is adopted on the BMS dataset to determine the calibrated version of the Perez model based on Colorado sky conditions. Solar measurements in all orientations of 90° and 40° on the south are used at the same time for calibration. A comparison between the Perez model with original and calibrated coefficients is shown in Table 14.

Table 14 - Performance of the proposed calibration method based on Colorado (BMS) data. The units of the statistical indicator are as following: RMSE(W/m^2), CV-RMSE (%), MAE (W/m^2)

		North 90°	East 90°	South 90°	West 90°	South 40°
Original Perez	RMSE	43.55	50.34	58.59	48.01	70.28
	CV-RMSE	36.45	16.51	15.91	19.92	13.21
	MAE	28.24	34.42	39.10	32.19	54.80
Calibrate Perez	RMSE	39.70	46.45	49.98	44.49	35.83
	CV-RMSE	30.99	13.08	12.25	16.23	10.41
	MAE	21.18	23.92	27.67	22.81	45.55

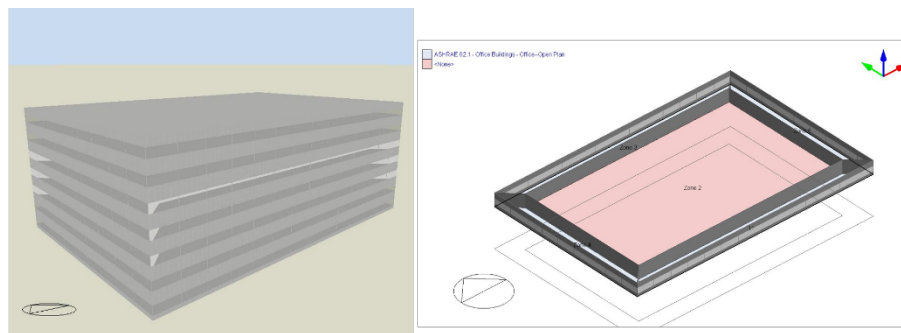
4-2-1-2 Result and discussion

The effects of opting for a calibrated Perez model and the impacts on a building's estimated energy performance are discussed in this section. The original Perez model coefficients for irradiance are replaced with the calibrated coefficients in EnergyPlus software, and both the original and calibrated sky models are then tested on a typical building energy model. This study has modified the EnergyPlus source code collected from the development repository available from [194].

In this study, two separate simulations based on the availability of measured data from the two locations performed. The effects of using a calibrated Perez model in Eindhoven is tested for the performance of PV panels, as the focus of calibration is only on the south façade. Also, the building cooling and heating loads are evaluated for a specific zone in Eindhoven. On the other hand, BMS data from Colorado was calibrated on four main orientations due to the availability of measured data. This facilitated running whole building simulations and investigating the building's energy performance.

In this study, the term “Base-EP” refers to the default EnergyPlus code with original Perez coefficients and a ground reflection of 0.2. The term “Modified-EP” refers to the modified EnergyPlus code with calibrated Perez parameters and a ground reflectance.

The analysis related to comparisons of building heating/cooling loads is performed based on an energy model that is realized based on ASHRAE's large office Reference Building (Figure 27). All the templates and building configurations are assumed as ASHRAE's default settings. The whole building model as mentioned is involved in analysis related to Colorado data set while for the Eindhoven data only one zone is considered.



ASHRAE 901- OfficeLarge

Figure 27- ASHRAE 90.1, Large office. The case-study building energy model.

4-2-1-2-1 Effect of calibration on PV performance

To simulate the performance of PV panels at three inclinations of 90°, 30°, and 15°, simple geometry is considered with PV installed at the aforementioned inclinations. For each tilt angle, two simulations are performed based on the original and calibrated Perez coefficients. The heat transfer integration mode of PV in EnergyPlus is set to “*Decoupled Ulleberg Dynamic*” and the performance evaluation selected as “*Equivalent One-Diode*”. Table 19 and Figure 28 comprehensively report the results of the Base-EP and Modified-EP in predicting the electricity yield for each square meter. The percentage of error in Table 19 is calculated based on Eq.35 while Eq.36 quantifies the average error between the two cases of Base-EP and Modified-EP.

$$\text{Percentage of error} = \frac{\text{Modified}_{EP} - \text{Base}_{EP}}{\text{Modified}_{EP}} * 100 \quad (\text{Eq.35})$$

$$\text{Mean bias error} = \text{mean}(\text{Modified}_{EP} - \text{Base}_{EP}) \quad (\text{Eq.36})$$

The largest difference in the estimated electricity production is observed at 15° inclination, reaching as high as 9% (Table 15). This is related to the high exposure of 15° inclined panels to the sky as well as the sensitivity of this tilt to changes in Perez model characteristics. Also, it is notable that the Base-EP over-estimates the performance of PV panels, regardless of the orientation. The smallest variation (i.e. 2%) is observed at 90° inclination which underlines the low sensitivity of energy production on vertical PV to Perez Coefficients.

Table 15 - Comparison of energy produced between the Base EP and Modified EP

	PV 15	PV 30	PV90
Percentage of variation (%)	-9.41	-5.74	-1.99
Mean Bias variation (kWh)	-20.05	-14.06	-3.87

Figure 28 presents a comparison between the original Perez and the calibrated version, by resorting to the probability distributions of electricity produced by each square meter of PV. It is shown that the Base-EP underestimates the density of produced electricity for 15° and 30° of tilt, specifically in lower values, as demonstrable around the median of the probability distributions. In 90° however, the density of the produced electricity follows a similar pattern in both Base-EP and Modified-EP cases, yet, a shift of one W/m² is observed in the general trend.

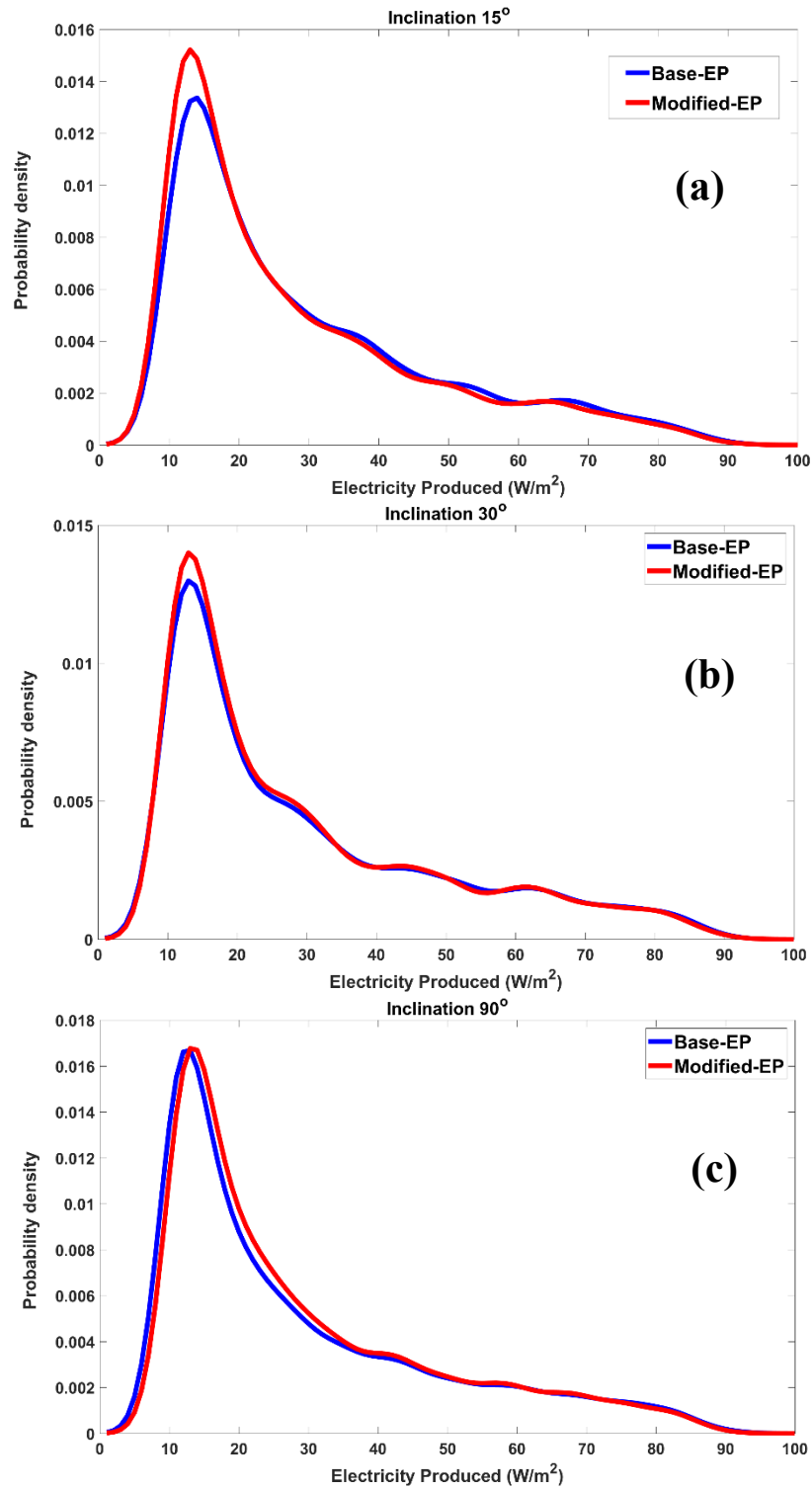


Figure 28- Comparison between the produced energy by simulated PVs based on Base-EP and Modified-EP, an illustration of the probability distribution. PVs are located with (a) 15°, (b) 30° and (c) 90° of inclination

Figure 29 indicates that the calibrated implementation of the Perez model returns different estimations of incident solar irradiation on vertical surfaces. It is understood that the Base-EP overestimates incident solar irradiation on the south facade. Also, it can be clearly observed how the calibrated model Perez shifts the estimations of solar irradiation with Modified-EP to real measurements.

To have a more robust observation of the calibration’s impact, a single thermal zone oriented due south is selected. The area of the studied zone is 340.72 m² and the studied zone is preserved from the adjacent indoor spaces by considering internal boundary conditions as adiabatic. In free-floating conditions, indoor comfort is strongly correlated by the building’s boundary conditions, and therefore, any changes in the surrounding environment can affect the indoor comfort conditions. The indoor temperature based on Base-EP and Modified-EP is compared in Table 16. The Modified-EP reported a smaller frequency of temperatures in comfort bound while the frequency of heating hours ($T < 20$) is increased.

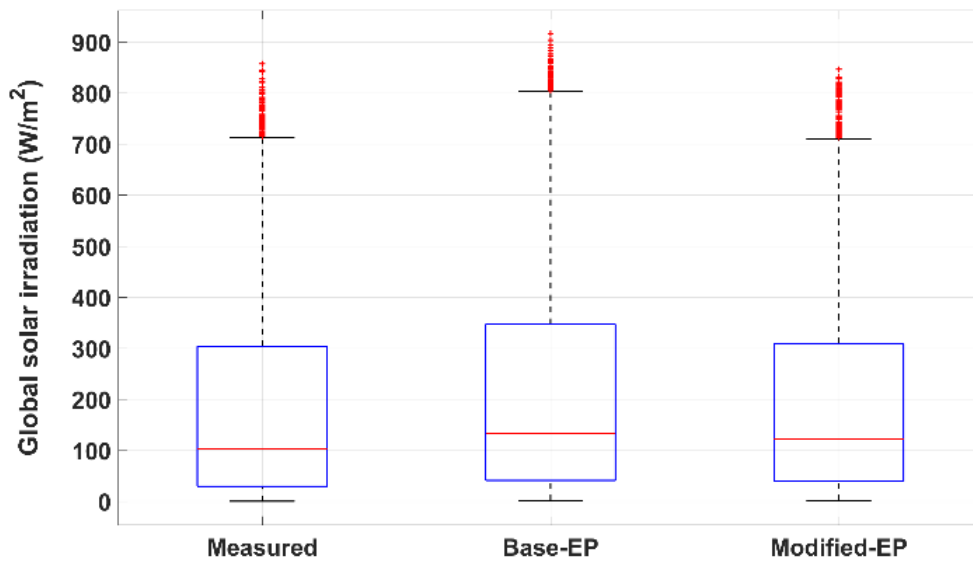


Figure 29- Comparison of incident solar irradiation on vertical surface

Table 16- Indoor temperature frequency in free-floating conditions

Indoor temperature (°C)	Base-EP (hours)	Modified-EP (hours)
$T < 20$	5805	6067
$20 \leq T \leq 26$	2715	2522
$T > 26$	240	171

Building’s heating and cooling loads are also compared using both default and modified EnergyPlus models. The results of annual heating and cooling loads reveal that the overestimation of solar irradiation by EnergyPlus mostly affects the cooling loads (Table 17). Consequently, the default Perez model overestimates the annual cooling load by approximately 12%, in the considered climate context. Moreover, the difference in the peak cooling loads obtained by the two models is significant (9%). On the other hand, it can be argued that the variation of annual heating energy use and peak heating load are negligible when a setpoint of 20°C is considered.

Table 17 - Effect of calibrated Perez model on the estimations of heating and cooling loads

	Annual energy (MWh)		Peak load (kW)	
	Heating	Cooling	Heating	Cooling
Base-EP	21.72	15.52	37.82	11.83
Modified-EP	22.48	13.75	37.87	10.85

Since the frequency of peak loads can affect the system sizing process, the cumulative distribution of all cooling loads is provided in Figure 30. It is observed that when opting for a 90% reliability, the Base-EP returns a cooling load of 5569 W, which corresponds to a cooling system with at least 5500 W of capacity. Meanwhile, the Modified-EP returns a cooling of 4933 W for the same level of reliability (90%), which corresponds to a smaller system with a capacity of 5000 W.

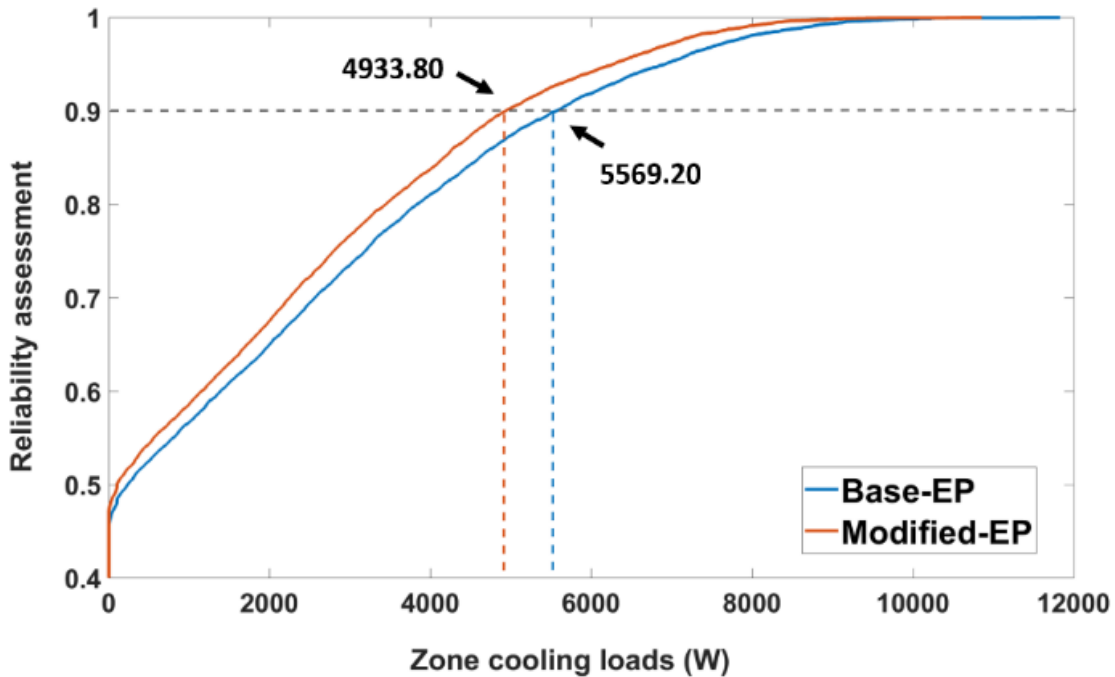


Figure 30 - Reliability assessment of the proposed cooling system

4-2-1-2-2 Effect of calibration on whole building energy performance

The first analysis is focused on the estimations of incident solar radiation on exterior surfaces, by comparing outputs of the default (original Perez) and modified (calibrated Perez) EnergyPlus variants. Figure 31 indicates that the calibrated implementation of the Perez model returns different estimations of incident solar irradiation on vertical surfaces. The boxplots in Figure 31 reveal under-estimation of incident solar radiation by Base-EP in Colorado recurring for all orientations. The effects of calibration on building energy quantities in terms of cooling and heating loads are also evaluated. For this, cooling and heating energy consumptions are extracted from both Base-EP and Modified-EP cases. The HVAC template of ASHRAE large office is set as a boiler with gas as the fuel for heating and chiller with electricity for cooling [195].

The results of whole building energy simulations are shown in Table 18. The percentage of error is calculated based on (Eq.35). Based on Table 8 the calibrated version of Perez has a notable effect on the estimation of heating energy consumption in Colorado, reaching 5%. Meanwhile, the variation in cooling energy consumption is negligible. These results are in line with the observations from the previous analysis, displaying lower solar radiation on the façade for the Base-EP scenario.

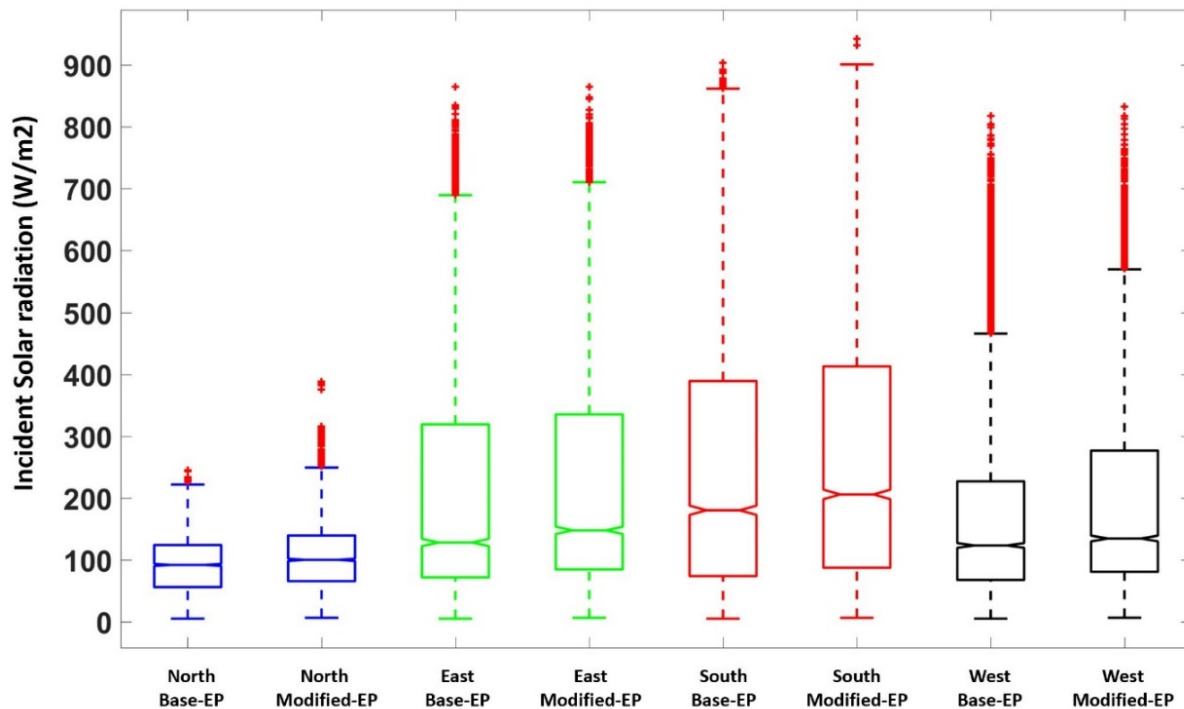


Figure 31- Incident solar radiation on building facades(W/m^2), comparison of Base-EP and Modified-EP

Table 18- Cooling and heating energy consumption in ASHRAE large office, a comparison the effect of calibrating Perez model in Base-EP and Modified-EP

Annual (MWh)	Base-EP	Modified-EP	Percentage of variation (%)
Cooling energy consumption (Electricity)	1417.36	1431.06	-0.96
Heating energy consumption (Gas)	1039.47	986.03	5.42

4-2-1-3 Conclusion

In this study, a method for calibrating the Perez sky diffuse model using Subset Simulation is proposed. The introduced method can minimize the multivariable objective function. i.e., MAE and CV-RMSE. Also, the sequential sampling nature of SuS enables smaller sample size and therefore, higher calibration speed. The proposed method is tested on measurements from three inclinations of 90°, 30° and 15° in Eindhoven, and afterwards further validated on a dataset of measurements obtained from Colorado for various orientations. The proposed calibration method can be easily adapted to other locations and is not case dependent.

The calibrated Perez model with modified sky condition coefficients is implemented into building energy simulation tool EnergyPlus. Results showed that the Perez model with default coefficients overestimates the PV electricity production in Eindhoven by 9%.

The effect of calibrating Perez model on whole building energy performance was also studied with measurements obtained from Colorado. Using default Perez coefficients in Colorado, however, results in the underestimation of the incident radiation on inclined surfaces. The effects are reflected in a 5% variation in the heating energy consumption of an office building.

Validation of the proposed method on more sites with different climate conditions and the impacts on building energy performance is still in high demand. Also, the current study was developed based on measurements with 15 minutes interval, and yet evaluated in the hourly performance of heating/cooling systems. Therefore, the evaluation of the proposed method for various timesteps is a high-potential direction for future studies.

4-2-2 Building energy model fine-tuning

In Chapter 3, DIVA is suggested as an appropriate tool for detailed modeling of solar radiation within an urban canyon. Climate and time steps, target and surrounding elements, sensor points, and RADIANCE parameters are introduced as the important hyperparameters that should be fine-tuned suitably.

The sensor points in DIVA have two attributes, i.e. orientation and direction. In DIVA, positive y-axis is assumed as North orientation. Direction of the sensors is assigned with values between $[-1, 1]$ for x, y, and z which can be located in horizontal or tilted conditions. Solar radiation is typically collected on horizontal surfaces (Figure 32-b), however, in this study, solar radiation on vertical surfaces is intended. To estimate incident solar radiation on building facades, a series of sensor points should be considered to be located vertically on the facade and due to target orientation (Figure 32- a).

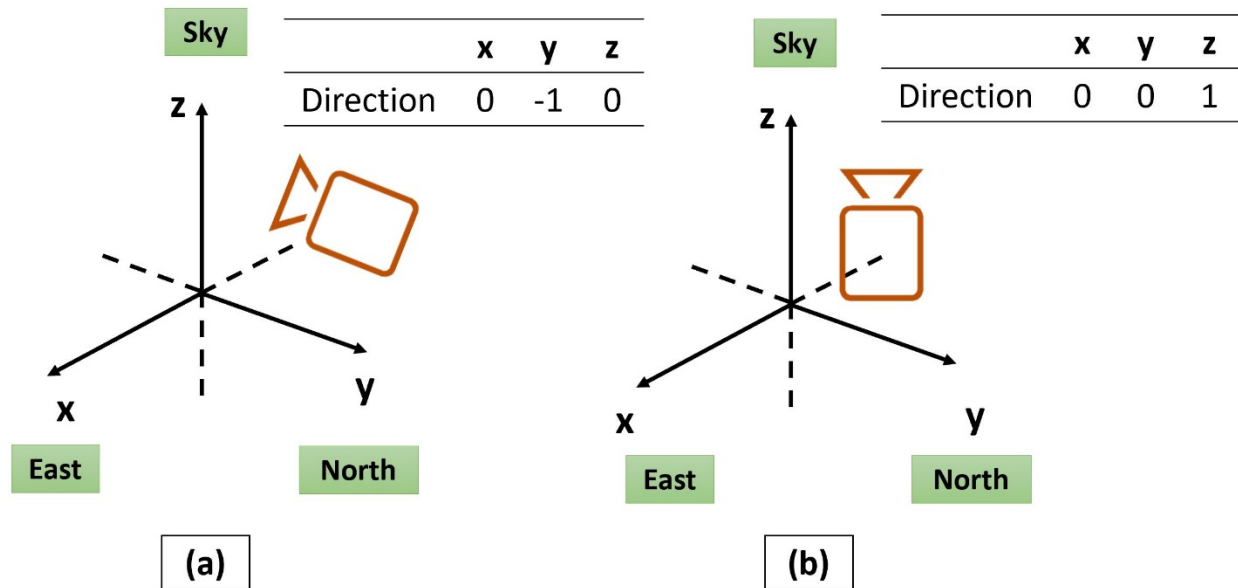


Figure 32- Samples of sensor direction and orientation settings in DIVA. (a) The camera (assumed as a sensor) is faced due to the south, collecting data on the vertical surface, (b) The camera is facing up, collecting data on horizontal surface

Ambient bounces (ab) is the most important among the RADIANCE parameters and, as mentioned in Chapter 3, the quality of results and computational time are affected by Ab. Therefore, ab should be carefully decided in initial steps. Moreover, since this research study needs numerous simulations the computational time is a key factor in deciding about the ambient bounce value.

Regarding that different choice of ambient bounces are tested for both simple and complex canyon. Some clarification is reported in Table 19. Besides the time of simulation, the R-squared (R^2) value is calculated to analyze the difference in the quality of estimations. In all comparison, the

simulation model with $ab=2$ is fixed in X-axis of regression plot, and the Y-axis varies between simulation models with $ab=5$, $ab=7$, and $ab=7$ (high-quality). Results of R^2 are also presented in Table 19.

Table 19- Comparison of different ambient bounces and simulation results for estimation solar radiation

Simulation model	Simulation time(s)		R-squared
ab2- low quality	120	-	-
ab5- custom quality	300	ab2 vs. ab5	0.999
ab7- custom quality	300	ab2 vs. ab7	0.9992
ab7- high quality	25200	ab2 vs. ab7 high quality	0.9989

Results revealed that unlike the illuminance analysis, effects of ambient bounces for solar radiation incident on exterior surfaces in DIVA simulations is negligible. Regarding the highlights in Table 19, the ambient bounce of two ($ab=2$) is considered for the uncertainty analysis of solar radiation within the urban canyon.

4-2-2-1 Investigation on modeling trees in the urban canyon

The representation of trees in the environment of building performance simulation is a significant challenge. Seasonal effects, shape/size, and transparency of trees are the main challenges concerning trees. In this section, an investigation on the best modeling approaches of trees within the urban canyon is presented. This section aims to render the best solutions to model trees regarding the following factors:

- The model should present the tree’s seasonal change
- The geometry of the model should be flexible for uncertainty analysis
- The computational time should be minimal
- The transparency of the trees should be reflected into the model

The first activities in this section are focused on defining the transparency of trees. As mentioned in section 3-3, by considering the tree leaves material as “trans” type in Radiance material database, it is possible to consider both seasonal change and the transparency of trees to direct solar radiation. As suggested by Tregenza et al. [188], the transmittance of trees can be anywhere from 0.38 in summer to 0.94 in winter, depending on the type and context of the tree. Figure 33 displays some proposed values.

Single plane tree transmittance / transmissivity values				
tree type	transmittance		transmissivity	
	Tn. winter	Tn. summer	Tns. winter	Tns. summer
urban tree	0.55	0.15	0.60	0.16
small decorative / immature tree	0.75	0.25	0.82	0.27
evergreen conifer	0.15	0.05	0.16	0.05
Simple volumetric tree transmittance & transmissivity values				
tree type	transmittance		transmissivity	
	Tn. winter	Tn. summer	Tns. winter	Tns. summer
urban tree	0.74	0.387	0.81	0.42
small decorative / immature tree	0.86	0.5	0.94	0.54
evergreen conifer	0.39	0.22	0.42	0.24

Figure 33- A screenshot from Diva4Rhino forum. Suggested values for tree transmittance for summer and winter [196]

The next step is related to defining the best geometry as a representative model of trees in this study. Regarding that, a sensitivity analysis is performed to find the best case. The first analysis is focused on the validity of the selected materials. Rays of solar radiation hit the face of trees which are exposed to the sun, from which some parts of them are reflected, some absorbed, and of the rest pass through the gaps between the tree’s foliage. The trans material provides the potential of importing these characteristics to geometry model. According to Tregenza et al. [188], the sphere geometry is the best choice to reflect the material’s property. In this step, the trans material is applied to two shapes, i.e. a box, and a sphere (Figure 34).

The solar radiation sensors are located on the studied area while simulations performed on sensors placed horizontally. The hourly values of incident solar radiation for one year of simulation is extracted. Results are compared for three levels, i.e., ground, middle to top floors. According to this observation, using the same material properties, the lowest values are recorded for the case with the tree as a box (Figure 34). This difference is related to the way that Radiance considers boxes and spheres. A box is assumed as geometry with six surfaces. Therefore, the incident ray on the box, enter to the geometry from a surface with defined transmittance (here,0.42), while the part passing through and already attenuated, departure from the other face of the box, and again is

affected by another 0.42 transmittance ratio. While the sphere is considered as geometry with one surface.

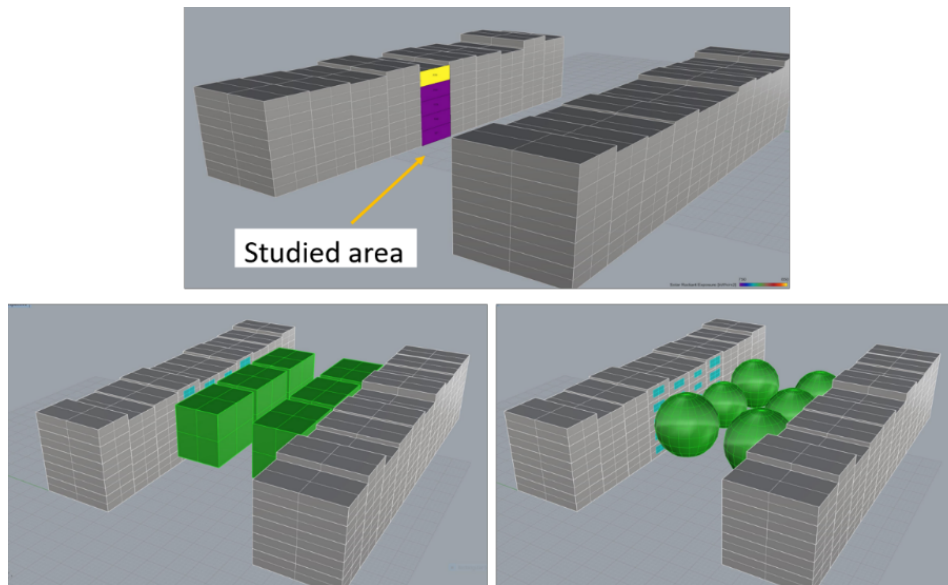


Figure 34 - Studied area (Up), Comparing the effect of trans material on two geometry for trees (Down)

Figure 35 Compares the availability of solar radiation on building façade in two different models of the urban canyon; (1) Trees modeled as a sphere, and (2) trees modeled as a box. From Figure 35 it is observed that the difference between modelling trees by sphere or box mainly affect the incident solar radiation on the middle floor.

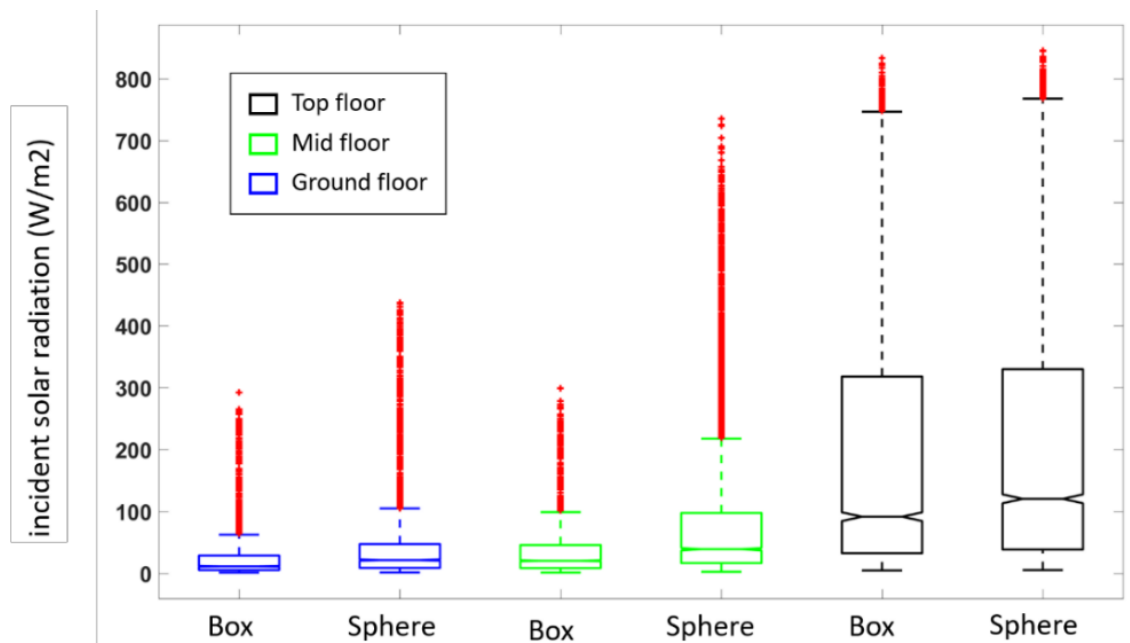


Figure 35- Contrast incident solar radiation on south facade affected by shadows from trees as box and as sphere

Therefore, the sphere is chosen as the default shape of trees in this study. In the next step, the transparency of trees is assessed through detailed modeling which considers the density of leaves. For this, two models of trees are considered: (1) a simple geometry with reflected winter/summer change in material properties attained by assigning different transmittance values, and (2) a detailed geometry where the seasonal change shaped by the changing the leaf area percentage (Figure 36 and 37).

In Figure 37 the green box-plots refer to the simple geometry, where the winter and summer transparency of trees to solar radiation selected is defined as 0.82 and 0.41, respectively. In the detailed models, leaf area percentage is randomized in Grasshopper to simulate the winter and summer shape of trees. The random value varies between 8-2, where 8 presents the most transparent state of the tree, while two can be considered as a fully covered condition in summer. A comparison between the simple and detailed geometries revealed that random sample 4 could suitably present winter transparency, while random sample 2 can be considered as the state of the tree in summer. However, such detailed modeling of trees significantly increases the computational time.

The simulation time of a highly dense single tree (random 2) was twice longer than that of a simple tree model. This extra computational time is utterly important for this study, since adding more trees along with other parameters inside the canyon such as windows, external shadings and cars add a significant load on the simulation time. Therefore, the UA of the urban canyon in this study is developed based on a simple tree geometry, with the winter/summer effects reflected within the material.

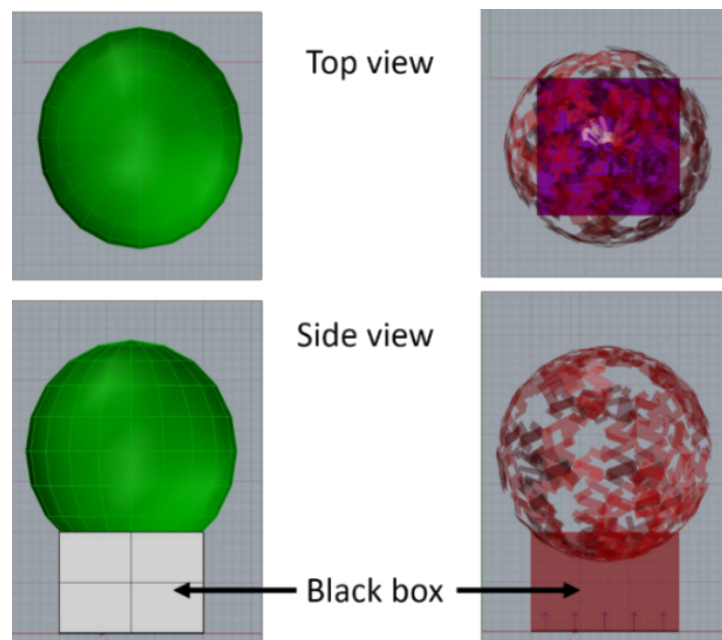


Figure 36- Detailed tree model is compared with the simple model.

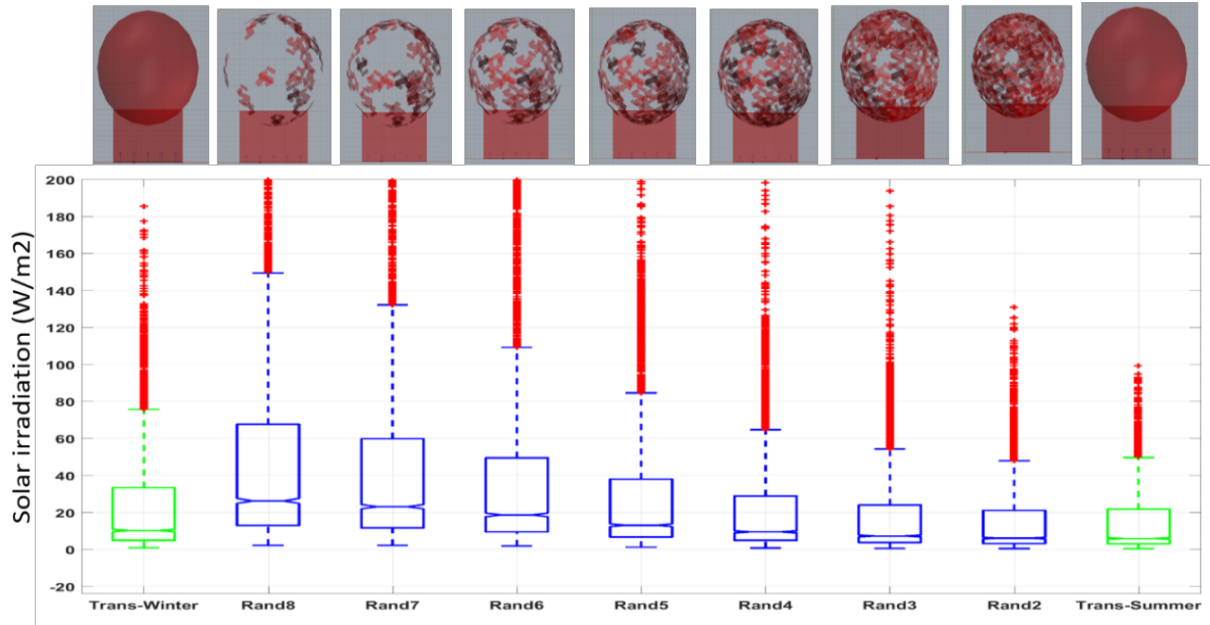


Figure 37- Sensitivity analysis of detailed tree modeling, the decision about modifying the material transparency or precise model

4-2-2-2 Uncertainty propagation

In this section propagating the uncertainty within the urban canyon model, including (1) the approach of propagations, (2) range of variation and (3) method of implementing in DIVA software is described.

Proposed hybrid sampling approach is adapted to generate random samples of the studied complex urban canyon. As mentioned in Chapter 3, in this study seven variables are selected as uncertain parameters in an urban canyon. Table 20 presents the details about each uncertain parameter.

Table 20- uncertain parameters in urban canyon and range of variation

Uncertain parameters	Unit	Variation	Definition of uncertainty
Ratio of building height	%	±10% (survey)	Probabilistic
WWR	%	[15,60] (survey)	Probabilistic
External shading	On/off	[0,1] (scenario)	Boolean
Exterior wall reflectance	-	[0.1,0.3] (survey)	Probabilistic
Trees crown dimeter	m	[4.5,10] ([197])	Probabilistic
Tree transmittance	-	[20,30] ([185])	Possibilistic
Cars reflectance	-	[0.05, 0.58] ([186])	Possibilistic

Parameters related to the geometry of the canyon can be considered as probabilistic uncertainty since enough data have been collected to fit a probability distribution function on the measurements. The term “survey” in Table 20 refers to observations from an actual urban canyon which is located in Milan, Italy. The basic height of surrounding buildings, glazed area (WWR) and reflectance of the opaque area are estimated based on the mentioned survey. The height of the surrounding buildings varies by $\pm 10\%$ against the baseline building height. A variation between 15%-60% is observed for WWR from surveying the canyon. The reflectance of surrounding buildings is defined based on the façade colors and materials.

In this study, uncertainty in the transparency of tree and reflectance of car bodies are assumed as possibilistic uncertainty because adequate data cannot be collected either on-site or from the literature. The transparency of tree and reflectance of car bodies, is derived from measurements obtained from [185] and [186], respectively.

Also, in chapter 3, it is discussed that random sampling based on possibilistic distribution should be performed through defining several α -cuts (see section 3-2-2-3). Therefore, three alpha-cuts are assumed for possibilistic distributions of this section and 6 different random samples are generated from the upper and lower bound of distribution in α -cut of 0, 0.5 and 1. Figure 38-a shows the distribution of transparency of the trees, while the variation in car body reflectance is illustrated in Figure 38-b.

The next step is implementing the samples generated by MATLAB in DIVA-Grasshopper. Figure 39 shows how imported values from MATLAB are assigned to building components in DIVA Grasshopper. Each random sample is a combination of building geometry parameters, tree features, and car body reflectances. All the algorithms and developed codes related to sampling procedure are reported in Annex 2.

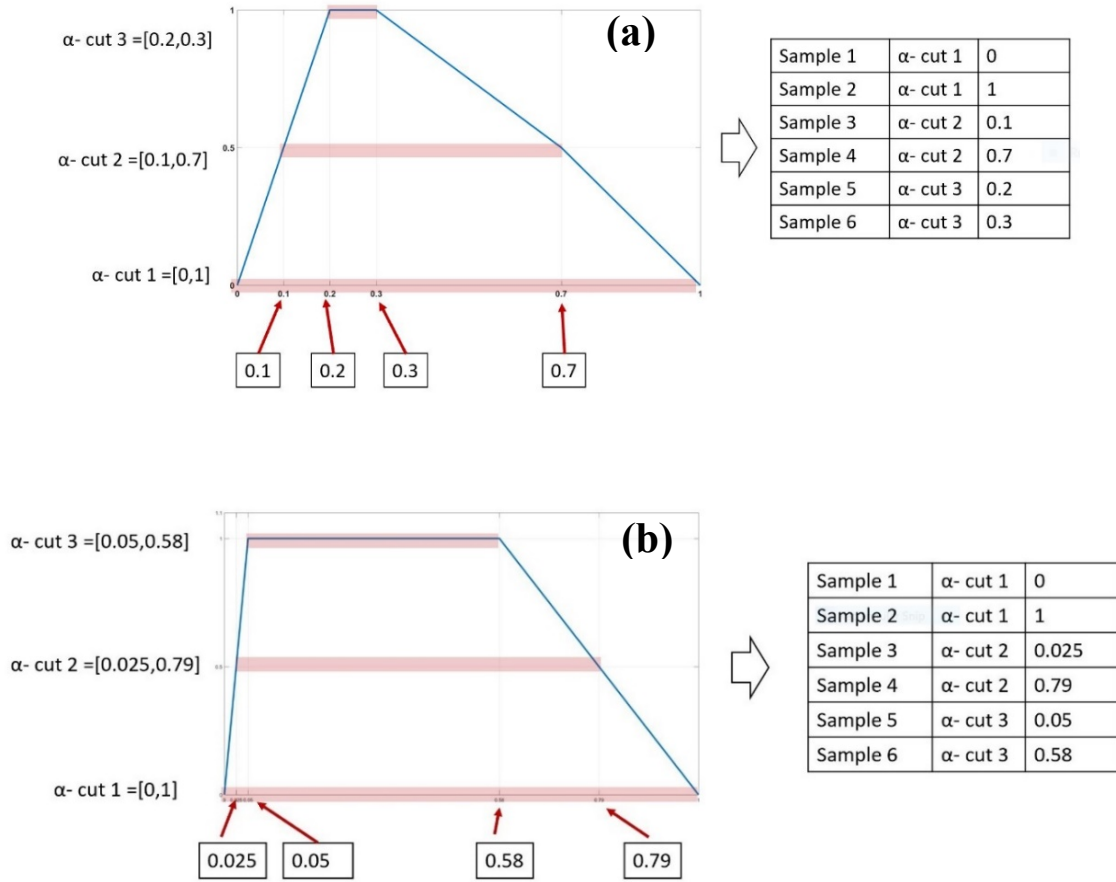


Figure 38- Possibility distribution of (a) transmittance of trees, (b) cars reflectance

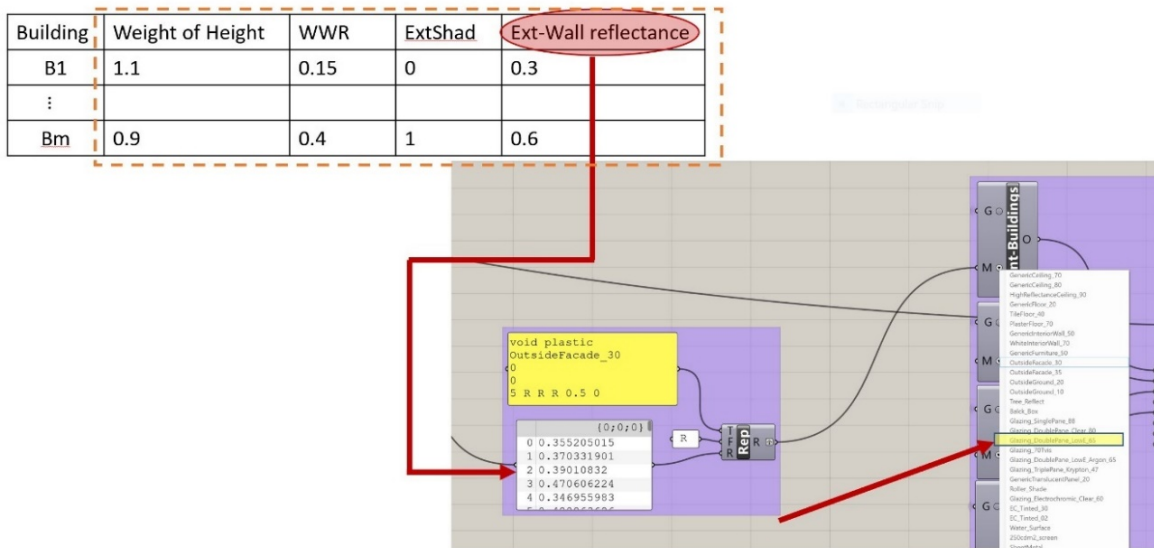


Figure 39- A sample of how each generated sample is assigned to Building geometry in Grasshopper

4-2-2-3 Sample canyon model

The framework of uncertainty quantification is tested on a sample case study. The case study is a canyon with an aspect ratio of 0.5. DIVA simulations are performed with two conditions: (1) a simple canyon according Figure 16, (2) sixty different random samples are generated with a range of uncertainty according to selective parameters (Figure 15). Ground, middle and top floors are targeted from the entire studied area, while hourly results of global, direct and diffuse solar radiation incident on the target surfaces are extracted from DIVA simulations. This study has focused on South façade.

Figure 40 provides a comparison between the typical condition of modeling urban canyon and the uncertainty approach. According to Figure 40 and based on the height of the building, the effects of surroundings may be dissimilar. For example, the maximum of variation in solar radiation on the ground floor is observed in the 90th percentile while the 75th percentile returned the maximum difference for the middle floor. In the upper floors, less variation of solar radiation is observed due to reducing the effect of trees, being the main challenging feature in the urban canyon.

Table 21 presents a numerical assessment of the variation in incident solar radiation on building façade, whilst regarding the uncertainties in boundary conditions. Based on Table 21, the difference between the lowest and highest solar availability obtained from 60 random samples in 90th percentile is 151 W/m² for the ground floor, while 59 W/m² of difference is observed for both middle and top floors in the 90th percentile. The difference between lowest and highest solar availability in 75th percentile is 64, 105 and 41 W/m² for ground, middle and top floor, respectively. The reported values of solar radiation in Figure 40 and Table 21 are related to global solar radiation. It is clear that the uncertainty of incident solar radiation mainly comes from the diffuse and ground reflection components of solar radiation, since the peak of variation is observed in the ground floor. The lower floors in the buildings within a complex urban canyon are strongly subjected to shading from trees and surrounding buildings. Also, effects of reflected solar radiation from ground and other elements such as parked cars mostly influence the incident solar radiation on lower floors of the buildings (e.g. ground floor, first floor). Therefore, the main part of global solar radiation comes from diffuse and ground reflected components rather than the direct components. Vice versa, in top floors where the effect of shadowing is minor, a smaller range of variation in solar radiation is observed. The highest variation is in the middle floor at the 75th percentile, which arise from the effect of both diffuse and direct components of solar radiation at this level.

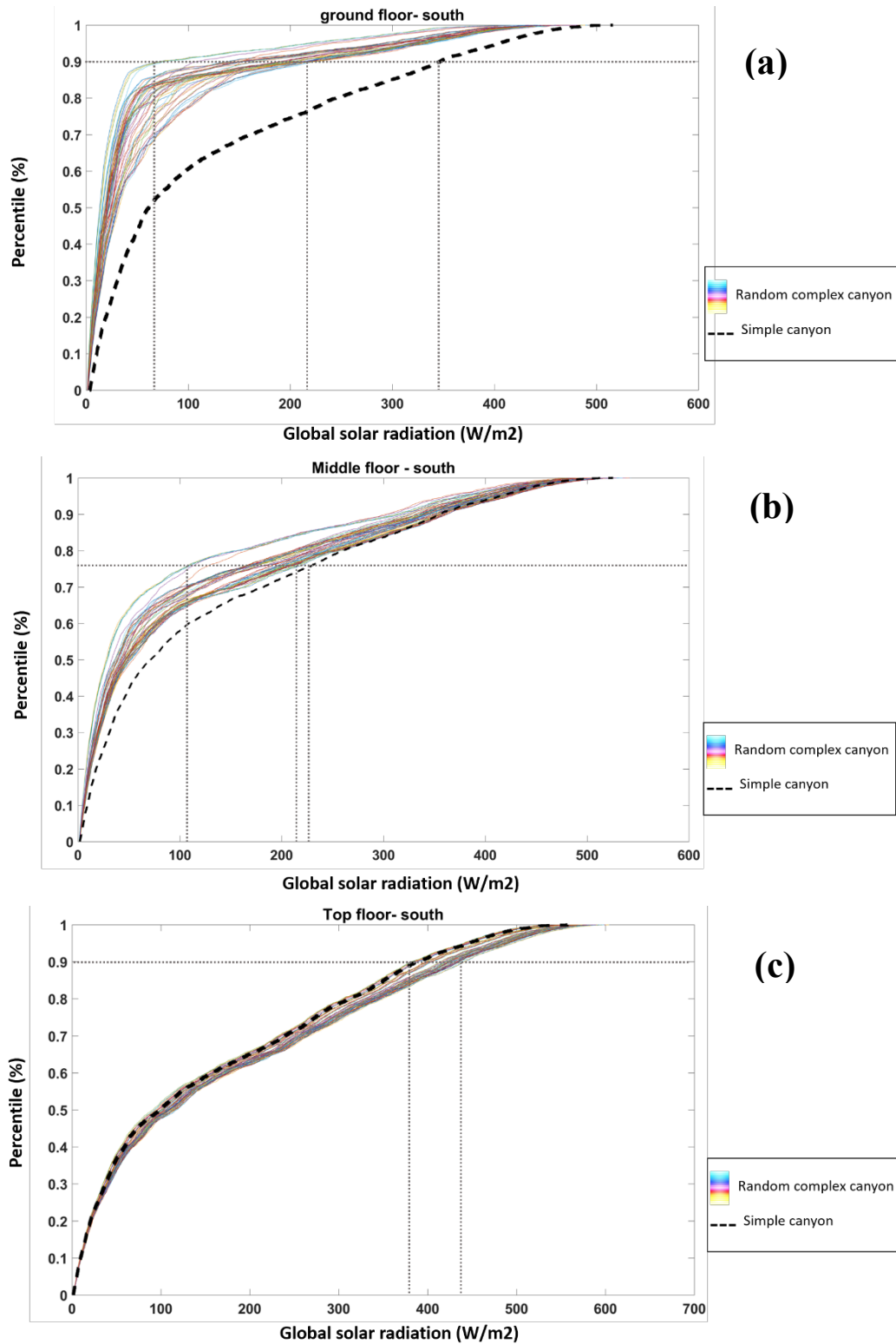


Figure 40- Uncertainty analysis of incident solar radiation on south façade on three floors: (a) ground floor, (b) middle floor, (c) top floor.

Table 21- Solar radiation (W/m²) among the 60 random samples in 75th and 90th percentiles

	90 th percentile [min, max]	75 th percentile [min, max]
Ground floor	[75 , 226]	[26 , 90]
Middle floor	[302 , 361]	[102 , 207]
Top floor	[381 , 440]	[266, 307]

To illustrate the variation of incident solar radiation based on uncertainties in boundary conditions, daily profile of typical solar days is compared with the Simple canyon as in Figures 41-43. Three representative days are selected as the summer, intermediate season and winter day. The highlighted days are selected based on highest, intermediate and lowest solar elevation during the year. Daily profiles are created for 21st March, 20th Jun, and 22nd December. Estimated incident solar radiation based on simple and random complex canyons are compared in the following figures. The first observation from Figures 41-43 points to the difference between the probabilistic approach and the deterministic approach of modelling the building boundary conditions. When the deterministic approach (as in Simple canyon) is considered a single value is obtained for every hour which may result in over/underestimation of the actual incident solar radiation. However, the probabilistic approach (random complex canyons) provides a range of variation for each hour of day, within which exists the actual incident radiation.

During the intermediate seasons (Figure 41), the high sensitivity of incident solar radiation that is affected by uncertainties in the boundary conditions, is observed at mid-day for the ground floor, when the sun has the highest solar elevation. While, in the middle floor, the highest sensitivity occurs during the morning and afternoon hours. The variation of solar radiation on the top floor is negligible.

In the summertime (Figure 42) the high sensitivity of incident solar radiation that is affected by uncertainties in boundary conditions, is observed at morning and afternoon for the ground floor. While, in the middle and top floors, a similar pattern of variation is observed during all day. The variation of solar radiation in the middle and top floors in this period shows a small sensitivity to the uncertainty in building surroundings.

During the winter period (Figure 43) as well as intermediate seasons, different patterns of sensitivity to building boundary conditions is observed. Since solar altitude in winter is low, the building surfaces mostly receive the diffuse radiation in a complex urban canyon during daytime. The most variation during the winter season is observed in the middle floor at mid-day.

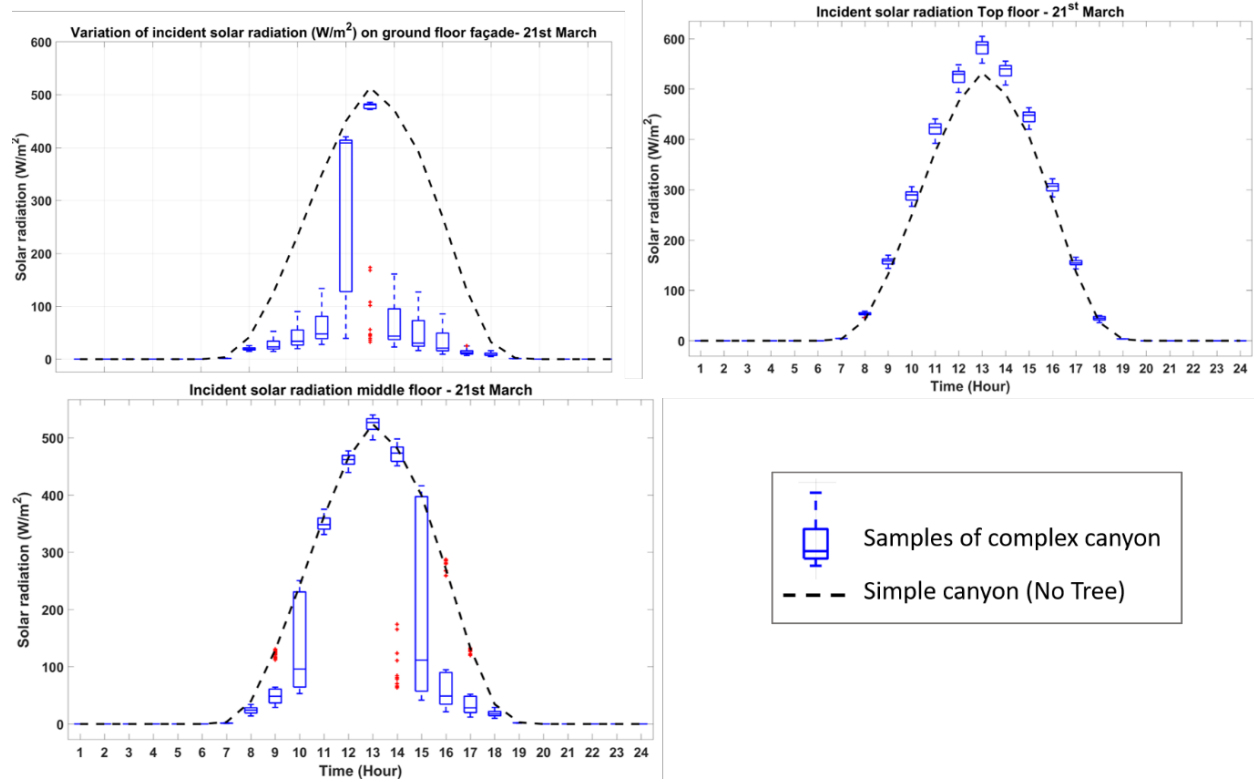


Figure 41 - Simple canyon vs. uncertainty propagated canyon - Daily profile of 21 March

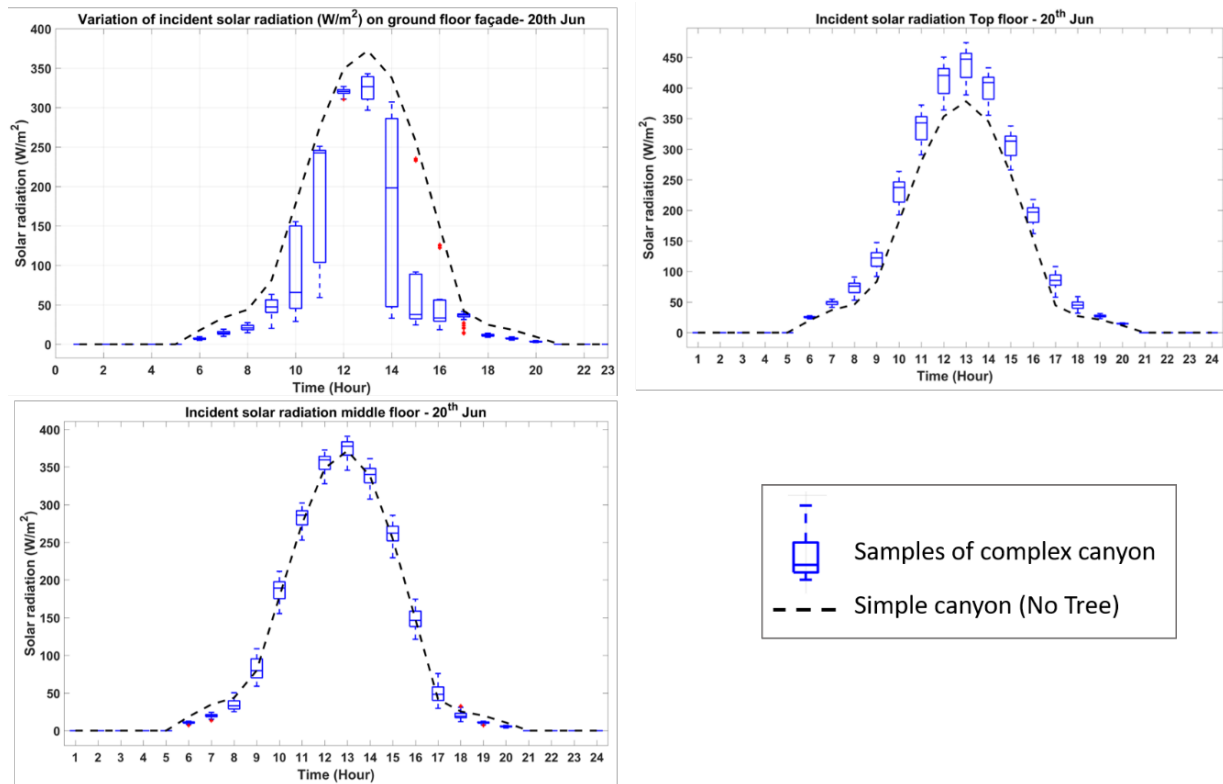


Figure 42-Simple canyon vs. uncertainty propagated canyon - Daily profile of 20 Jun

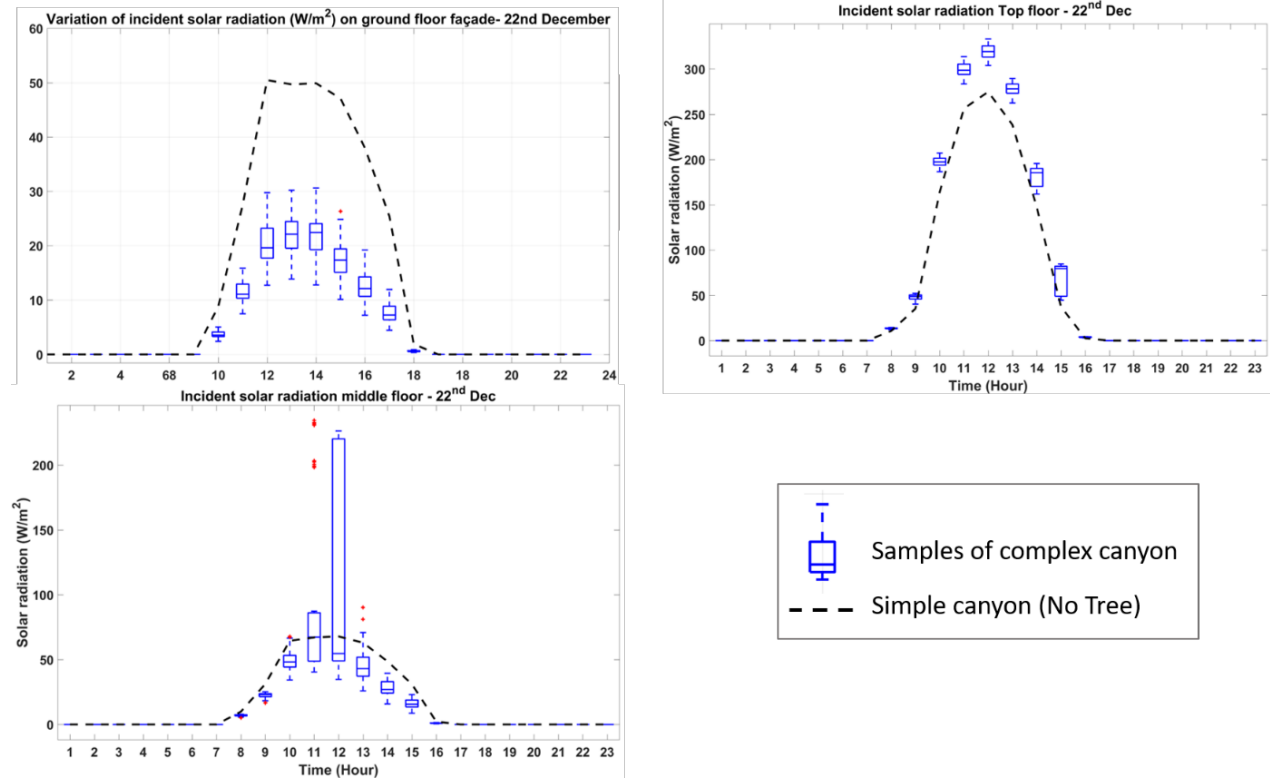


Figure 43- Simple canyon vs. uncertainty propagated canyon - Daily profile of 22 Dec

To evaluate the effect of solar radiation in an urban canyon, two scenarios are defined, i.e. supremum (upper/high) and infimum (lower/low) scenarios. The high scenario considers a random sample of the canyon with all complexity, where the highest values of solar radiation on the studied area are observed; while the low scenario is selected based on the exact opposite conditions (Figure 44).

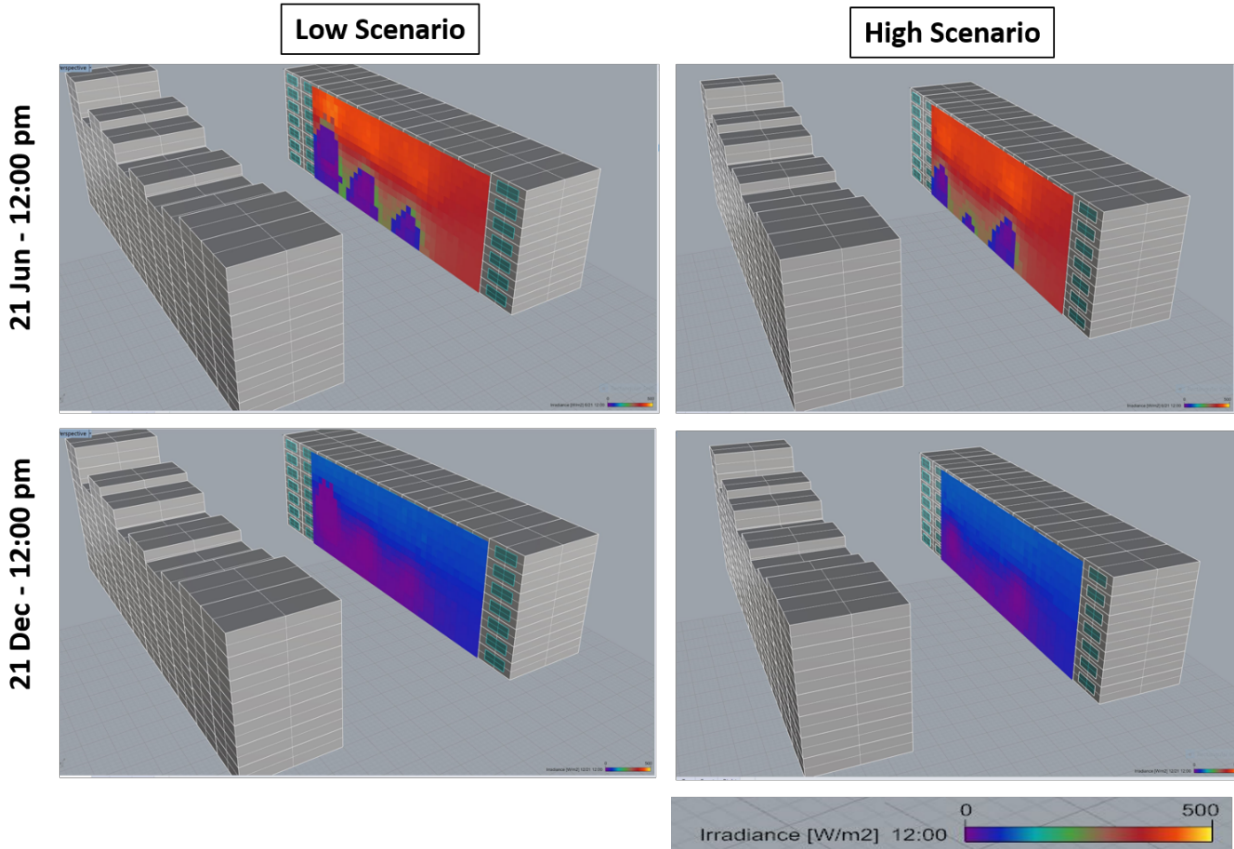


Figure 44- Incident solar radiation (W/m^2) on building facades during 21 Jun and 21 December in two candidate scenarios: low (Left) and high (Right). For a better presentation of the results, trees and cars are hidden however the effects are clear.

4-2-3 Uncertainty of solar radiation and daylight analysis

Indeed, one of the first consequences of over/under-estimating of solar radiation on the building surfaces is perceived on building daylight availabilities. In this step, the quantified solar radiation through UA is fed into daylight simulations. The effects on useful daylight illuminance (UDI), daylight factor (DF) and annual lighting energy are discussed in the following.

The daylight analysis performed on three scenarios as described in the previous section, using two sets of radiance parameters. The UDI is calculated with ambient bounce (ab) of 2, while other evaluations are estimated based on $ab=5$. The DAYLIGHT and DAYLIGHTFACTOR components in DIVA for Grasshopper are selected as the calculation tool.

The building located in the center of the studied urban canyon is selected for daylight analysis. An area of 100 m^2 on each floor is specified to host the illuminance sensors. The distance between the sensors is set to 1 meter while placed at 0.8 meters high from each floor.

4-2-3-1 Useful Daylight Illuminance (UDI)

Nabil et al. [198] presented the Useful Daylight Illuminance metric (UDI) based on a wide set of experiments on occupant behavior in different daylight conditions. The UDI paradigm is suggested for time series analysis where the hourly values of daylight illuminance are the focus on the study. In this study, hourly daylight illuminance levels are categorized into three conditions:

- 1- Under sunlit area: Hourly values of daylight illuminance less than 100 lux
- 2- UDI: Hourly values of daylight illuminance between 100 and 2000 lux
- 3- Over sunlit area: Hourly values of daylight illuminance greater than 2000 lux

The UDI is used by the U.S. Green Building Council's LEED v4 green building rating system.

The percentage of hours related to the aforementioned categories (extracted from scenarios and distances from the window) is illustrated in Figures 45-47. Accordingly, the embedded uncertainty of solar radiation within the UDI calculations reveals the sensitivity of UDI to building surrounding elements as well as the simulated building height. The variation of UDI in the ground is more than that of other floors, which is in line with the uncertainty analysis of incident solar radiation obtained from Figure 40. The variation of UDI on the top floor is almost negligible due to low uncertainty of incident solar radiation on upper floors.

As observed, the approach of modeling urban canyon and complex features can assist in embedding uncertainty in the calculation of useful daylight illuminance. These uncertainties vary based on the height of the studied area. The error range of variation is estimated through:

$$\%UA = \left[\frac{((UDI_{high}) - (UDI_{low}))}{\frac{(UDI_{high}) + (UDI_{low})}{2}} \right] * 100 \quad (\text{Eq.37})$$

Therefore, in the three representative floors among the considered scenarios, the UDI has changed in the range of $\pm 22\%$ for ground floor and $\pm 12\%$ in the middle floor (Figure 45).

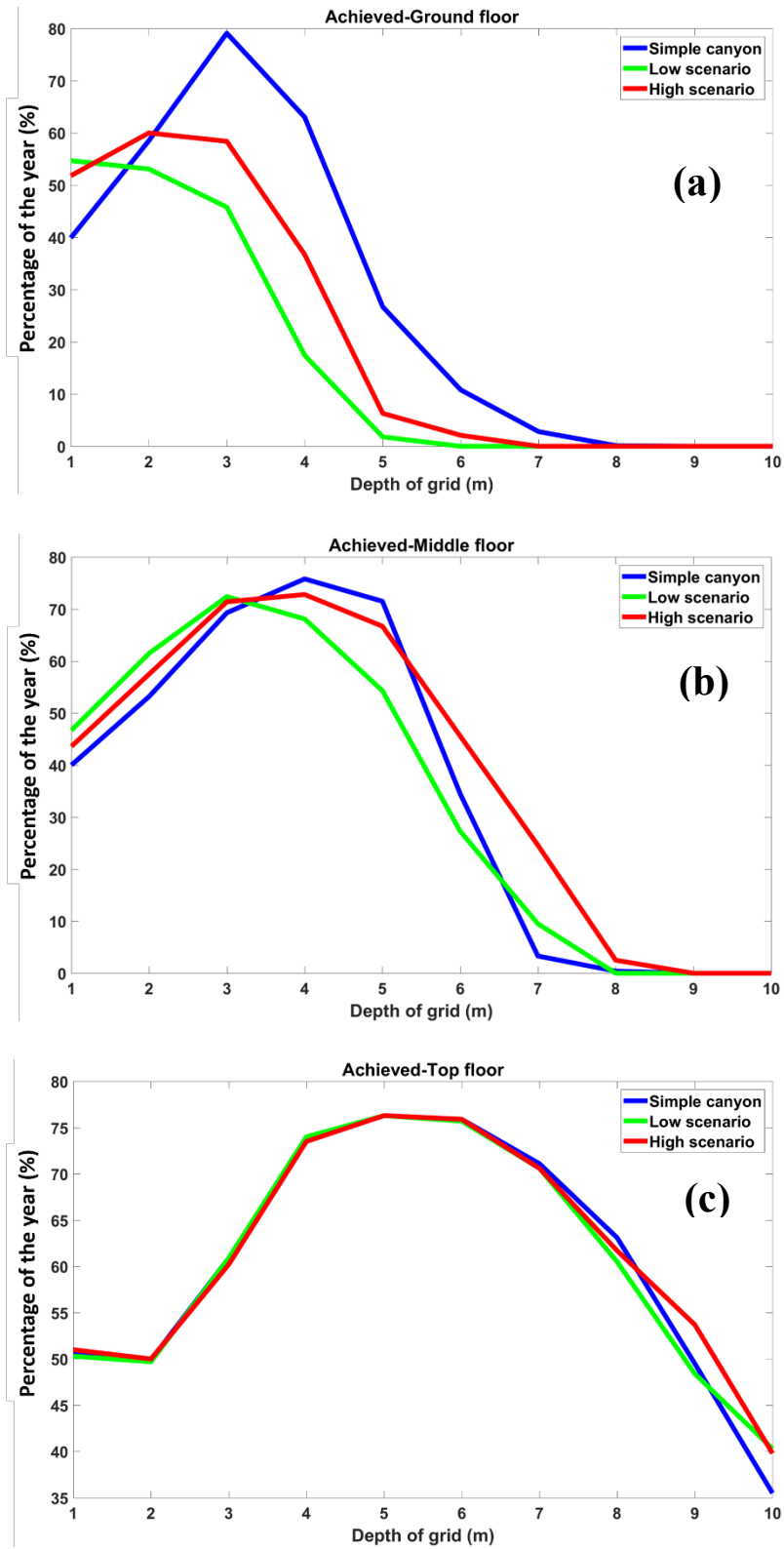


Figure 45 – Comparison of percentage of the year when the illuminance is occurred in UDI metrics for three scenarios. (a) ground floor, (b) middle floor and (c) top floor.

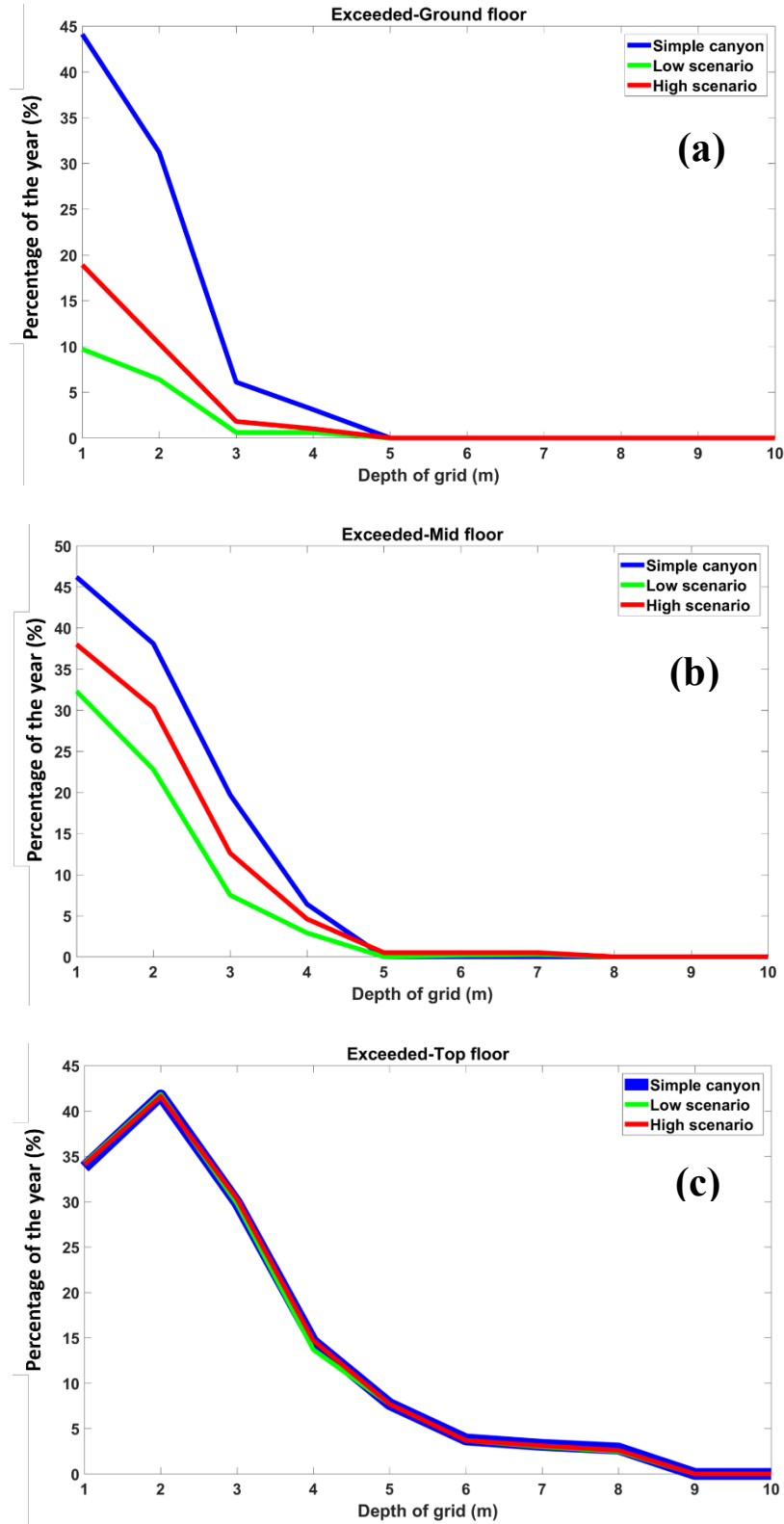


Figure 46- Comparison of percentage of the year when the illuminance is exceeded of UDI metrics for three scenarios. (a) ground floor, (b) middle floor and (c) top floor

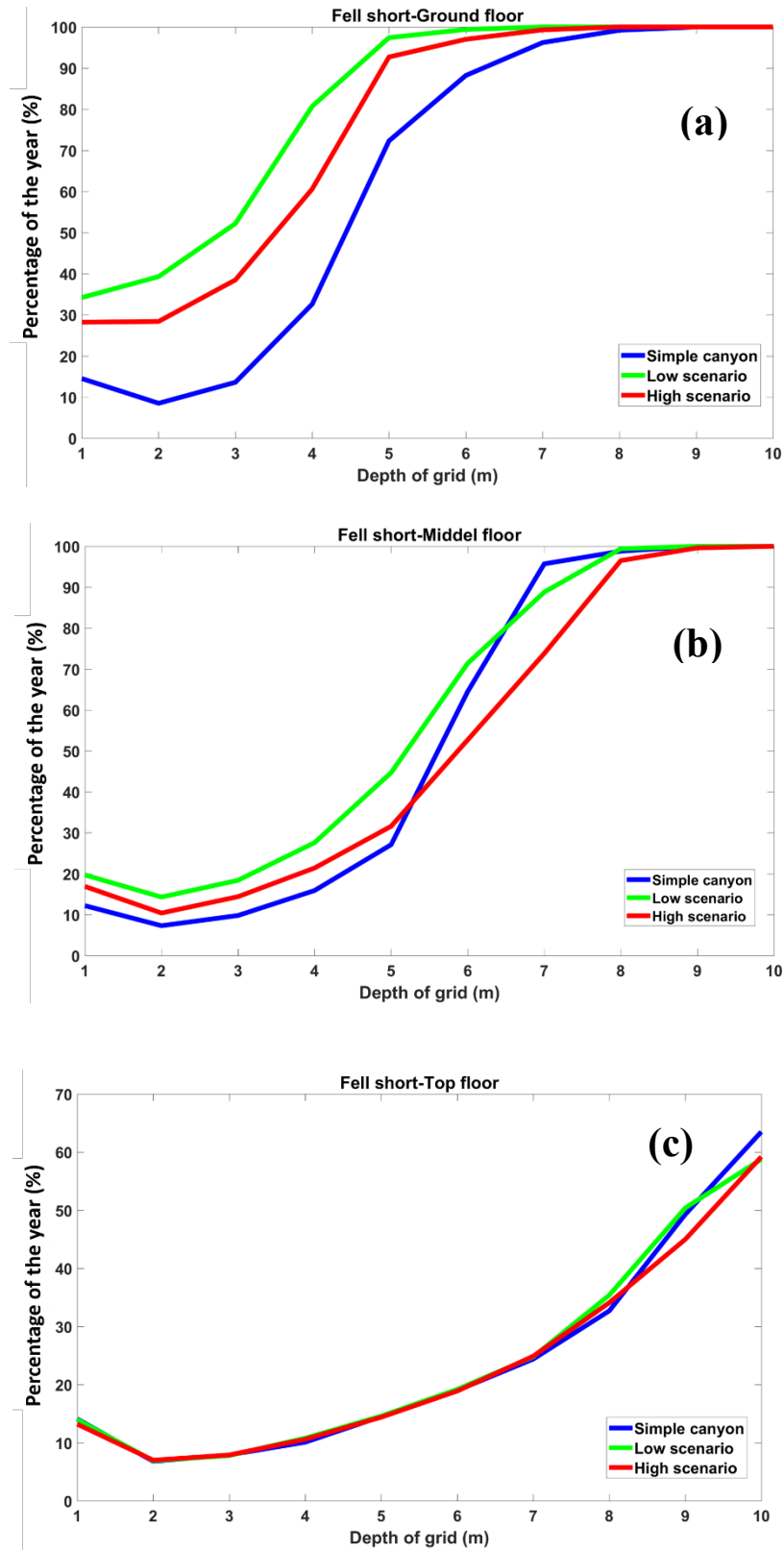


Figure 47- Comparison of percentage of the year when the illuminance is lower than UDI metrics for three scenarios. (a) ground floor, (b) middle floor and (c) top floor

4-2-3-2 Daylight factor (DF)

Daylight factor is recognized as a metric for indoor natural illuminance. Daylight factor is calculated based on the ratio of indoor to outdoor illuminance when the sky conditions are considered as overcast.

According to Figure 48 and as expected, a significant difference between the simple scenario (Blue line) and complex ones (Red and Green) is observed. Since in the simple scenario the incident solar radiation did not show a noticeable variation between the selected floors, a similar trend is also followed in calculations of DF. Meanwhile, the DF may reach twice as high as the simple case.

As shown before, the higher floors receive more direct solar radiation since the effects of shadowing elements are reduced. This is also observed in DF estimations of the top floor, and as reported in Figure 48 the difference of DF between the two scenarios are unimportant.

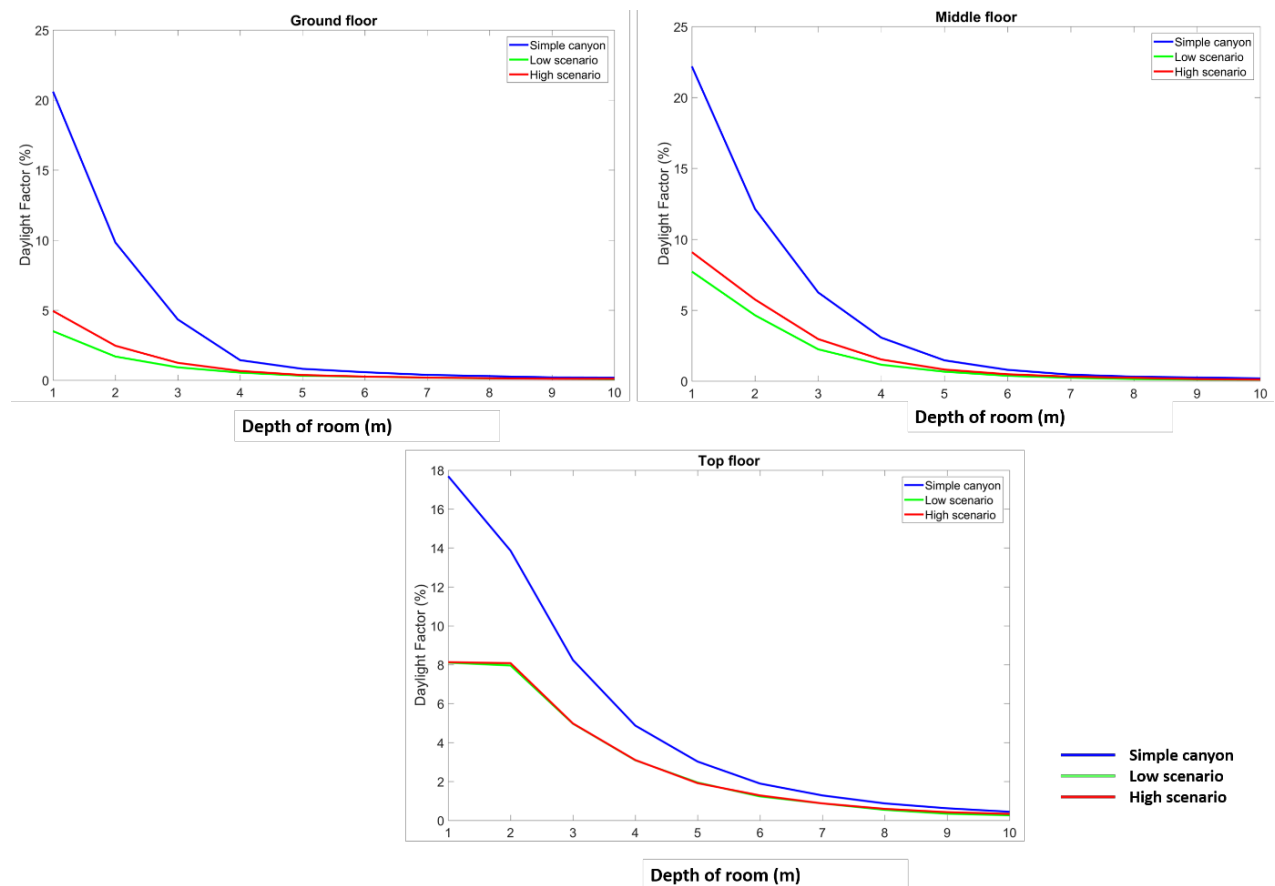


Figure 48 - Daylight factor (%), comparison between simple, low and high scenarios. Depth of room refers to distance of each point from the window. Window is located at 1

4-2-3-4 Annual electricity

The quantified solar scenarios are also evaluated regarding the impacts on electricity consumption. Table 22 reports the total energy consumption of each grid located on the ground, middle and top floors, respectively. Comparing the value of Table 22 with the trend of daylight factor in Figure 54 reveals that in general the electricity power is under-estimated in building energy calculations since the simple canyon is typical modeling of building and surroundings.

The fractional error between the electricity consumption in the simple canyon and presented scenarios is calculated by:

$$Variation_{lowerBound} = \left[\frac{(LowScenario - SimpleScenario)}{SimpleScenario} \right] * 100 \quad (Eq.38)$$

$$Variation_{higherBound} = \left[\frac{(HighScenario - SimpleScenario)}{SimpleScenario} \right] * 100 \quad (Eq.39)$$

$$\%variation = \max(Variation_{lowerBound}, Variation_{higherBound}) \quad (Eq.40)$$

Table 22 -Annual lighting energy used per grid (kWh).

	Simple canyon	Low scenario	High scenario	Variation between high and low scenarios (%)
Ground floor	3039.9	3933.8	3888.6	± 29.41
Middle floor	2473.3	3599.3	3565.8	± 45.52
Top floor	1947	2843.9	2751.3	± 46.07

4-2-3-5 Quantification of glare uncertainty as a support for decision making

Determining the window to wall ratio (WWR) of the building is one of the bases of building daylight design phase. In this section, the importance of considering the uncertainty in building surroundings during the design phase of windows are investigated. Therefore, a series of parametric simulations are applied to the studied urban canyon as a support for decision makers. Regarding that, the window to wall ratio is varied between 30% to 80%, with 10% steps, and applied on a building in the middle of the studied urban canyon. The hourly interior illuminance is extracted for three levels of ground, middle and top floor. Similar to previous sections, simulations are performed for both high and low scenarios (Figure 53), using an ambient bounce of $ab=5$. The illuminance sensors are the same as the previous analysis of UDI and daylight factor.

To estimate the potential of the glare, defining a reliable threshold is necessary. This threshold may vary between 2000 – 3000 Lux according to the literature [199]. In this study, the potential of glare is counted for the hours in which the illuminance exceeds 2500 Lux.

The next set of analyses focus on the variation of interior illuminance on building floors while changing in WWR. Figures 49-55 render the fraction of year in which the illuminance exceeds the threshold (>2500 Lux), indicating a possibility for glare. Also, the fraction of floor area in which high illuminance occurs, is displayed in the figures. This fraction defines the percentage of studied floor area subject to illuminance values higher than the threshold.

Figures 49 and 50 present the results of glare analysis related to the ground floor for low and high scenarios, respectively. Figure 53 provides a comparison between the two, i.e., low and high scenarios. The difference between transparent and solid surfaces in Figure 53, underlines the effect of building surrounding on potential glare. As expected, the potential of the glare increases with higher WWR. However, a notable jump is observed on the ground floor of both scenarios after WWR 50%. While in the low scenario around 6% of the year renders a high risk of glare, this value is doubled (around 12%) in the high scenario with the same WWR. Also, a larger fraction of the floor is subjected to glare in the high scenario, when compared to equal conditions in the low scenario (Figure 53). The same illustrations are prepared for the middle floor as presented in Figures 54.

However, the top floor (as already shown in previous daylight analysis) has a lower sensitivity to canyon complexities, which is also reflected in glare risk assessments analysis. Therefore, only one figure (Figure 55) is presented for the top floor, rendering trivial difference between high and low scenarios.

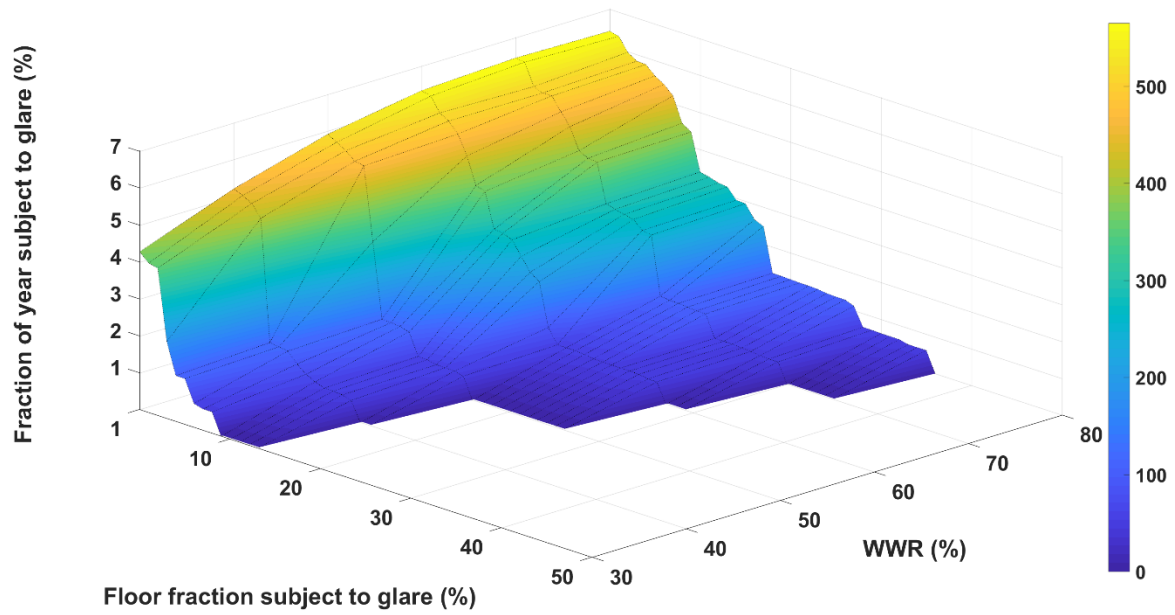


Figure 49 – Risk of glare based on variation in WWR on the low scenario for ground floor

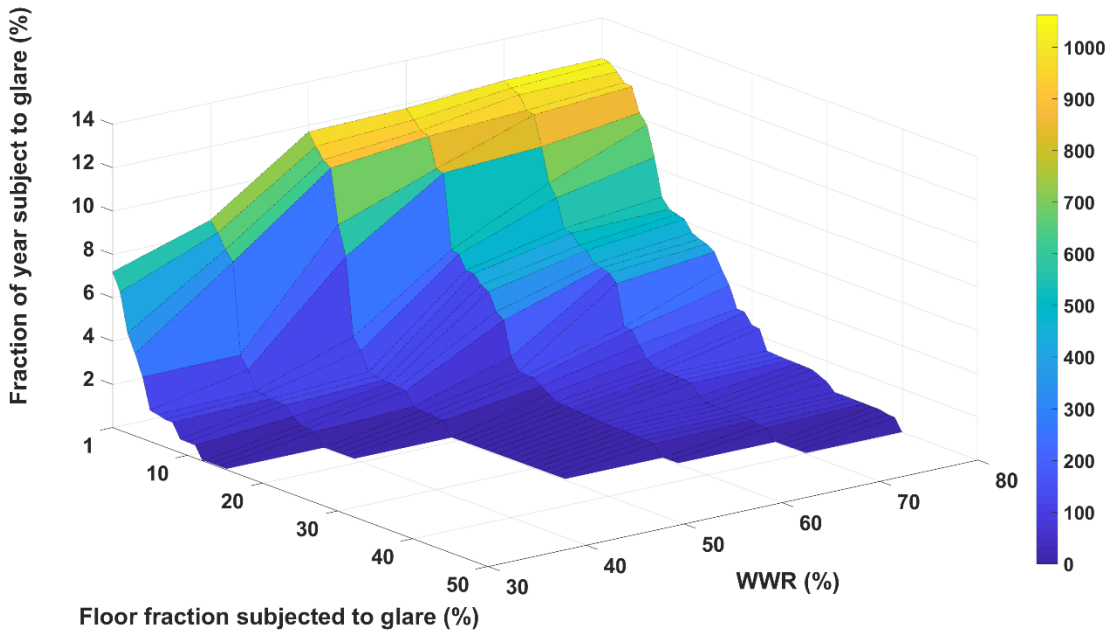


Figure 50 - Risk of glare based on variation in WWR on the high scenario for ground floor

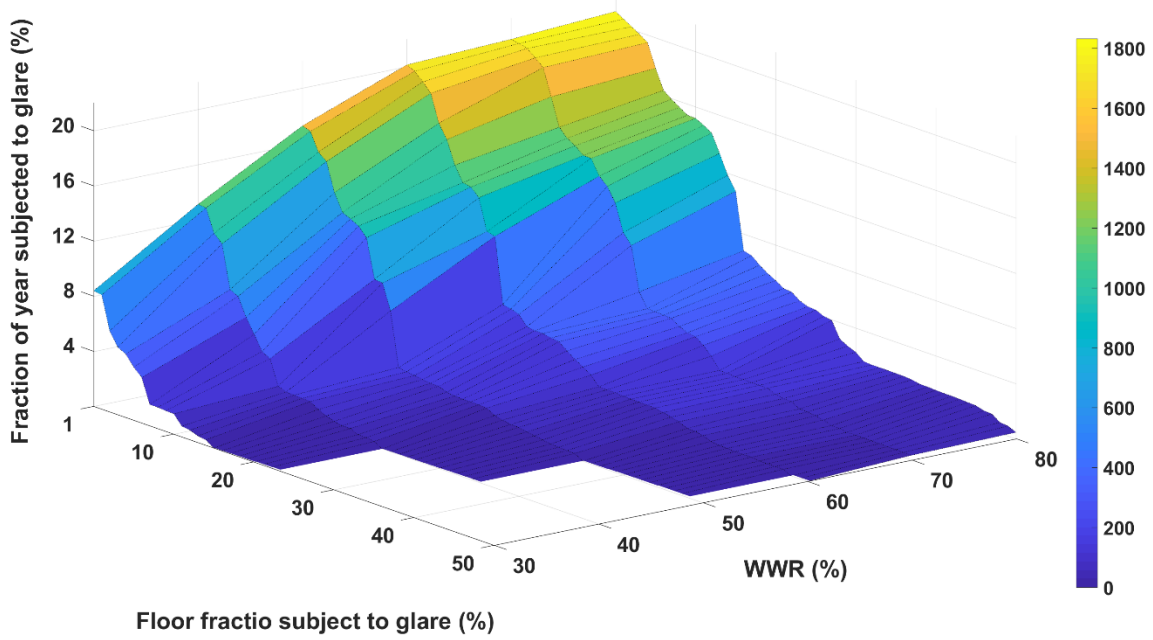


Figure 51 - Risk of glare based on variation in WWR on the low scenario for the middle floor

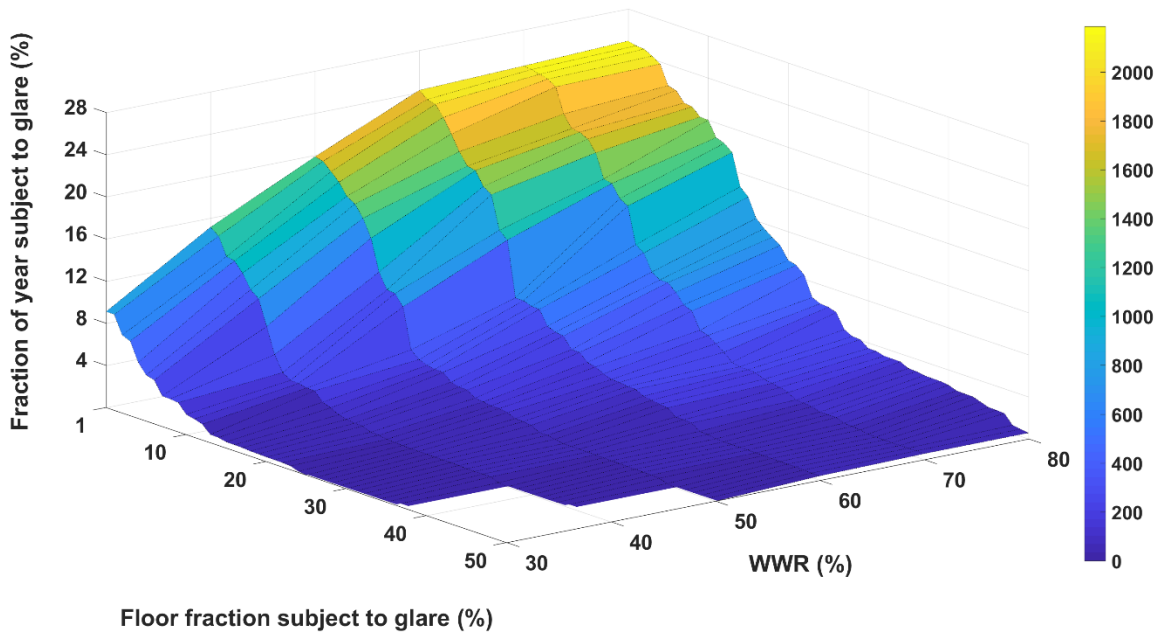


Figure 52-Risk of glare based on variation in WWR on the high scenario for the middle floor

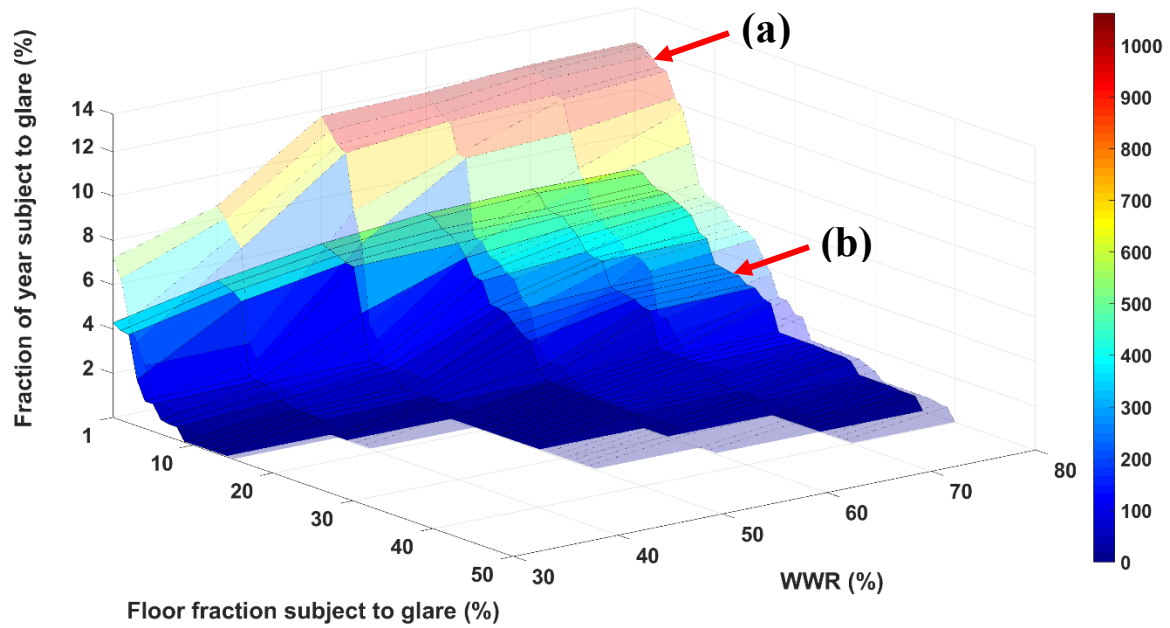


Figure 53 – Fraction of floor subject to glare in the ground floor. A comparison between high scenario (a) transparent mesh, and low scenario (b) solid

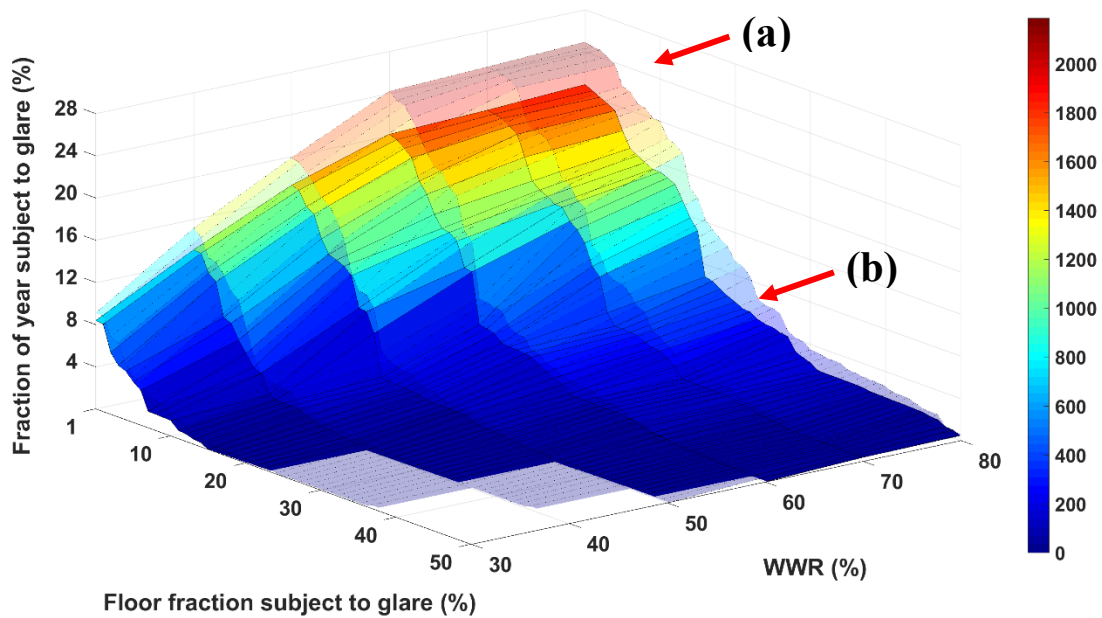


Figure 54- Fraction of floor subject to glare in the middle floor. A comparison between high scenario (a) transparent mesh, and low scenario (b) solid

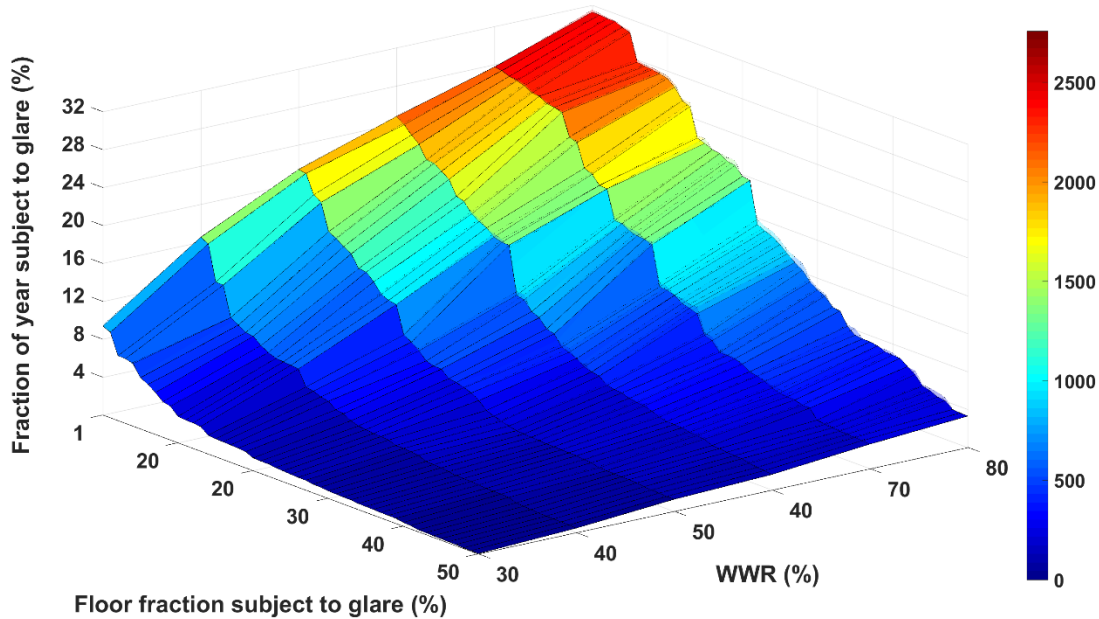


Figure 55- Fraction of floor subject to glare in the *top floor*. Similar performance of high and low scenario

4-2-4 Connect solar radiation analysis to building energy simulations

The objective of this section is to quantify how using detailed solar radiation within the urban canyon, affects building energy performance. The incident solar radiation can be extracted from building energy simulations. This value is calculated based on the solar radiation from weather data which after is used in heat balance equations. The main challenge of implementing DIVA results into building energy calculations is to incorporate the incident radiation into the heat balance calculations.

4-2-4-1 uncertainty in solar radiation and indoor comfort

The whole building energy simulation tool, WUFI Plus (V. 3.1.1.0), can perform both thermal and hygrothermal calculations of building performance [200].

Once the representative samples of canyon models are Hourly external weather conditions including the temperature, relative humidity, wind, and solar radiation are involving in WUFI hygrothermal simulations. To modify a certain weather file for using in WUFI simulations, the WAC format of weather data provides the liberty to choose between different data sources and weather elements. WUFI can involve the measured solar radiation over a certain inclination in hygrothermal calculations. To do this, the weather data should be generated in WAC format and

the type of solar radiation in weather data should be considered as “solar measured” [201]. The hourly global solar radiation of specified scenarios is extracted from DIVA analysis and replaced in solar radiation column of WAC weather data as “solar measured”. Accordingly, three series of weather data are generated for high, low and as well as simple scenarios.

Figure 56 shows the simulated building energy model in WUFI Plus. The building characteristics including building components assembly, infiltration rate, and system characteristics are chosen based on typical buildings for Milan city [202]. Detailed about the building envelop characteristics are presented in Annex3.

The target zone in these simulations is fixed as the middle floor while other floors are considered to have adiabatic partitions between conditioned spaces. Samples are assumed to be conditioned only during the heating period. In the estimated solar radiations obtained from DIVA, the effect of ground reflectance and surrounding elements are already taken into account. Therefore, the model in WUFI is created as a single zone with the ground reflectivity set to zero, as well as no shading components. Indoor temperature and relative humidity are extracted from all simulation models to be applied to the comfort-based analyses using the PMV model.

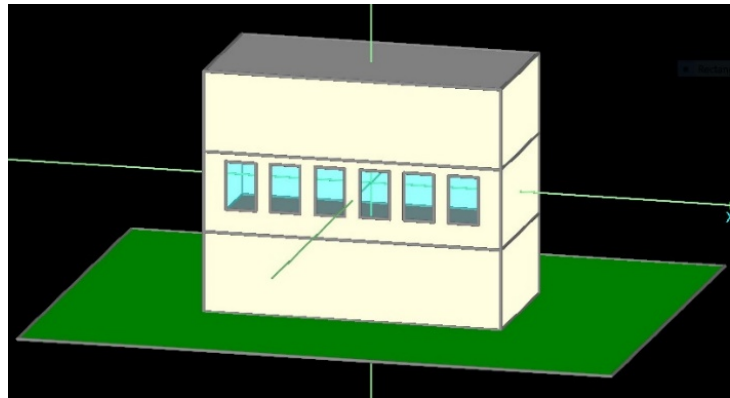


Figure 56- building energy model in WUFI, the middle zone, and its external walls are simulated

The radiation map component in DIVA estimates incident solar radiation. Global, direct and diffuse components of solar radiation are extracted separately from DIVA simulations. These quantities are fed into Eq.26 to calculate the ERF_{solar} and the following MRT_{solar} . Table 23 reports the essential input parameters as well as the values utilized in this study to calculate MRT_{solar} .

To determine the f_p , the proposed values by [189] are studied in this step. Kubaha et al proposed a model to define the detailed f_p of both seated and standing postures, which varies based on sun azimuth and altitude during the daylight hours.

Table 23- Input parameters for calculating MRT solar, Units and used values in the following calculations

Input parameters	Unit	Value
f_{eff}	-	0.755
f_{svv}	-	0.28
I_{diff}	W/m ²	Hourly -simulated
I_{global}	W/m ²	Hourly -simulated
I_{dir}	W/m ²	Hourly -simulated
R_{floor}	-	0.2
A_p	m ²	Hourly -calculated
f_{bes}	-	0.3
A_D	m ²	1.8
T_{sol}	-	0.71
α_{sw}	-	0.67
α_{Lw}	-	0.67
f_p	-	Hourly -calculated
Window Width	m	1
Window Height	m	1.6
Occupant distance to the window	m	0.5

The hourly values of f_p for seated posture are stated based on Figure 57 i.e. a fitted curve on the reported sun azimuth/altitude and projected area factor. The mentioned fit is an interpolated surface on parameters of Figure 57(b) and extracted by MATLAB curve fitting tool. The hourly values of f_p are extracted from fit function as reported in Eq.41.

$$f_p(h_i) = FittedModel(SunAzimuth_{h_i}, SunAltitude_{h_i}) \quad (Eq.41)$$

Where, $f_p(h_i)$ returns to hourly projected area factor, $SunAzimuth_{h_i}$ refers to hourly solar azimuth angle and $SunAltitude_{h_i}$ is the solar altitude of the same hour.

After calculating solar based MRT, the PMV metric is estimated for current indoor conditions. Indoor temperatures, relative humidity, and MRT_{solar} are considered to calculate PMV, these parameters vary in six simulation models (high/low scenarios multiplied by three levels). However, the constant values of metabolic rate (1.2), clothing rate (1) and air movement (0.1 m/s) are vectorized for each sample of simulation to obtain the hourly variation of PMV. The sacless of PMV is decided based on ASHRAE thermal sensation scales which are reported in Chapter 3, Table 8.

The number of hours outside comfort conditions are counted for each simulated model and reported in Table 24. It is important to note that uncomfortable episodes are observed during the heating season when the building model is assumed to be conditioned. This shows how the effect

of short-wave radiation may be underestimated in the design phase and can result in overheating during winter. From Table 24, it is observed that the percentage of error between high and low scenarios, during conditioning seasons, concerning ground, middle and top floors is 7%, 4.5%, and 9%, respectively.

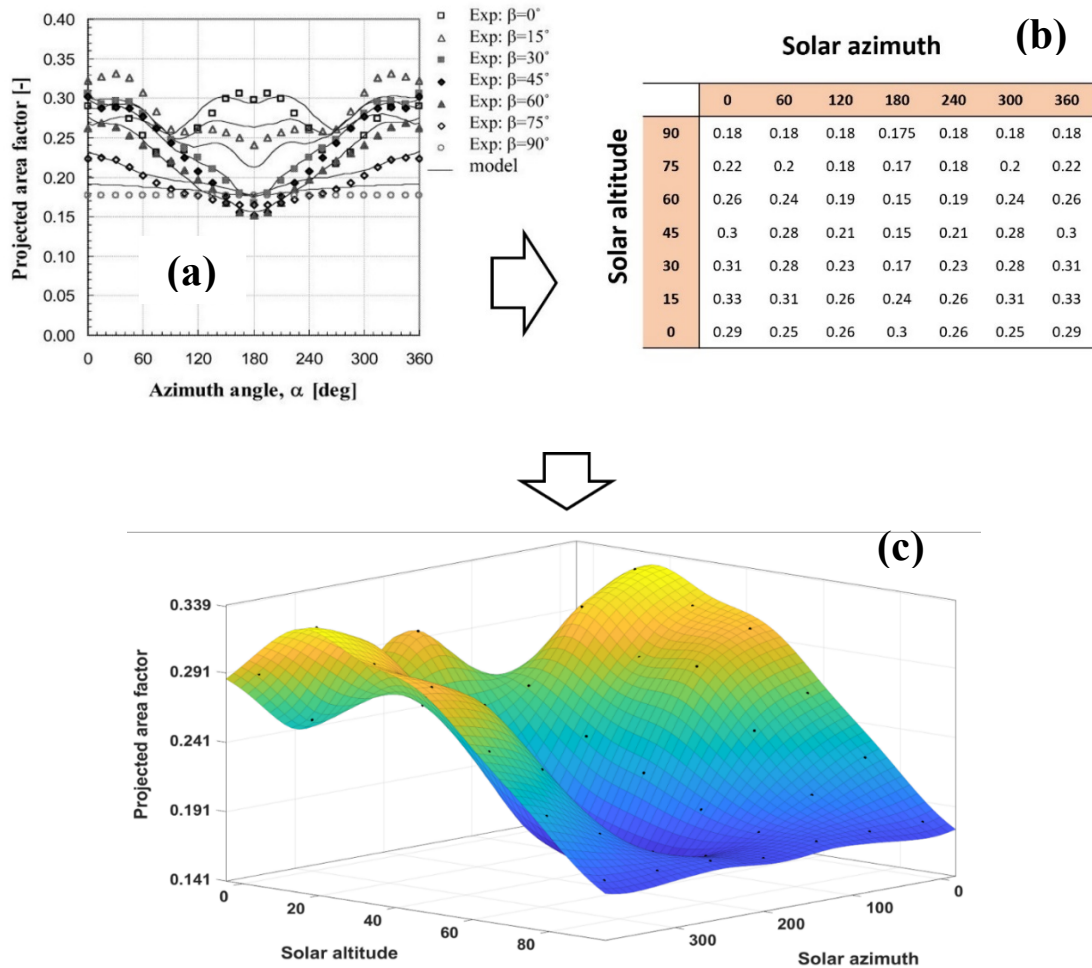


Figure 57- Projected area factor (f_p) based on solar azimuth and altitude for seated posture [189] (a) and (b), interpolate fit on the value of projection factor (c)

Table 24 – Hours outside of comfort in candidate scenarios, results of PMV solar-based

	High Scenario		Low Scenario	
	Heating season	Intermediate + Cooling season	Heating season	Intermediate + Cooling season
Ground level	54	3243	37	3018
Middle level	129	3531	279	3380
Top level	677	3799	647	3454

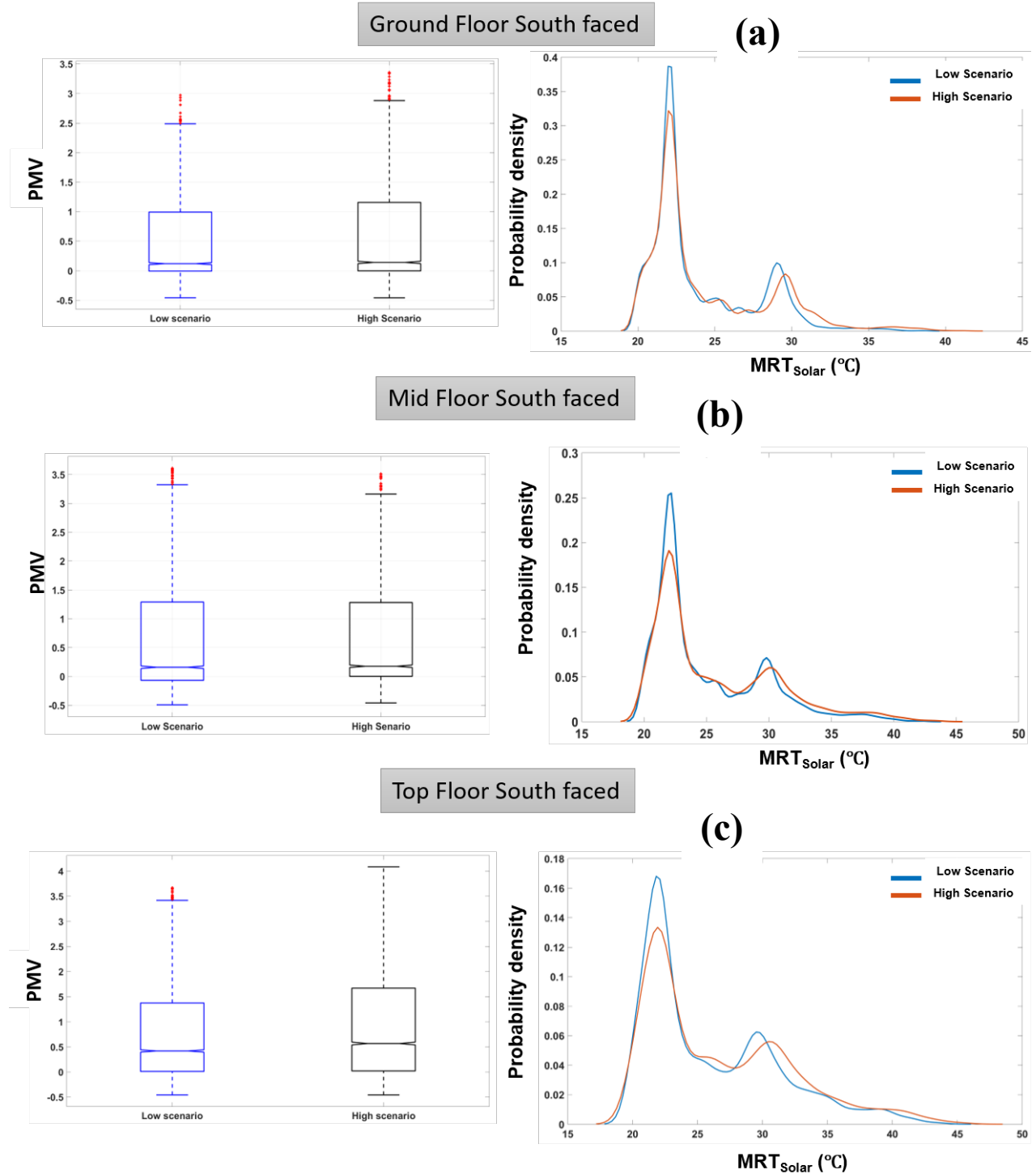


Figure 58- Variation of PMV and MRT solar in high and low scenarios for ground (a), middle (b) and top (c) floor

Figure 58 illustrates how the variation of solar radiation on different levels can affect the decision about comfort. From Figure 58 based on low scenarios in candidate floors, lower values of MRT occurs as well.

Figure 59 presents the time-series of indicated uncomfortable hours based on the PMV index for both low and high scenario and with a focus on the middle floor. The Y-axis presented the comfort indicators, regarding all the certain natural hours ($-0.5 \leq PMV \leq 0.5$) are settling down in $y=0$. The $y=0.5$ defines the edge between the natural and slightly warm hours where the $0.5 < PMV < 1$ and the $y=1,2,3$ are covering the PMV in the category of slightly warm, warm and hot, respectively. The notable frequency is happening in January and December since during these periods the heating system is working and again it is showing how the underestimation of solar radiation during the design phase can increase the risk of overheating even in winter period.

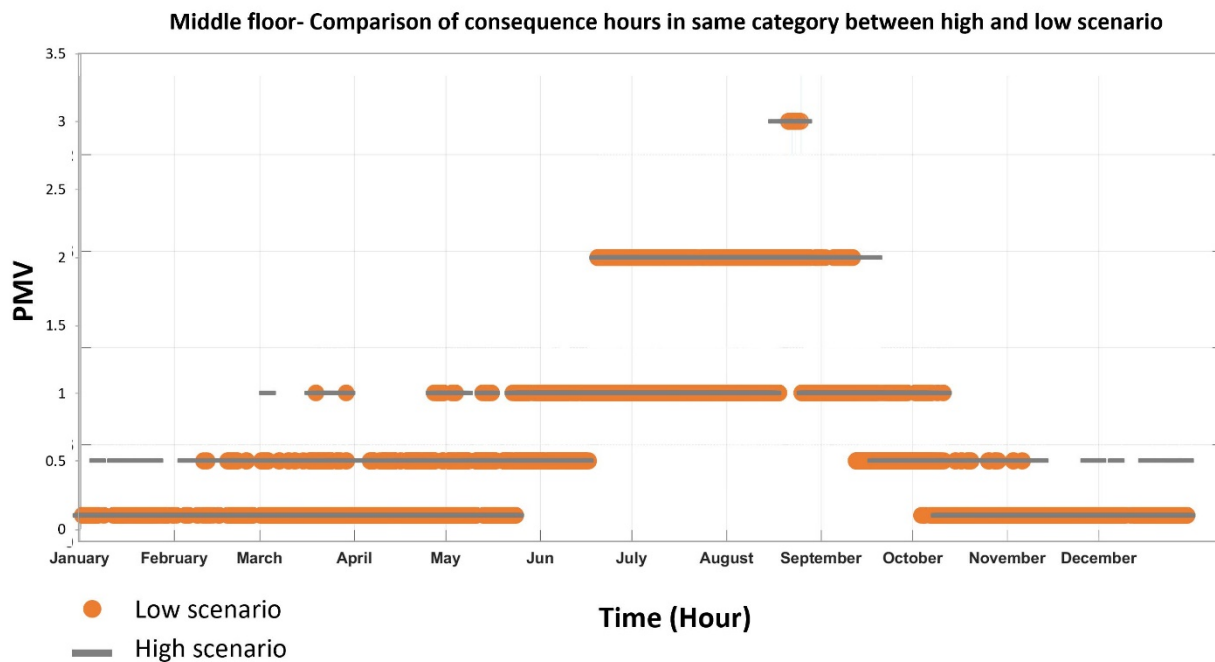


Figure 59- Frequency of different thermal sensation based on ASHRAE division and PMV calculations.

Figure 60 shows the variation of hours during a year which fall in PMV index categories for different floors and two scenarios. A different trend of hours in warm and hot categories is observed for the top floor. This arise from patterns of skylines in the candidate scenarios. In this study, the low and high scenarios are selected based on the state of incident solar radiation at the middle floor to avoid the overfitting of the analysis on high variation in ground floor or underfitting the results and resorting to low variation in the top floor. However, results from Figure 60 reveal that the candidate scenarios can change in different levels of the buildings.

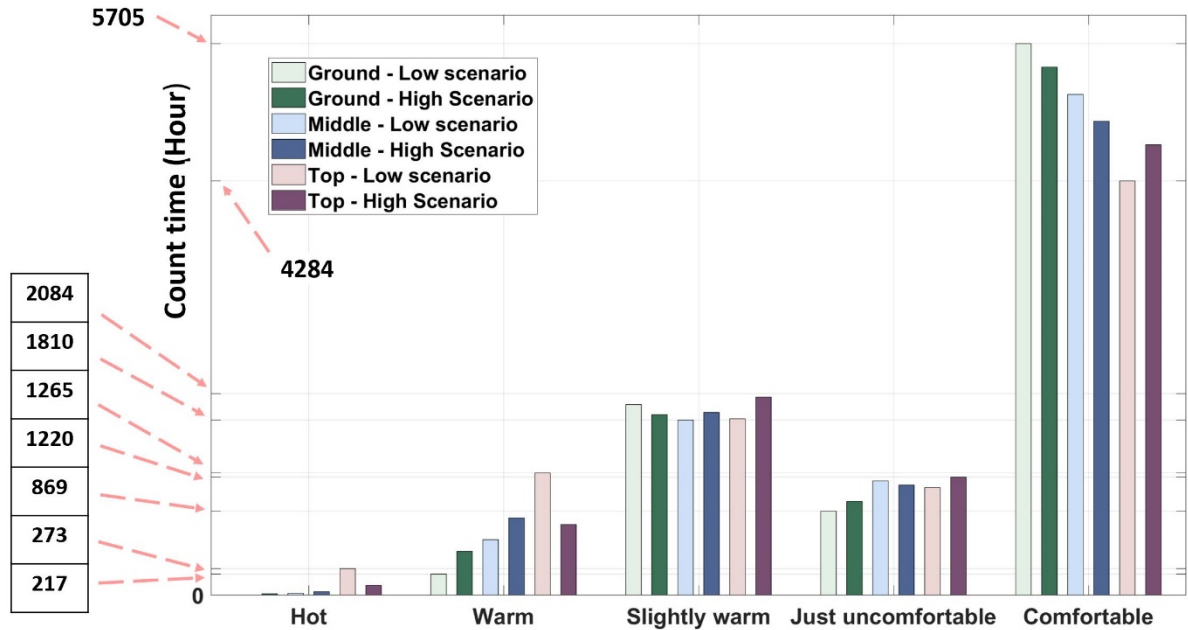


Figure 60- Variation hours in PMV categories affected by uncertainty in building surroundings

Figure 61 compares thermal sensation categories for the middle floor concerning simple and complex scenarios. Underestimation of comfort hours and overestimation in warm and hot hours in the Simple scenario are two interesting points of Figure 61, which mainly arise from neglecting the shadowing effect of trees.

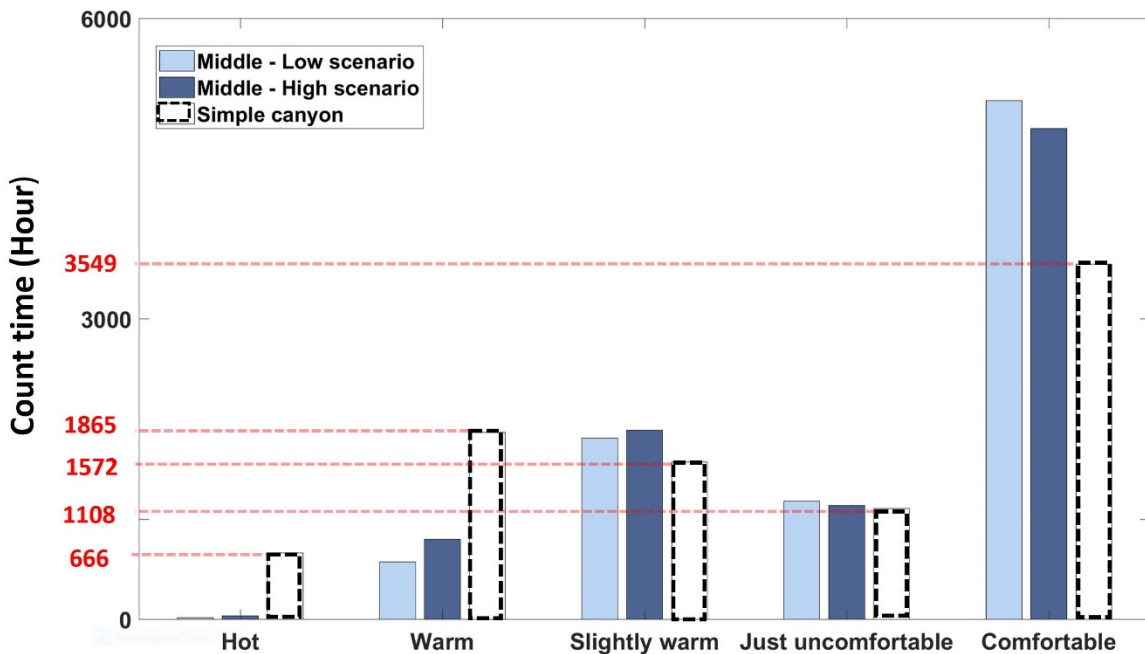


Figure 61- Variation of thermal sensation based on simple and complex urban canyon scenarios

The impact of the hybrid uncertainty treatment of urban canyon features on indoor comfort is also studied. Figure 62 reports the variation in uncomforted hours presented through the solar-based PMV. The graph displays the effect of resorting to probabilistic and possibilistic variables separately. The limiting criteria for comfort is set to $PMV \pm 0.5$.

The studied building model is based on typical residential buildings assumptions in Milan with a working heating system during winter and no active cooling system for summer time.

Black lines (dash/solid) represent the effect of the seasonal change in trees (transparency) on the comfort conditions. As mentioned before, this variable is treated according to the theory of possibility and applied to the canyon model. The Red lines (dash/solid) report the effect of uncertainty for probabilistic variables (Table 20) on comfort hours. Figure 62 underlines the shadowing effect of trees on building performance within a complex canyon.

The difference of uncomfortable hours between lower bounds (black dash) and upper bounds (black solid) of possibilistic variables is 349 hours during a year, while this difference is 10 times smaller in the case of probabilistic variables.

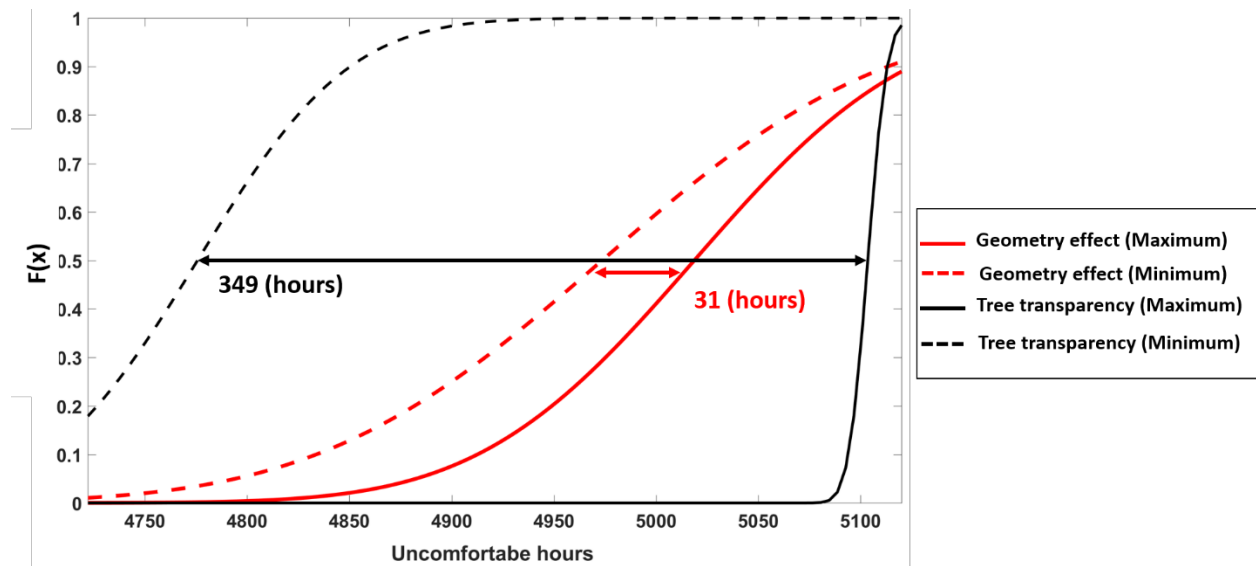


Figure 62- Contrasting the effect of probabilistic and possibilistic variables on thermal comfort

Finally, a comparison between the adaptive comfort model which does not consider the effect of short-wave radiation and PMV solar based is performed (Table 25). Results show that the adaptive model reported higher hours in comfort zone, while in more realistic situations the comfort hours may be drastically affected when the heating/cooling system is off.

Table 25 - Percentage of hours outside the comfort condition, A comparison of adaptive comfort model and PMV solar based

		PMV (%)	Adaptive (%)
High scenario	Top floor	48.7	67.1
	Middle floor	58.1	77.8
	Ground level	64.6	82.7
Low scenario	Top floor	52.8	79.7
	Middle floor	54.2	72.6
	Ground floor	61	79.7

4-2-5 Conclusion

This section has focused on associating the uncertainty of solar radiation on building façade to estimate building energy quantities. Accordingly, a series of daylight analysis, indoor comfort, and building cooling/heating assessments are performed. All the analysis highlighted the importance of the considering the incident solar radiation as a parameter in the urban canyon which vary in parallel of building surroundings.

Buildings in urban canyons generally are considered as simple scenarios in this study. However, the evaluations of daylight factor revealed that typical modeling of canyons, however, may result in over-estimating the daylight factor. Moreover, adding complexity in urban canyons has a significant effect on electricity loads and resulting difference in lighting energy need for each floor.

The solar radiation within the urban canyon is also assessed within the context of building indoor comfort through the MRT measure. The Predicted Mean Vote (PMV) is also calculated by resorting to on solar-based MRT. PMV solar base compared with Adaptive comfort model which neglected the effect of solar radiation in indoor comfort. Results reveal the noticeable difference between the two approaches.

Chapter 5 - Conclusions

There is a gap between actual and estimated building performance. The uncertainty in input parameters of building simulation tools is known as one of the most important sources of the performance gap. Among the uncertain input parameters, assumptions of climatic properties – which are typically implemented through the weather data – are of great importance. Re-scaling the climatic parameters the mesoscale to the microscale is one of the proposed solutions to reduce the climate-related uncertainty. Among the weather parameters, estimations of incident solar radiation on building facades are associated with uncertainty from two main perspectives, i.e., the accuracy of calculation models as well as the inputs fed into the models. The inadequacy of measurements and lack of interoperability between simulations tools are the main barriers for these kinds of studies. Therefore, there is a necessity for a holistic framework which describes proper quantification, propagation, and post-processing of uncertainty in an urban canyon. This Ph.D. study was an attempt to tackle the raise challenge while rendering the effects of opting for a suitable uncertainty treatment framework.

The current study is designed to provide information for architects, building engineers, urban planners/designers, as well as policymakers. Architects define the façade of the building and often choose the properties of opaque and transparent surfaces. The framework introduced in this study, not only helps architects to assign proper characteristic to the transparent surfaces (glazing) of their building placed within a canyon, but also, to evaluate the effect of the buildings glazed and opaque reflections (specularity) of other buildings within the canyon. Building engineers who work alongside architects can evaluate the performance of their shading devices and consequently the availability of daylight, occupant comfort, and energy performance with more realistic realizations of the surrounding environment. Urban designers and planners who define the aspect ratio of the urban canyons, as well as the urban furniture (vegetation, parking spaces, etc.), ought to have a deep understanding of the interaction between the buildings as well as urban furniture within an urban canyon. Therefore, resorting to the framework in this study will not only provide them with adequate knowledge to assess the suitability of characteristics of urban canyons, but also deliver well-informed foundation for new design and planning. Finally, policymakers working in the municipal, district, and national levels can opt for the introduce framework to set regulations and policies regarding the overall characteristic of a canyon, be it minimum and maximum range of specularity and reflectance, suitable margins for tree spacing and species, as well as regulations on the canyon skyline.

5-1 Summary

This research investigated the preparation of raw weather data as an input of building energy simulations, theory of uncertainty and the importance of its propagation, improving the accuracy of a solar model, and finally quantification of uncertainty-associated solar radiation in complex urban canyons. All proposed methods in this study were developed based on actual weather conditions, however, it was proved that they are not case specific and are extendable to other climates and urban canyons.

Long-term missing data in raw measurements of weather parameters were infilled by resorting to neural networks. The method was validated for temperature and relative humidity. Availability of measurements from a network of weather stations is necessary for a guaranteed level of accuracy. The trained neural network was able to predict three consecutive weeks of missing hourly values with suitable accuracy.

A deep survey on the theory of uncertainty was performed. Introducing possibilistic and hybrid approaches for uncertainty propagation aside from the conventional probabilistic approach was the main novelty of this part. It was discussed that based on the nature of the uncertainty and availability of data, choosing the correct approach for representing and propagating uncertainty within the model can affect the knowledge for decision support.

The accuracy of Perez sky diffuse model as one of the most popular models in building energy simulation tools was also evaluated. Future investigation on the accuracy of the model for different locations and sky conditions was proposed by the model developer. Regarding that, a calibration method was developed to calibrate multiple parameters. The calibration can be applied to the measured data from different orientations and inclinations in one run. The method uses the subset simulation approach which significantly reduces the computational time. Also, the calibrated Perez was implemented in EnergyPlus. The method was developed based on measurements from a specific site, however, location independence of the calibration method was proved as well. Applying the calibrated Perez model in EnergyPlus revealed how under/over-estimations of incident solar radiation by the default model can affect the reliability of estimations in building energy loads and photovoltaic performance.

In this study, the complexity of modeling urban canyons was challenged and compared with the current simplifications concerning building surroundings. This approach to solar radiation within the urban canyon is a first of its kind, as previous studies, mainly focused on solar availability in micro-urban scales or the glare analysis in a case-specific condition. It was observed that details of urban canyon such as variation in height of adjacent buildings and reflectivity or transparency of surroundings can drastically affect the thermal comfort, visual comfort, as well as lighting energy consumption. It was also shown that the effects of complexity in the urban canyon are

sensitive to the target height and vary on different floors. The annual electricity is the most sensitive parameter among the selected outputs with a variation of $\pm 46\%$. Also, the experience of the indoor comfort for different floors may vary up to $\pm 7\%$ due to the uncertainty in the urban canyon parameters. It was found that the effect of variables with high uncertainty (treated according to the theory of possibility) can be up to 10 times greater than features with lower levels of uncertainty (treated based on the theory of probability). The detailed modeling of the trees was also deeply discussed and the suitable representation of trees for uncertainty analysis was proposed. The model is a balance between the complexity and simplification.

Aside from all the novelties of the presented research study, a few (sub) objectives were not fully addressed.

The calibrated Perez model is not evaluated in the urban canyon scale regarding the limitation of measured solar radiation. Since the studies in the urban canyon are developed based on Milano climatic conditions, measurements of solar radiation on tilted surfaces were not available.

The framework of propagating the uncertainty in the urban canyon is performed based on a dialog between MATLAB and DIVA in Grasshopper. Automation of the entire process in Grasshopper could potentially be a topic for enhancing the framework.

This study presented estimations of solar radiation in urban canyons regarding the effects of uncertain parameters, while the effects on building performance are clarified. However, the results can be involved in different design strategies and decision making such as reliability assessments of different shading systems, yet, not covered here since it is out of the aims and scope of this research.

More detailed daylight analysis still merits consideration based on the uncertainty of solar radiation in an urban canyon. For instance, an investigation on the case-specific conditions within highly glazed canyons is less explored in this study.

5-2 Future studies

Actual Meteorological Year (AMY) is important for real-time building energy simulations. The proposed method of resorting to neural networks for infilling the missing values can be adopted in real-time or near real-time energy simulations that are executed on cloud servers. However, defining the minimum number of stations, distance of the stations within a network, etc., are important factors that have been overlooked, as it has been out of the scope of this study. Therefore, optimizing the properties of weather datasets as an input for real-time weather data is a potential subject for future studies.

Although, the accuracy of the proposed neural network for infilling the missing weather parameters in this study is evaluated by testing the quality of prediction based on another trusted weather dataset. However, a comparison with other methods such as “closest station method,” “multiple regression analysis,” “cubic spline method,” etc., could be useful to assess the proposed method from both aspects of computational time and prediction accuracy.

The proposed method for calibrating the Perez model is validated on two case studies. However, further evaluations based on different climatic and sky conditions are highly recommended. Also, the effect of a calibrated Perez on daylight analysis can expand the current study.

The proposed method of uncertainty quantification of solar radiation is only tested for the south façade as the most critical surface in the northern hemisphere. To prevent redundancy, other orientations has been skipped in this study, however, applying the proposed method on various inclinations and orientations is highly recommended. This issue may be more challenging for daylight analysis in east and west orientations.

Another research potential derived from the introduced framework in this study is the effectiveness of urban morphology indicators (e.g. FAR, canyon aspect ratio, greenery density, etc.) as well as reference/prototype building models (e.g. ASHRAE reference buildings) on promoting optimal solar behavior within the canyon.

In this study, results were post-processed as a support for decision makings. However, explicit feedbacks as a result of the decision has been less explored. A reliability assessment of different shading strategies performance regarding complex urban canyons can be a future research built on the basis of results extracted from this study.

The area of the building’s façade for applying BIPVs can also be another research founded on the achievements of this study. In case of availability of data, the framework can be used to validate the estimations against the actual performance of BIPV within a canyon.

References

- [1] “Sims, R. ‘Cities, Towns and Renewable Energy–Yes In My Front Yard.’ Paris, France: International (2009).”
- [2] M. Santamouris, “Cooling the buildings – past , present and future,” vol. 128, pp. 617–638, 2016.
- [3] Y. Toparlar, B. Blocken, B. Maiheu, and G. J. F. van Heijst, “A review on the CFD analysis of urban microclimate,” *Renew. Sustain. Energy Rev.*, vol. 80, pp. 1613–1640, Dec. 2017.
- [4] “American Meteorological Society, cited 2019: Microclimate. Glossary of Meteorology. [Available online at <http://glossary.ametsoc.org/wiki/Microclimate>].” .
- [5] M. Santamouris, “On the energy impact of urban heat island and global warming on buildings,” *Energy Build.*, vol. 82, pp. 100–113, 2014.
- [6] M. Santamouris, “On the energy impact of urban heat island and global warming on buildings,” *Energy Build.*, vol. 82, pp. 100–113, Oct. 2014.
- [7] D. Li, G. Liu, and S. Liao, “ScienceDirect Solar potential in urban residential buildings,” *Sol. Energy*, vol. 111, pp. 225–235, 2015.
- [8] M. Nunez and T. R. Oke, “The energy balance of an urban canyon,” *J. Appl. Meteorol.*, vol. 16, no. 1, pp. 11–19, 1977.
- [9] T. R. Oke, “Boundary layer climates. 2nd,” *Methuen, 289p*, vol. 548, 1987.
- [10] C. S. B. Grimmond *et al.*, “Initial results from Phase 2 of the international urban energy balance model comparison,” vol. 272, no. October 2010, pp. 244–272, 2011.
- [11] P. De Wilde, “The gap between predicted and measured energy performance of buildings: A framework for investigation,” *Autom. Constr.*, vol. 41, pp. 40–49, 2014.
- [12] Y. Sun, “Closing the building energy performance gap by improving our predictions,” no. August, 2014.
- [13] A. Marshall *et al.*, “Domestic building fabric performance: Closing the gap between the in situ measured and modelled performance,” *Energy Build.*, vol. 150, pp. 307–317, 2017.
- [14] C. Shrubsole *et al.*, “Bridging the gap: The need for a systems thinking approach in understanding and addressing energy and environmental performance in buildings.”
- [15] S. Attia, M. Hamdy, W. O’Brien, and S. Carlucci, “Assessing gaps and needs for integrating building performance optimization tools in net zero energy buildings design,” *Energy Build.*, vol. 60, pp. 110–124, 2013.
- [16] R. Haas, H. Auer, and P. Biermayr, “The impact of consumer behavior on residential energy demand for space heating,” *Energy Build.*, vol. 27, pp. 195–205, 1998.
- [17] P. de Wilde, “The gap between predicted and measured energy performance of buildings: A framework for investigation,” *Autom. Constr.*, vol. 41, pp. 40–49, May 2014.
- [18] A. C. Menezes, A. Cripps, D. Bouchlaghem, and R. Buswell, “Predicted vs. actual energy performance of non-domestic buildings: Using post-occupancy evaluation data to reduce the performance gap,” *Appl. Energy*, vol. 97, pp. 355–364, 2012.
- [19] R. Paolini, M. Zinzi, T. Poli, E. Carnielo, and A. G. Mainini, “Effect of ageing on solar spectral reflectance of roofing membranes: Natural exposure in Roma and Milano and the impact on the energy needs of commercial buildings,” *Energy Build.*, vol. 84, pp. 333–343, 2014.
- [20] D. B. Crawley, Y. J. Huang, and L. Berkeley, “Does It Matter Which Weather Data You

- Use in Energy Simulations ?,” *Build. Energy Simul. User News*, vol. 18, no. 1, pp. 25–31, 1997.
- [21] A. L. S. Chan, “Developing a modified typical meteorological year weather file for Hong Kong taking into account the urban heat island effect,” *Build. Environ.*, vol. 46, pp. 2434–2441, 2011.
- [22] M. Royapoor and T. Roskilly, “Building model calibration using energy and environmental data,” *Energy Build.*, vol. 94, pp. 109–120, 2015.
- [23] M. Hosseini, B. Lee, and S. Vakilinia, “Energy performance of cool roofs under the impact of actual weather data,” *Energy Build.*, vol. 145, pp. 284–292, 2017.
- [24] M. David, L. Adelard, P. Lauret, and F. Garde, “A method to generate Typical Meteorological Years from raw hourly climatic databases,” *Build. Environ.*, vol. 45, no. 7, pp. 1722–1732, Jul. 2010.
- [25] “Energy Climate and Change World Energy Outlook Special Report.”
- [26] K. Gobakis and D. Kolokotsa, “Coupling building energy simulation software with microclimatic simulation for the evaluation of the impact of urban outdoor conditions on the energy consumption and indoor environmental quality,” *Energy Build.*, vol. 157, pp. 101–115, 2017.
- [27] M. Heidarnejad, S. K. Nikkho, J. Liu, N. Mattise, and J. Srebric, “ScienceDirect Quantify Impacts of Local Urban Microclimate on Local Airflow Patterns Quantify Impacts of Local Urban Microclimate on Local Airflow Patterns,” *Procedia Eng.*, vol. 205, no. 00, pp. 1983–1989, 2017.
- [28] U. Berardi, “The outdoor microclimate benefits and energy saving resulting from green roofs retrofits,” *Energy Build.*, vol. 121, pp. 217–229, 2016.
- [29] Y. Liu, R. Stouffs, A. Tablada, N. H. Wong, and J. Zhang, “Comparing micro-scale weather data to building energy consumption in Singapore,” *Energy Build.*, vol. 152, pp. 776–791, 2017.
- [30] S. Tsoka, K. Tolika, T. Theodosiou, K. Tsikaloudaki, and D. Bikas, “A method to account for the urban microclimate on the creation of ‘typical weather year’ datasets for building energy simulation, using stochastically generated data,” *Energy Build.*, vol. 165, pp. 270–283, 2018.
- [31] A. Vallati, A. De, L. Vollaro, I. Golasi, E. Barchiesi, and C. Caranese, “On the impact of urban micro climate on the energy consumption of buildings,” *Energy Procedia*, vol. 82, pp. 506–511, 2015.
- [32] A. Gros, E. Bozonnet, C. Inard, and M. Musy, “Simulation tools to assess microclimate and building energy – A case study on the design of a new district,” *Energy Build.*, vol. 114, pp. 112–122, 2016.
- [33] Y. Sun, Y. Heo, M. Tan, H. Xie, C. F. Jeff Wu, and G. Augenbroe, “Uncertainty quantification of microclimate variables in building energy models,” *J. Build. Perform. Simul.*, vol. 7, no. 1, pp. 17–32, 2014.
- [34] T. Vermeulen, L. Merino, C. Knopf-Lenoir, P. Villon, and B. Beckers, “Periodic urban models for optimization of passive solar irradiation,” 2018.
- [35] E. S. Krayenhoff, A. Christen, A. Martilli, and T. R. Oke, “A Multi-layer Radiation Model for Urban Neighbourhoods with Trees,” *Boundary-Layer Meteorol.*, vol. 151, no. 1, pp. 139–178, 2014.
- [36] Y. Cascone, V. Corrado, and V. Serra, “Calculation procedure of the shading factor under complex boundary conditions,” *Sol. Energy*, vol. 85, no. 10, pp. 2524–2539, 2011.

- [37] M. M. E. van Esch, R. H. J. Looman, and G. J. de Bruin-Hordijk, “The effects of urban and building design parameters on solar access to the urban canyon and the potential for direct passive solar heating strategies,” *Energy Build.*, vol. 47, pp. 189–200, 2012.
- [38] N. A. Kelly and T. L. Gibson, “Improved photovoltaic energy output for cloudy conditions with a solar tracking system,” *Sol. Energy*, vol. 83, no. 11, pp. 2092–2102, 2009.
- [39] N. Jakica, “State-of-the-art review of solar design tools and methods for assessing daylighting and solar potential for building-integrated photovoltaics,” *Renew. Sustain. Energy Rev.*, vol. 81, no. January 2017, pp. 1296–1328, 2018.
- [40] V. L. Castaldo *et al.*, “ScienceDirect Thermal comfort in the historical urban canyon: the effect of innovative materials,” *Energy Procedia*, vol. 134, pp. 151–160, 2017.
- [41] N. Nasrollahi and E. Shokri, “Daylight illuminance in urban environments for visual comfort and energy performance,” *Renew. Sustain. Energy Rev.*, vol. 66, pp. 861–874, 2016.
- [42] B. De Bsrn *et al.*, “General Solar Position Calculations,” *World Renew. Energy Forum*, vol. 76, no. September, pp. 1–2, 2012.
- [43] M. David, P. Lauret, and J. Boland, “Evaluating tilted plane models for solar radiation using comprehensive testing procedures, at a southern hemisphere location,” *Renew. Energy*, vol. 51, pp. 124–131, 2013.
- [44] R. Perez, R. Seals, P. Ineichen, R. Stewart, and D. Menicucci, “A new simplified version of the perez diffuse irradiance model for tilted surfaces,” *Sol. Energy*, vol. 39, no. 3, pp. 221–231, 1987.
- [45] G. Pernigotto, A. Prada, P. Baggio, A. Gasparella, and A. Mahdavi, “IMPACT OF SOLAR IRRADIATION MODELS ON SIMULATED HOURLY ENERGY PERFORMANCE OF BUILDINGS University of Padova , Dep . of Management and Engineering , Italy Free University of Bozen-Bolzano , Faculty of Science and Technology , Italy University of Trento , D,” *Build. Simul. Conf.*, pp. 2809–2816, 2015.
- [46] A. Prada, G. Pernigotto, P. Baggio, and A. Gasparella, “Effect of solar radiation model on the predicted energy performance of buildings,” *3rd Int. Hight Perform. Build. Conf. Purdue*, 2014.
- [47] S. Lou, D. H. W. Li, J. C. Lam, and E. W. M. Lee, “Estimation of obstructed vertical solar irradiation under the 15 CIE Standard Skies,” *Build. Environ.*, vol. 103, pp. 123–133, 2016.
- [48] F. Ali-Toudert and H. Mayer, “Numerical study on the effects of aspect ratio and orientation of an urban street canyon on outdoor thermal comfort in hot and dry climate,” *Build. Environ.*, vol. 41, no. 2, pp. 94–108, 2006.
- [49] F. Bourbia and H. . Awbi, “Building cluster and shading in urban canyon for hot dry climate: Part 1: Air and surface temperature measurements,” *Renew. Energy*, vol. 29, no. 2, pp. 249–262, 2004.
- [50] J. Allegrini, V. Dorer, and J. Carmeliet, “Impact of radiation exchange between buildings in urban street canyons on space cooling demands of buildings,” *Energy Build.*, vol. 127, pp. 1074–1084, 2016.
- [51] S. Freitas, C. Catita, P. Redweik, and M. C. Brito, “Modelling solar potential in the urban environment: State-of-the-art review,” *Renew. Sustain. Energy Rev.*, vol. 41, pp. 915–931, 2015.
- [52] P. J. Rosado, G. Ban-Weiss, A. Mohegh, and R. M. Levinson, “Influence of street

- setbacks on solar reflection and air cooling by reflective streets in urban canyons,” *Sol. Energy*, vol. 144, pp. 144–157, 2017.
- [53] Y. Qin, “Urban canyon albedo and its implication on the use of reflective cool pavements,” *Energy Build.*, vol. 96, pp. 86–94, 2015.
- [54] M. Sleiman *et al.*, “Soiling of building envelope surfaces and its effect on solar reflectance – Part II : Development of an accelerated aging method for roofing materials,” 2014.
- [55] K. A. Al-Sallal and L. Al-Rais, “A novel method to model trees for building daylighting simulation using hemispherical photography,” *J. Build. Perform. Simul.*, vol. 6, no. 1, pp. 38–52, 2012.
- [56] J. Konarska *et al.*, “Transpiration of urban trees and its cooling effect in a high latitude city,” *Int. J. Biometeorol.*, vol. 60, no. 1, pp. 159–172, Jan. 2016.
- [57] C.-M. Hsieh, “Effects of tree shading and transpiration on building cooling energy use,” *Energy Build.*, vol. 159, pp. 382–397, 2017.
- [58] H. J. Moon and G. Augenbroe, “Assessing mold risks in buildings under uncertainty,” *Coll. Archit.*, vol. Doctor of, no. August, p. 245, 2005.
- [59] S. H. Kim and G. Augenbroe, “Uncertainty in developing supervisory demand-side controls in buildings: A framework and guidance,” *Autom. Constr.*, vol. 35, pp. 28–43, Nov. 2013.
- [60] C. J. Hopfe and J. L. M. Hensen, “Uncertainty analysis in building performance simulation for design support,” *Energy Build.*, vol. 43, no. 10, pp. 2798–2805, 2011.
- [61] I. Macdonald, “Quantifying the effects of uncertainty in building simulation,” 2002.
- [62] S. Bucking, R. Zmeureanu, and A. Athienitis, “A methodology for identifying the influence of design variations on building energy performance,” *J. Build. Perform. Simul.*, vol. 7, no. 6, pp. 411–426, 2014.
- [63] F. Domínguez-Muñoz, B. Anderson, J. M. Cejudo-López, and A. Carrillo-Andrés, “Uncertainty in the thermal conductivity of insulation materials,” *Energy Build.*, vol. 42, no. 11, pp. 2159–2168, Nov. 2010.
- [64] F. S. Westphal and R. Lamberts, “Building Simulation Calibration Using Sensitivity Analysis,” *9Th Int. IBPSA Conf.*, pp. 1331–1338, 2005.
- [65] H. Breesch and A. Janssens, “Building Simulation To Predict the Performances of Natural Night Ventilation : Uncertainty and Sensitivity Analysis,” *Build. Res. Inf.*, pp. 115–122, 2005.
- [66] H. Brohus, P. Heiselberg, a Simonsen, and K. C. Sørensen, “Uncertainty of energy consumption assessment of domestic buildings,” *Build. Simul. 2009*, pp. 1022–1029, 2009.
- [67] S. Burhenne, D. Jacob, and G. P. Henze, “SAMPLING BASED ON SOBOL SEQUENCES FOR MONTE CARLO TECHNIQUES APPLIED TO BUILDING SIMULATIONS Fraunhofer Institute for Solar Energy Systems , Freiburg , Germany University of Colorado , Boulder , USA Corresponding author . E-mail address : sebastian.burhen,” pp. 14–16, 2011.
- [68] G. Calleja Rodríguez, A. Carrillo Andrés, F. Domínguez Muñoz, J. M. Cejudo López, and Y. Zhang, “Uncertainties and sensitivity analysis in building energy simulation using macroparameters,” *Energy Build.*, vol. 67, pp. 79–87, Dec. 2013.
- [69] A. Capozzoli, H. E. Mechri, and V. Corrado, “Impacts of Architectural Design Choices on Building Energy Performance: Applications of Uncertainty and Sensitivity Techniques,” *Build. Simul. 2009*, vol. 15217, pp. 1000–1007, 2009.

- [70] V. Corrado and H. E. Mechri, “Uncertainty and Sensitivity Analysis for Building Energy Rating,” *J. Build. Phys.*, vol. 33, no. 2, pp. 125–156, 2009.
- [71] B. Eisenhower, Z. O. Neill, V. a Fonoberov, and I. Mezi, “Uncertainty and sensitivity decomposition of building energy models,” *J. Build. Perform. Simul.*, vol. 00, pp. 1–18, 2011.
- [72] P. Heiselberg, H. Brohus, A. Hesselholt, H. Rasmussen, E. Seinre, and S. Thomas, “Application of sensitivity analysis in design of sustainable buildings,” *Renew. Energy*, vol. 34, no. 9, pp. 2030–2036, Sep. 2009.
- [73] Y. Heo, R. Choudhary, and G. A. Augenbroe, “Calibration of building energy models for retrofit analysis under uncertainty,” *Energy Build.*, vol. 47, pp. 550–560, Apr. 2012.
- [74] K. Hilliaho, E. Mäkitalo, and J. Lahdensivu, “Energy saving potential of glazed space: Sensitivity analysis,” *Energy Build.*, vol. 99, pp. 87–97, Jul. 2015.
- [75] A. H. Holm and H. M. Kuenzel, “Practical application of an uncertainty approach for hygrothermal building simulations—drying of an AAC flat roof,” *Build. Environ.*, vol. 37, no. 8–9, pp. 883–889, Aug. 2002.
- [76] J. S. Hygh, J. F. DeCarolis, D. B. Hill, and S. Ranji Ranjithan, “Multivariate regression as an energy assessment tool in early building design,” *Build. Environ.*, vol. 57, pp. 165–175, Nov. 2012.
- [77] A. Ioannou and L. C. M. Itard, “Energy performance and comfort in residential buildings: Sensitivity for building parameters and occupancy,” *Energy Build.*, vol. 92, pp. 216–233, 2015.
- [78] Y.-J. Kim, K.-U. Ahn, and C.-S. Park, “Decision making of HVAC system using Bayesian Markov chain Monte Carlo method,” *Energy Build.*, vol. 72, pp. 112–121, 2014.
- [79] J. C. Lam and S. C. M. Hui, “Sensitivity analysis of energy performance of office buildings,” *Build. Environ.*, vol. 31, no. 1, pp. 27–39, 1996.
- [80] J. Le Dréau and P. Heiselberg, “Sensitivity analysis of the thermal performance of radiant and convective terminals for cooling buildings,” *Energy Build.*, vol. 82, pp. 482–491, Oct. 2014.
- [81] I. Macdonald and P. Strachan, “Practical application of uncertainty analysis,” *Energy Build.*, vol. 33, no. 3, pp. 219–227, Feb. 2001.
- [82] A. S. Silva and E. Ghisi, “Uncertainty analysis of user behaviour and physical parameters in residential building performance simulation,” *Energy Build.*, vol. 76, pp. 381–391, Jun. 2014.
- [83] C. Spitz, L. Mora, E. Wurtz, and A. Jay, “Practical application of uncertainty analysis and sensitivity analysis on an experimental house,” *Energy Build.*, vol. 55, pp. 459–470, Dec. 2012.
- [84] W. Tian and R. Choudhary, “A probabilistic energy model for non-domestic building sectors applied to analysis of school buildings in greater London,” *Energy Build.*, vol. 54, pp. 1–11, Nov. 2012.
- [85] W. Tian and P. de Wilde, “Uncertainty and sensitivity analysis of building performance using probabilistic climate projections: A UK case study,” *Autom. Constr.*, vol. 20, no. 8, pp. 1096–1109, Dec. 2011.
- [86] L. Wang, P. Mathew, and X. Pang, “Uncertainties in energy consumption introduced by building operations and weather for a medium-size office building,” *Energy Build.*, vol. 53, pp. 152–158, 2012.
- [87] P. de Wilde and W. Tian, “Predicting the performance of an office under climate change:

- A study of metrics, sensitivity and zonal resolution,” *Energy Build.*, vol. 42, no. 10, pp. 1674–1684, Oct. 2010.
- [88] S. de Wit and G. Augenbroe, “Analysis of uncertainty in building design evaluations and its implications,” *Energy Build.*, vol. 34, no. 9, pp. 951–958, 2002.
- [89] J. Strømmand Andersen and P. A. Sattrup, “The urban canyon and building energy use: Urban density versus daylight and passive solar gains,” *Energy Build.*, vol. 43, pp. 2011–2020, 2011.
- [90] E. Krüger, D. Pearlmutter, and F. Rasia, “Evaluating the impact of canyon geometry and orientation on cooling loads in a high-mass building in a hot dry environment,” *Appl. Energy*, vol. 87, pp. 2068–2078, 2009.
- [91] N. Shishegar, “Street Design and Urban Microclimate: Analyzing the Effects of Street Geometry and Orientation on Airflow and Solar Access in Urban Canyons,” *J. Clean Energy Technol.*, 2013.
- [92] C. Chatzipoulka, R. Compagnon, and M. Nikolopoulou, “Urban geometry and solar availability on façades and ground of real urban forms: using London as a case study,” *Sol. Energy*, vol. 138, pp. 53–66, 2016.
- [93] R. Emmanuel, H. Rosenlund, and E. Johansson, “Urban shading—a design option for the tropics? A study in Colombo, Sri Lanka,” *Int. J. Climatol. Int. J. Clim.*, vol. 27, pp. 1995–2004, 2007.
- [94] A. J. Arnfield, “REVIEW TWO DECADES OF URBAN CLIMATE RESEARCH: A REVIEW OF TURBULENCE, EXCHANGES OF ENERGY AND WATER, AND THE URBAN HEAT ISLAND,” *Int. J. Climatol. Int. J. Clim.*, vol. 23, pp. 1–26, 2003.
- [95] L. Kleerekoper, M. van Esch, and T. Baldiri Salcedo, “How to make a city climate-proof, addressing the urban heat island effect,” *Resources, Conserv. Recycl.*, vol. 64, pp. 30–38, 2011.
- [96] J. Allegrini, “A wind tunnel study on three-dimensional buoyant flows in street canyons with different roof shapes and building lengths,” *Build. Environ.*, vol. 143, pp. 71–88, Oct. 2018.
- [97] M. Garau, M. Grazia Badas, S. Ferrari, A. Seoni, and G. Querzoli, “Turbulence and Air Exchange in a Two-Dimensional Urban Street Canyon Between Gable Roof Buildings,” *Boundary-Layer Meteorol.*, vol. 167, pp. 123–143, 2018.
- [98] F. Ali-Toudert and H. Mayer, “Effects of asymmetry, galleries, overhanging façades and vegetation on thermal comfort in urban street canyons,” *Sol. Energy*, vol. 81, no. 6, pp. 742–754, Jun. 2007.
- [99] E. Arens, T. Hoyt, X. Zhou, L. Huang, H. Zhang, and S. Schiavon, “Modeling the comfort effects of short-wave solar radiation indoors,” *Build. Environ.*, vol. 88, pp. 3–9, 2015.
- [100] M. Daoudi, “[No Title],” *J. Vis. Lang. Comput.*, vol. 11, no. 3, pp. 287–301, 2000.
- [101] A. P. de A. Rocha, J. Goffart, L. Houben, and N. Mendes, “On the uncertainty assessment of incident direct solar radiation on building facades due to shading devices,” *Energy Build.*, vol. 133, pp. 295–304, 2016.
- [102] K. Steemers, N. Baker, D. Crowther, and M. Nikolopoulou, “Radiation absorption and urban texture Building Open-source: To what extent does WikiHouse apply the open-source model to architecture? View project,” 2010.
- [103] S. Kotthaus, T. E. L. Smith, M. J. Wooster, and C. S. B. Grimmond, “Derivation of an urban materials spectral library through emittance and reflectance spectroscopy,” *ISPRS J. Photogramm. Remote Sens.*, vol. 94, pp. 194–212, 2014.

- [104] “Spectral Library of Impervious Urban Materials.” [Online]. Available: <http://www.met.reading.ac.uk/micromet/LUMA/SLUM.html>.
- [105] M. Santamouris, “Using cool pavements as a mitigation strategy to fight urban heat island-A review of the actual developments,” *Renew. Sustain. Energy Rev.*, vol. 26, pp. 224–240, 2013.
- [106] M. Revesz, S. M. Oswald, H. Trimmel, P. Weihs, and S. Zamini, “Potential increase of solar irradiation and its influence on PV facades inside an urban canyon by increasing the ground-albedo,” *Sol. Energy*, vol. 174, pp. 7–15, Nov. 2018.
- [107] P. R. Tregenza, “Uncertainty in daylight calculations.”
- [108] J. E. Hay, “CALCULATION OF MONTHLY MEAN SOLAR RADIATION FOR HORIZONTAL AND INCLINED SURFACES,” Pergamon Press Ltd, 1979.
- [109] B. Liu and R. Jordan, “Daily insolation on surfaces tilted towards equator,” *ASHRAE J.:(United States)*, vol. 10, 1961.
- [110] D. T. Reindl, W. A. Beckman, and J. A. Duffie, “Evaluation of hourly tilted surface radiation models,” *Sol. energy*, vol. 45, no. 1, pp. 9–17, 1990.
- [111] C. Gueymard, “An anisotropic solar irradiance model for tilted surfaces and its comparison with selected engineering algorithms,” *Sol. Energy*, vol. 38, no. 5, pp. 367–386, 1987.
- [112] J. Boland, B. Ridley, and B. Brown, “Models of diffuse solar radiation,” *Renew. Energy*, vol. 33, no. 4, pp. 575–584, 2008.
- [113] T. M. Klucher, “Evaluation of models to predict insolation on tilted surfaces,” *Sol. energy*, vol. 23, no. 2, pp. 111–114, 1979.
- [114] Y. S. Khoo *et al.*, “Optimal orientation and tilt angle for maximizing in-plane solar irradiation for PV applications in Singapore,” *IEEE J. Photovoltaics*, vol. 4, no. 2, pp. 647–653, 2014.
- [115] S. Dervishi and A. Mahdavi, “Computing diffuse fraction of global horizontal solar radiation: A model comparison,” *Sol. Energy*, vol. 86, no. 6, pp. 1796–1802, Jun. 2012.
- [116] A. M. Noorian, I. Moradi, and G. A. Kamali, “Evaluation of 12 models to estimate hourly diffuse irradiation on inclined surfaces,” *Renew. Energy*, vol. 33, no. 6, pp. 1406–1412, 2008.
- [117] C. Demain, M. Journée, and C. Bertrand, “Evaluation of different models to estimate the global solar radiation on inclined surfaces,” *Renew. Energy*, vol. 50, pp. 710–721, 2013.
- [118] R. Wattan and S. Janjai, “An investigation of the performance of 14 models for estimating hourly diffuse irradiation on inclined surfaces at tropical sites,” 2016.
- [119] Z. Li, H. Xing, S. Zeng, J. Zhao, and T. Wang, “Comparison of Anisotropic Diffuse Sky Radiance Models for Irradiance Estimation on Building Facades,” *Procedia Eng.*, vol. 205, pp. 779–786, 2017.
- [120] M. de Simón-Martín, C. Alonso-Tristán, and M. Díez-Mediavilla, “Diffuse solar irradiance estimation on building’s façades: Review, classification and benchmarking of 30 models under all sky conditions,” *Renew. Sustain. Energy Rev.*, vol. 77, no. April, pp. 783–802, 2017.
- [121] K. Lee, H. Yoo, and G. J. Levermore, “Quality control and estimation hourly solar irradiation on inclined surfaces in South Korea,” *Renew. Energy*, vol. 57, pp. 190–199, 2013.
- [122] C. A. Gueymard and D. R. Myers, “Validation and Ranking Methodologies for Solar Radiation Models.”

- [123] C. A. Gueymard, “Direct and indirect uncertainties in the prediction of tilted irradiance for solar engineering applications,” *Sol. Energy*, vol. 83, pp. 432–444, 2008.
- [124] B. E. Psiloglou and H. D. Kambezidis, “Estimation of the ground albedo for the Athens area, Greece,” *J. Atmos. Solar-Terrestrial Phys.*, vol. 71, no. 8–9, pp. 943–954, 2009.
- [125] M. Sengupta *et al.*, “Best Practices Handbook for the Collection and Use of Solar Resource Data for Solar Energy Applications Best Practices Handbook for the Collection and Use of Solar Resource Data for Solar Energy Applications(www.nrel.gov/publications),” *Tech. Rep. - NREL/TP-5D00-63112*, no. February, pp. 1–255, 2015.
- [126] D. Yang, “Solar radiation on inclined surfaces: Corrections and benchmarks,” *Sol. Energy*, vol. 136, pp. 288–302, 2016.
- [127] “TRNSYS 17,” 2009.
- [128] “EnergyPlus Documentation Engineering Reference,” 1996.
- [129] C. F. Reinhart, “Tutorial on the Use of Daysim Simulations for Sustainable Design,” *Harvard Des. Sch.*, pp. 1–114, 2010.
- [130] R. Perez, P. Ineichen, R. Seals, J. Michalsky, and R. Stewart, “Modeling daylight availability and irradiance components from direct and global irradiance,” *Sol. Energy*, vol. 44, no. 5, pp. 271–289, 1990.
- [131] J. A. Ruiz-Arias and C. A. Gueymard, “Worldwide inter-comparison of clear-sky solar radiation models: Consensus-based review of direct and global irradiance components simulated at the earth surface,” *Sol. Energy*, no. February, pp. 1–20, 2018.
- [132] M. Diez-Mediavilla, A. De Miguel, and J. Bilbao, “Measurement and comparison of diffuse solar irradiance models on inclined surfaces in Valladolid (Spain),” 2005.
- [133] G. Notton, C. Cristofari, and P. Poggi, “Performance evaluation of various hourly slope irradiation models using Mediterranean experimental data of Ajaccio,” 2005.
- [134] A. Padovan and D. Del Col, “Measurement and modeling of solar irradiance components on horizontal and tilted planes,” *Sol. Energy*, vol. 84, pp. 2068–2084, 2010.
- [135] S. A. Khalil and A. M. Shaffie, “A comparative study of total, direct and diffuse solar irradiance by using different models on horizontal and inclined surfaces for Cairo, Egypt,” 2013.
- [136] M. David, P. Lauret, and J. Boland, “Evaluating tilted plane models for solar radiation using comprehensive testing procedures, at a southern hemisphere location,” *Renew. Energy*, vol. 51, pp. 124–131, 2013.
- [137] P. G. Loutzenhiser *et al.*, “Empirical validation of models to compute solar irradiance on inclined surfaces for building energy simulation,” *Sol. Energy*, vol. 81, no. 2, pp. 254–267, 2007.
- [138] L. Robledo and A. Soler, “Modelling irradiance on inclined planes with an anisotropic model,” *Energy*, vol. 23, no. 3, pp. 193–201, 1998.
- [139] Y. Sun, H. Su, C. F. J. Wu, and G. Augenbroe, “Uncertainty quantification of solar diffuse irradiation on inclined surfaces for building energy simulation,” *Proc. BS 2013 13th Conf. Int. Build. Perform. Simul. Assoc.*, vol. 1493, no. September 2016, pp. 71–78, 2013.
- [140] D. Yang *et al.*, “Bidirectional irradiance transposition based on the Perez model,” 2014.
- [141] M. F. Jentsch, A. S. Bahaj, and P. A. B. James, “Climate change future proofing of buildings-Generation and assessment of building simulation weather files,” *Energy Build.*, vol. 40, no. 12, pp. 2148–2168, 2008.
- [142] J. Estévez, P. Gavilán, and J. V. Giráldez, “Guidelines on validation procedures for

- meteorological data from automatic weather stations,” *J. Hydrol.*, vol. 402, no. 1–2, pp. 144–154, May 2011.
- [143] M. A. Shafer, C. A. Fiebrich, D. S. Arndt, S. E. Fredrickson, and T. W. Hughes, “Quality Assurance Procedures in the Oklahoma Mesonet.”
- [144] D. Y. Graybeal, A. T. Degaetano, and K. L. Eggleston, “Improved Quality Assurance for Historical Hourly Temperature and Humidity: Development and Application to Environmental Analysis.”
- [145] M. Hasanpour Kashani and Y. Dinpashoh, “Evaluation of efficiency of different estimation methods for missing climatological data,” *Stoch. Environ. Res. Risk Assess.*, vol. 26, pp. 59–71, 2012.
- [146] T. C. Pagano, Q. J. Wang, H. A. P. Hapuarachchi, D. L. Shrestha, and D. E. Robertson, “Evaluation of numerical weather prediction model precipitation forecasts for short-term streamflow forecasting purpose,” *Hydrol. Earth Syst. Sci.*, vol. 17, no. 5, pp. 1913–1931, 2013.
- [147] A. K. Yadav and S. S. Chandel, “Solar radiation prediction using Artificial Neural Network techniques: A review,” *Renew. Sustain. Energy Rev.*, vol. 33, pp. 772–781, May 2014.
- [148] S. Rehman and M. Mohandes, “Artificial neural network estimation of global solar radiation using air temperature and relative humidity,” *Energy Policy*, vol. 36, no. 2, pp. 571–576, 2008.
- [149] M. Bilgili, B. Sahin, and A. Yasar, “Application of artificial neural networks for the wind speed prediction of target station using reference stations data,” *Renew. Energy*, vol. 32, no. 14, pp. 2350–2360, Nov. 2007.
- [150] F. Khayatian, L. Sarto, and G. Dall’O’, “Application of neural networks for evaluating energy performance certificates of residential buildings,” *Energy Build.*, vol. 125, pp. 45–54, Aug. 2016.
- [151] E. Zio, *The Monte Carlo simulation method for system reliability and risk analysis*. Springer, 2013.
- [152] M. H. DeGroot and M. J. Schervish, *Probability and Statistics*. 2011.
- [153] L. A. Zadeh, “Fuzzy sets as a basis for a theory of possibility,” *Fuzzy Sets Syst.*, vol. 1, no. 1, pp. 3–28, 1978.
- [154] D. R. Tobergte and S. Curtis, *Uncertainty Theory*, vol. 53, no. 9. 2013.
- [155] D. Kurowicka and R. Cooke, “Uncertainty Analysis with High Dimensional Dependence Modelling,” *Recherche*. p. 302, 2006.
- [156] Y. Jiang, Z. Nan, and S. Yang, “Risk assessment of water quality using Monte Carlo simulation and artificial neural network method,” *J. Environ. Manage.*, vol. 122, pp. 130–136, 2013.
- [157] P. Zhang, W. Li, S. Li, Y. Wang, and W. Xiao, “Reliability assessment of photovoltaic power systems: Review of current status and future perspectives,” *Appl. Energy*, vol. 104, pp. 822–833, 2013.
- [158] I. Macdonald, “Quantifying the Effects of Uncertainty in Building Simulation,” *Regulation*, vol. Ph D, no. July, p. 267, 2002.
- [159] B. D. Lee, Y. Sun, G. Augenbroe, and C. J. J. Paredis, “Towards better prediction of building performance : a workbench to analyze uncertainty in building simulation,” *BS2013 13th Conf. Int. Build. Perform. Simul. Assoc. Chambéry, Fr. August 26-28*, pp. 1231–1238, 2013.

- [160] S. S. Sawilowsky, “Trivials : The Birth , Sale , And Final Production Of,” vol. 2, no. 1, 2003.
- [161] A. Darwiche, *Modeling and reasoning with Bayesian networks*. Cambridge University Press, 2009.
- [162] P. Gärdenfors, *Knowledge in flux: Modeling the dynamics of epistemic states*. The MIT press, 1988.
- [163] L. A. Zadeh, “Is there a need for fuzzy logic?,” *Inf. Sci. (Ny)*, vol. 178, no. 13, pp. 2751–2779, 2008.
- [164] B. R. Cobb and P. P. Shenoy, “A comparison of Bayesian and belief function reasoning,” *Inf. Syst. Front.*, vol. 5, no. 4, pp. 345–358, 2003.
- [165] D. Dubois and H. Prade, “Possibility theory, probability theory and multiple-valued logics: A clarification,” *Ann. Math. Artif. Intell.*, vol. 32, no. 1, pp. 35–66, 2001.
- [166] D. Dubois, H. Prade, and P. Smets, “Representing partial ignorance,” *IEEE Trans. Syst. Man, Cybern. A Syst. Humans*, vol. 26, no. 3, pp. 361–377, 1996.
- [167] J. Kohlas and P.-A. Monney, *A mathematical theory of hints: An approach to the Dempster-Shafer theory of evidence*, vol. 425. Springer Science & Business Media, 2013.
- [168] J. A. Cooper, S. Ferson, and L. Ginzburg, “Hybrid processing of stochastic and subjective uncertainty data,” *Risk Anal.*, vol. 16, no. 6, pp. 785–791, 1996.
- [169] C. Baudrit, D. Dubois, and N. Perrot, “Representing parametric probabilistic models tainted with imprecision,” *Fuzzy sets Syst.*, vol. 159, no. 15, pp. 1913–1928, 2008.
- [170] D. Dubois, E. Kerre, R. Mesiar, and H. Prade, “Fuzzy interval analysis,” in *Fundamentals of fuzzy sets*, Springer, 2000, pp. 483–581.
- [171] D. Dubois and H. Prade, “When upper probabilities are possibility measures,” *Fuzzy sets Syst.*, vol. 49, no. 1, pp. 65–74, 1992.
- [172] G. Shafer, *A mathematical theory of evidence*, vol. 1. Princeton university press Princeton, 1976.
- [173] D. Guyonnet, B. Bourguine, D. Dubois, H. Fargier, B. Côme, and J.-P. Chilès, “Hybrid Approach for Addressing Uncertainty in Risk Assessments,” *J. Environ. Eng.*, vol. 129, no. 1, pp. 68–78, 2003.
- [174] P. Baraldi and E. Zio, “A Combined Monte Carlo and possibilistic approach to uncertainty propagation in event tree analysis,” *Risk Anal.*, vol. 28, no. 5, pp. 1309–1325, 2008.
- [175] D. Dubois, H. Fargier, and J. Fortin, “The empirical variance of a set of fuzzy intervals,” in *The 14th IEEE International Conference on Fuzzy Systems, 2005. FUZZ'05.*, 2005, pp. 885–890.
- [176] C. Baudrit, D. Dubois, and D. Guyonnet, “Joint propagation and exploitation of probabilistic and possibilistic information in risk assessment,” *IEEE Trans. fuzzy Syst.*, vol. 14, no. 5, pp. 593–608, 2006.
- [177] D. Guyonnet, ; Bernard Bourguine, ; Didier Dubois, ; Hé Lè Ne Fargier, ; Bernard Côme, and J.-P. Chilè, “Hybrid Approach for Addressing Uncertainty in Risk Assessments.”
- [178] Z. Gong, F. DiazDelaO, M. B.- Risk, R. and Safety, and undefined 2016, “Bayesian model calibration using subset simulation,” *books.google.com*.
- [179] S.-K. Au and J. L. Beck, “Estimation of small failure probabilities in high dimensions by subset simulation,” *Probabilistic Eng. Mech.*, vol. 16, no. 4, pp. 263–277, Oct. 2001.
- [180] A. Srivastav, A. Tewari, and B. Dong, “Baseline building energy modeling and localized uncertainty quantification using Gaussian mixture models,” *Energy Build.*, vol. 65, pp. 438–447, 2013.

- [181] T.K.Moon, “The Expectatio Maximization Algorithm,” pp. 47–60, 1996.
- [182] S. Crone, “Radiance users manual,” *Glass*, no. November, 1992.
- [183] “Solemma, LLC.” [Online]. Available: <https://www.solemma.com>.
- [184] J. A. Jakubiec and C. Reinhart, “DIVA-FOR-RHINO 2.0: Environmental parametric modeling in Rhinoceros/Grasshopper using RADIANCE, Daysim and EnergyPlus,” in *Conference proceedings of building simulation*, 2011.
- [185] L. V. de Abreu-Harbich, L. C. Labaki, and A. Matzarakis, “Effect of tree planting design and tree species on human thermal comfort in the tropics,” *Landsc. Urban Plan.*, vol. 138, pp. 99–109, 2015.
- [186] R. Levinson, H. Pan, G. Ban-Weiss, P. Rosado, R. Paolini, and H. Akbari, “Potential benefits of solar reflective car shells: Cooler cabins, fuel savings and emission reductions,” *Appl. Energy*, vol. 88, pp. 4343–4357, 2011.
- [187] C. L. Bueno-bartholomei and L. C. Labaki, “HOW MUCH DOES THE CHANGE OF SPECIES OF TREES AFFECT THEIR SOLAR RADIATION ATTENUATION ? *,” pp. 2–5, 1996.
- [188] P. Tregenza and M. Wilson, *Daylighting: architecture and lighting design*. Routledge, 2013.
- [189] K. Kubaha, · D Fiala, · J Toftum, and · A H Taki, “Human projected area factors for detailed direct and diffuse solar radiation analysis,” *Int J Biometeorol*, vol. 49, pp. 113–129, 2004.
- [190] “full-text.”
- [191] P. O. Fanger, A. K. Melikov, H. Hanzawa, and J. Ring, “Air Turbulence and Sensation of Draught,” 1988.
- [192] T. Andreas, A.; Stoffel, “NREL Solar Radiation Research Laboratory (SRRL): Baseline Measurement System (BMS).” .
- [193] J. L. Loeppky, J. Sacks, and W. J. Welch, “Choosing the sample size of a computer experiment: A practical guide,” *Technometrics*, vol. 51, no. 4, pp. 366–376, 2009.
- [194] “NREL/ENERGYPLUS.” [Online]. Available: <https://github.com/NREL/EnergyPlus>.
- [195] S. Goel *et al.*, “Enhancements to ASHRAE Standard 90.1 Prototype Building Models,” 2014.
- [196] “Tree transmittance/transmissivity.”
- [197] K. Perini and A. Magliocco, “Effects of vegetation, urban density, building height, and atmospheric conditions on local temperatures and thermal comfort,” *Urban For. Urban Green.*, vol. 13, no. 3, pp. 495–506, Jan. 2014.
- [198] A. Nabil and J. Mardaljevic, “Useful daylight illuminances: A replacement for daylight factors.”
- [199] S. Torres and V. R. M. Lo, “Comparative analysis of simplified daylight glare methods and proposal of a new method based on the cylindrical illuminance,” vol. 78, pp. 699–704, 2015.
- [200] F. Antretter and M. Winkler, “WUFI ® Plus 3.0 Manual,” 2015.
- [201] “Creating weather files | WUFI (en).” [Online]. Available: <https://wufi.de/en/service/downloads/creating-weather-files/>.
- [202] R. Paolini *et al.*, “The hygrothermal performance of residential buildings at urban and rural sites: Sensible and latent energy loads and indoor environmental conditions,” *Energy Build.*, vol. 152, pp. 792–803, 2017.

Annexes:

Annex 1: Basis of DIVA solar radiation simulations

Inputs of Radiation Map can categorize in four groups: (1) climate and time steps, (2) target building and surroundings, (3) sensor points (area of interest) and (4) radiation parameters. A brief introduction of each input is mentioned in the following:

(1) Climate and time step: As mentioned before, DIVA performs daylight analysis based on climate-base calculation method, therefore, local weather parameter should import through “Loc” input as an EPW file. Also, it is possible to set the period of calculations in Radiation Map component for a certain moment, a specific period (summer/winter) or for whole year by hourly time steps.

(2) Target building and surroundings: Studied building and shading elements such as adjacent buildings and trees should be given representation in DIVA calculation through the “Obj” input port. The right material which reproduces the intended optical properties should be assigned on each object before connecting to Radiation Map component. The material in DIVA are assigned based on the RADAINACE format definition which depend on the type of material, set value of reflectance, transmittance or specularly of material.

(3) Sensor points: Solar radiation on studied area is collecting by a series of sensor points. These points can record illuminance as well as solar radiation. Two important setting should be noticed for each sensor point, i.e. sensor orientation (north, east, south, west) and direction (horizontal, tilted). Sensor points are imported to DIVA components via “Grid” port.

(4) Radiance parameter: A set of parameters are defined to control backward raytracing calculations in RADIANCE ([129] page 26). Backward raytracing algorithm estimate the light on target area by trace it back to the source of the light [182]. One of the most effective hyper parameters is the ambient bounce (ab). This parameter defines the number of rays which should bounced from a certain sensor point in RADIANCE. RADIANCE parameters are possible to set in “RP” port.

Annex 2: Uncertainty propagation - Code in MATLAB and connection to Grasshopper

The following MATLAB code is used to define the range of variation for selected features within an urban canyon as well as propagating the uncertainty based on hybrid method. The results export in separates .csv files for each uncertain feature and store in a folder which is already connected to DIAV-Grasshopper. After that in Grasshopper, geometry of each sample urban canyon generates.

```
# Define the number of random samples and number of urban canyon features
```

```
Number_of_Building=20;  
NumberofTarget=4;  
NumberRandom=10;  
NumberofFloors=7;  
NumberofAlpha=6;  
NumberofTotal_Sample=NumberofAlpha*NumberRandom;
```

```
# Propagate the uncertainty in height of surrounding buildings
```

```
BuildinHeight_Dist=makedist('normal','mu',1,'sigma',0.1);  
SBHeigh t=random (BuildinHeight_Dist,[NumberRandom,Numberof_Building]);
```

```
# Make the final number of samples; In this step the generated random for each probability distribution should merge with the number of random from possibility distribution
```

```
[Ratio_BuildingHeight]=SetRandomWith_Alphacut(SBHeight,NumberofTotal_Sample,  
NumberRandom,NumberofAlpha);
```

```
# Propagate the uncertainty in WWR of surroundings
```

```
WWR_Dist=makedist('normal','mu',0.45,'sigma',0.1);  
rW=random(WWR_Dist,[NumberRandom,NumberofTarget]);  
S_WWR=round(rW,2);  
[WWR]=SetRandomWith_Alphacut(S_WWR,NumberofTotal_Sample,  
NumberRandom, NumberofAlpha);
```

```

# Propagate the uncertainty in Opaque material (External walls) of surroundings
WallReflectance_Dist=makedist('normal','mu',0.37,'sigma',0.091);
nC=NumberofFloors*NumberofTarget;
Opaq_Ref=zeros(NumberRandom,nC);
One=ones(NumberofTarget,NumberofFloors);
for i=1:NumberRandom
    a11=random(WallReflectance_Dist,[1,NumberofTarget]);
    a22=transpose(a11);
    a33=One.*a22;
    a33=a33';
    a44=reshape(a33,1,nC);
    Opaq_Ref(i,:)=a44;
end
SExtWall_Ref=round(Opaq_Ref,2);
[ExternalWall_Reflectance]=SetRandomWith_Alphacut(SExtWall_Ref,
NumberofTotal_Sample, NumberRandom, NumberofAlpha);

# All about tree/ size and material
# Uncertainty propagation of random tree transmittance
Tree_alphacut_0=[0;1];
Tree_alphacut_05=[0.1;0.7];
Tree_alphacut_1=[0.2;0.3];
All_AlphaT=[Tree_alphacut_0;Tree_alphacut_05;Tree_alphacut_1];
Samples_Tree_Tans=repmat(All_AlphaT,NumberRandom,1);

# Propagate the uncertainty in tree radius
NumberofTree=6;
TreeRadiuse_Dist=makedist('normal','mu',7.5,'sigma',1);
SRadTree=random(TreeRadiuse_Dist,[NumberRandom,NumberofTree]);
[TreeCrown_Radius]=SetRandomWith_Alphacut(SRadTree,NumberofTotal_Sample,
NumberRandom,NumberofAlpha);

```

```
# Propagate the uncertainty in car material
```

```
Car_alphacut_0=[0;1];
```

```
Car_alphacut_05=[0.03;0.8];
```

```
Car_alphacut_1=[0.05;0.58];
```

```
All_alphacut_Car=[Car_alphacut_0;Car_alphacut_05;Car_alphacut_1];
```

```
CarReflectance= repmat(All_alphacut_Car,NumberRandom,1);
```

```
# Extract the csv file of each feature which calls later in Grasshopper as an input of data analysis module
```

```
str1=sprintf('TreeCrown_Radius.csv');
```

```
str2=fullfile('C:\...\Gh_Inputs',str1);
```

```
csvwrite(str2,TreeCrown_Radius)
```

```
# Intermediate function to arrange the random numbers with alpha-cut numbers
```

```
function
```

```
[RandomSet]=SetRandomWith_Alphacut(randomVar,NumberofTotal_Sample,  
NumberRandom, NumberofAlpha)
```

```
nRt=size(randomVar,2);
```

```
RandomSet=zeros(NumberofTotal_Sample,nRt);
```

```
for i=1:NumberRandom
```

```
    at=randomVar(i,:);
```

```
    bt=repmat(at,NumberofAlpha,1);
```

```
    r1=6*i-5;
```

```
    r2=6*i;
```

```
    RandomSet(r1:r2,:)=bt;
```

```
end
```

```
end
```

Annex3: Building energy model assumption in WUFI Plus

WUFI weather data generator provides the possibility to opt for different units for each weather parameter. The weather generator accepts solar radiation in W/m² while providing the liberty to choose between different data sources as shown in Figure 63. Regarding that, the results of solar radiation on vertical facades obtained from DIVA, could be replaced in WUFI weather data as measured solar radiation.

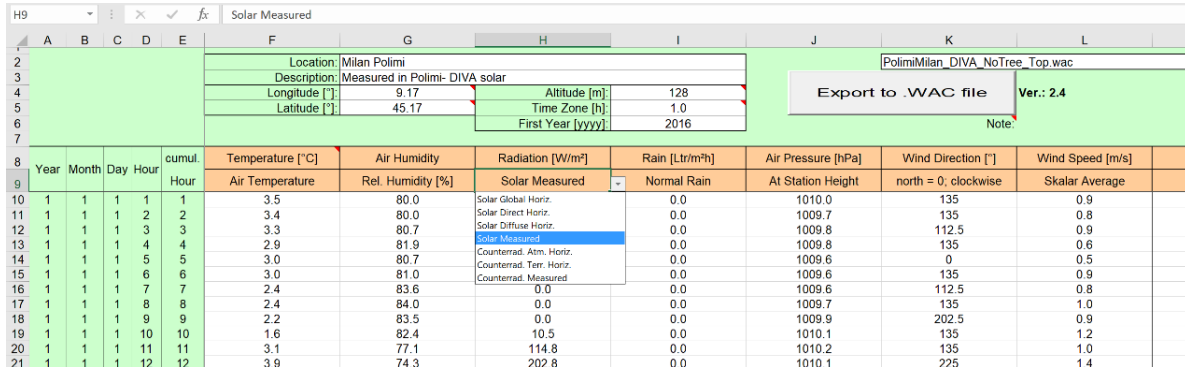


Figure 63 - WUFI weather generator

The characteristics of the exposing wall and window to solar radiation is presented in the following figures and tables.

Table 26 - Opaque and glazed area on target building façade

Exposure surface to solar radiation	Area	Orientation	Direction
Glazed area	9.6 m ²	South	Vertical
Opaque area	17.4 m ²	South	Vertical

Table 27 - Window properties: Detailed of simulated building energy model in WUFI

Window type:	
Low -e Double glazing on surface	
U-Value [W/m ² K]	1.99
Frame factor [-]	0.7
SHGC hemispherical [-]	0.53
Long wave radiation emissivity (mean glazing/frame) [-]	0.2

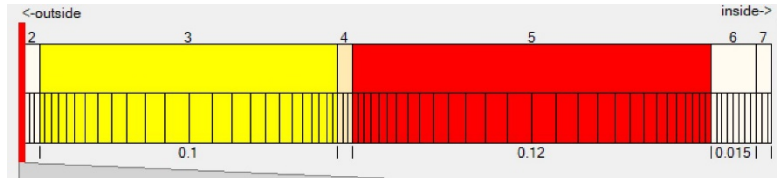

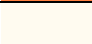




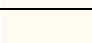


Figure 64 - Exterior wall assembly

Table 28- Exterior wall: Detailed of simulated building energy model in WUFI

Nr.	Material	ρ	c	λ	Thickness	color
	(from outside to inside)	[kg/m ³]	[J/kgK]	[W/mK]	[m]	
1	Quarzolite tonachino plus	1600	1000	1.28	0.002	
2	Cement Plaster	2000	850	1.2	0.005	
3	EPS	30	1500	0.04	0.1	
4	Mineral Plaster	1900	850	0.8	0.005	
5	Aerated Clay Brick	600	850	0.12	0.12	
6	Cement Lime Plaster	1900	850	0.8	0.015	
7	Interior Plaster	850	850	0.2	0.005	
Overall U-value		0.268W/m²K				